

# bradscholars

## Geometric modelling and shape optimisation of pharmaceutical tablets. Geometric modelling and shape optimisation of pharmaceutical tablets using partial differential equations.

Item Type	Thesis
Authors	Ahmat, Norhayati
Rights	<p><a href="http://creativecommons.org/licenses/by-nc-nd/3.0/">&lt;a rel="license" href="http://creativecommons.org/licenses/by-nc-nd/3.0/"&gt;&lt;img alt="Creative Commons License" style="border-width:0" src="http://i.creativecommons.org/l/by-nc-nd/3.0/88x31.png" /&gt;&lt;/a&gt;&lt;br /&gt;</a>The University of Bradford theses are licenced under a <a href="http://creativecommons.org/licenses/by-nc-nd/3.0/">&lt;a rel="license" href="http://creativecommons.org/licenses/by-nc-nd/3.0/"&gt;Creative Commons Licence&lt;/a&gt;.</a></p>
Download date	2026-03-15 02:57:24
Link to Item	<a href="http://hdl.handle.net/10454/5702">http://hdl.handle.net/10454/5702</a>



## **University of Bradford eThesis**

This thesis is hosted in [Bradford Scholars](#) – The University of Bradford Open Access repository. Visit the repository for full metadata or to contact the repository team



© University of Bradford. This work is licenced for reuse under a [Creative Commons Licence](#).

**GEOMETRIC MODELLING AND SHAPE**  
**OPTIMISATION OF PHARMACEUTICAL TABLETS**

Geometric Modelling and Shape Optimisation of Pharmaceutical Tablets Using  
Partial Differential Equations

Norhayati Binti AHMAT

Submitted for the degree of  
Doctor of Philosophy.

School of Computing, Informatics and Media  
University of Bradford

2012

## Abstract

**Keywords:** Geometric modelling, PDE Method, Parametric surfaces, Pharmaceutical tablets, Shape optimisation.

Pharmaceutical tablets have been the most dominant form for drug delivery and they need to be strong enough to withstand external stresses due to packaging and loading conditions before use. The strength of the produced tablets, which is characterised by their compressibility and compactibility, is usually determined through a physical prototype. This process is sometimes quite expensive and time consuming. Therefore, simulating this process before hand can overcome this problem.

A technique for shape modelling of pharmaceutical tablets based on the use of Partial Differential Equations is presented in this thesis. The volume and the surface area of the generated parametric tablet in various shapes have been estimated numerically. This work also presents an extended formulation of the PDE method to a higher dimensional space by increasing the number of parameters responsible for describing the surface in order to generate a solid tablet. The shape and size of the generated solid tablets can be changed by exploiting the analytic expressions relating the coefficients associated with the PDE method.

The solution of the axisymmetric boundary value problem for a finite cylinder subject to a uniform axial load has been utilised in order to model a displacement component of a compressed PDE-based representation of a flat-faced round tablet. The simulation results, which are analysed using the Heckel model, show that the developed model is capable of predicting the compressibility of pharmaceutical powders since it fits the experimental data accurately. The optimal design of pharmaceutical tablets with particular volume and maximum strength has been obtained using an automatic design optimisation which is performed by combining the PDE method and a standard method for numerical optimisation.

## Dedications

*Thank you ALLAH*

*To my dear mum, Chek Pou Md Zin and mother in law, Hadibah Noor*

*and*

*To my beloved husband, Muhamad Raymee Jaafar*

## **Acknowledgements**

I would like to express my deepest gratitude to my supervisors, Prof. Hassan Ugail and Dr. Gabriela González Castro, for their understanding, encouragement and support throughout this research. This work could not have been possible without their inspiring advice and continuous guidance. I would also like to thank my examiners, Dr. Lihua You and Dr. Stan Ipson, who made my viva an enjoyable, stimulating and challenging afternoon.

I would like to thank Prof. Anant Paradkar and Dr. Ravindra Dhumal from Institute of Pharmaceutical Innovation, University of Bradford for valuable discussions and providing experimental data of compressed Lactose. I would also like to thank Dr. Chuan-Yu Wu, who kindly shares his numerical data from the FEM simulation. In addition, I must sincerely thank Helen Jones, who patiently proofread this entire thesis.

I am grateful to have met many friends in this department, who have supported me throughout this journey. The special note of thanks goes to Mokhairi Makh-tar, Syadiah Nor and Nur Baini Ismail.

Lastly, I am heartily thankful to Ministry of Higher Education, Malaysia and Universiti Pendidikan Sultan Idris for giving me the opportunity to further my study.

## **Declaration**

I hereby declare that the work presented in this thesis is my original work. Wherever contributions of others are involved, every effort is made to indicate this clearly, with due reference to the literature, and acknowledgement of collaborative research and discussions.

The work was done under the guidance of Professor Hassan Ugail and Dr Gabriela González Castro, at the Centre for Visual Computing, University of Bradford, UK.

# Table of Contents

<b>Abstract</b> .....	<b>I</b>
<b>Dedications</b> .....	<b>II</b>
<b>Acknowledgements</b> .....	<b>III</b>
<b>Declaration</b> .....	<b>IV</b>
<b>List of Tables</b> .....	<b>VIII</b>
<b>List of Figures</b> .....	<b>IX</b>
<b>Chapter 1 Introduction</b> .....	<b>1</b>
1.1 Motivation .....	1
1.2 Objectives .....	4
1.3 Research Contributions .....	6
1.4 Publications .....	7
1.5 Structure of the Thesis .....	9
1.6 Summary .....	11
<b>Chapter 2 On the Compaction of Pharmaceutical Tablets</b> .....	<b>12</b>
2.1 Introduction .....	12
2.2 Compaction Properties of Pharmaceutical Powders .....	14
2.2.1 Compressibility of Pharmaceutical Powders .....	17
2.2.2 Compactibility of Tablets .....	22
2.3 Summary .....	27
<b>Chapter 3 Techniques for Geometric Modelling</b> .....	<b>28</b>

3.1	Introduction .....	28
3.2	History .....	29
3.3	Spline-Based Surface .....	32
3.4	Parametric Surfaces Based on the Use of Partial Differential Equations .....	37
3.4.1	Introduction to the PDE Method .....	40
3.4.2	Applications of PDE Surfaces .....	48
3.5	Design Optimisation .....	52
3.6	Summary .....	56
<b>Chapter 4</b>	<b>The PDE Method for Tablet Shape Modelling .....</b>	<b>58</b>
4.1	Introduction .....	58
4.2	Modelling Parametric Representation of Tablet Shapes .....	59
4.2.1	The Surface Area and Volume of a Parametric Tablet .....	64
4.3	Three-Dimensional Mesh Generation Using the PDE Method .....	70
4.4	Manipulation of PDE-Based Objects .....	75
4.4.1	Examples of Tablet Shape and Size Manipulation .....	79
4.5	Summary .....	82
<b>Chapter 5</b>	<b>Modelling the Mechanical Behaviour of Pharmaceutical Tablets.</b>	<b>84</b>
5.1	Introduction .....	84
5.2	Solution of the Love's Stress Function in Cylindrical Coordinates .....	85
5.2.1	Simulation of Axial Compression on the PDE-based Tablets .....	90
5.2.2	Results and Discussion .....	95
5.3	Elastic-Plastic Contact Deformation of a Spherical Granule .....	101
5.3.1	Deformation of a PDE-Based Spherical Tablet .....	106
5.3.2	Results and Discussion .....	107
5.4	Summary .....	114
<b>Chapter 6</b>	<b>Automatic Design Optimisation .....</b>	<b>115</b>

---

6.1	Introduction .....	115
6.2	Optimal Design of Pharmaceutical Tablets for Strength .....	116
6.2.1	The Flat-faced Round Tablet .....	119
6.2.2	The Spherical Tablet .....	124
6.2.3	The Spherical Capsule .....	129
6.3	Summary .....	136
<b>Chapter 7</b>	<b>Conclusions .....</b>	<b>138</b>
7.1	Summary .....	138
7.2	Contributions .....	141
7.3	Research Limitations .....	145
7.4	Future Work .....	147
	<b>Bibliography.....</b>	<b>149</b>
	<b>Appendix A .....</b>	<b>160</b>
	<b>Appendix B .....</b>	<b>162</b>
	<b>Appendix C .....</b>	<b>168</b>

## List of Tables

3.1	Algorithms offered by the MATLAB Optimisation Toolbox for solving linear and nonlinear programming problems . . . . .	55
4.1	Parameters and properties of each PDE-based representation of tablet configurations used in this project . . . . .	60
4.2(a)	Comparison between estimated and theoretical values of surface area and volume of a flat-faced round tablet . . . . .	67
4.2(b)	Comparison between estimated and theoretical values of surface area and volume of a spherical tablet . . . . .	68
4.3	Surface area and volume of shallow convex round, shallow convex oval and oblong tablets . . . . .	69
4.4	Number of nodes and time required to create the geometries shown in Figure 4.5. . . . .	74
4.5	Changes made to the design parameters of the original tablet shape. . . . .	81
5.1	Heckel's parameters for $\alpha$ -lactose from experiment and simulation . . . . .	98
5.2	Mechanical characteristics of the examined materials by compression. . . . .	108
5.3	The parameters of best-fit linear regression line for PDE coefficients. . . . .	110
6.1	Values used for the design parameters associated with the round tablet. . . . .	124
6.2	Values for the design parameters associated with the spherical tablet used in the optimisation. . . . .	128

## List of Figures

2.1	Tablet strength measurement in (a) diametrical test and (b) axial compressive strength. This figure is reproduced from Han et al. (2008) . . . . .	23
2.2	Front and side elevation of (a) a flat-faced round, (b) convex-faced round and (c) convex-faced elongated tablet. Figure adapted from Pitt and Heasley (2011) . . . . .	25
3.1	Bicubic Bézier surface. Figure extracted from Lavoué (2008) . . . . .	33
3.2	The boundary $\partial\Omega$ in the $(u, v)$ space is mapped to the three-dimensional space, $(x, y, z)$ . . . . .	41
3.3	Shape of PDE surfaces generated by the Biharmonic equation. (a) The boundary curves and (b) the corresponding surface shape. The effect on the shape of the surface by (c) resizing and (e) translating the derivative curves. The resulting manipulated surface shape in (d) and (f) . . . . .	45
3.4	Example of a two-patch PDE surface subject to a specific set of boundary conditions outlined in (a) . . . . .	47
4.1	Generating curves for a flat-faced round tablet. . . . .	60
4.2	Different shapes of pharmaceutical tablets created using either two or three PDE surface patches accordingly. The boundary curves for each shape are shown together with the corresponding spine in (a), (d), (g), (j) and (m). The interior part of each generated parametric tablet is illustrated in (c), (f), (i), (l) and(o) . . . . .	61

---

4.3	Independent variables in the extended PDE method . . . . .	71
4.4	Cuboid mesh generation process. (a) Generated nodes. (b) Generating Face1 faces parallel to $yz$ -plane from front layer to $sx$ -layer. (c) Generating Face2 faces parallel to $xy$ -plane from bottom layer to $sz$ -layer. (d) Generating Face3 faces parallel to $zx$ -plane from right layer to $sy$ -layer . . . . .	72
4.5	Cuboid mesh of a spheroid; (a) 800, (b) 3800 and (c) 7600 cuboids . . . . .	74
4.6	Solid PDE-based representation of tablets; (a) Flat-faced round, (b) Spherical, (c) Convex round, (d) Convex oval and (e) Oblong tablets . . . . .	75
4.7	Different tablet shapes obtained by changing the design parameters . . . . .	80
5.1	Stresses in cylindrical coordinates where $\sigma_z$ , $\sigma_\theta$ and $\sigma_r$ are the normal stress components in the $z$ , $\theta$ and $r$ directions respectively. . . . .	86
5.2	Schematic representation of the powder compaction process . . . . .	91
5.3	Heckel plot of compressed $\alpha$ -lactose monohydrate using experimental data. . . . .	96
5.4	Comparison between the Heckel plot of the simulated compression and the experimental result on Lactose powder . . . . .	98
5.5	Density-pressure linear regression lines of FEM versus PDE simulations on Lactose powder . . . . .	100
5.6	Compression of a spherical granule. (a) The slow compression of a spherical granule with two contact points. (b) The shape of a granule after the elastic-plastic deformation . . . . .	104

---

5.7	Force-displacement curve of a spherical granule during compression. This graph has been reproduced from Antonyuk et al. (2010) . . . . .	105
5.8	PDE coefficients representing the height and contact area of the compressed spherical (a) Lactose and (b) Köstrolith . . . . .	109
5.9	Comparison between the radius of contact area of the theoretical and PDE-based spherical (a) Lactose and (b) Köstrolith . . . . .	111
5.10	Solid PDE-based representation of compressed spherical tablets at different force values . . . . .	112
5.11	Heckel plot of theoretical and PDE-based model for the compressed spherical tablet . . . . .	113
6.1	Optimisation flow diagram . . . . .	119
6.2	Optimal shapes of tablets with maximum tensile strength: (a) straight and (b) curved-edge round tablets . . . . .	124
6.3	Spheroidal tablets with maximum tensile strength. (a) Resulting configuration with a tensile strength equal to $77.1736 \text{ N/mm}^2$ . The tensile strength of a spheroidal tablet in (b) is $69.1043 \text{ N/mm}^2$ . . . . .	128
6.4	(a) Surface shape of upper hemisphere of the shell. (b) Solid PDE-based representation of a spherical soft shell . . . . .	130
6.5	Mathematical representation of the compression test for a spherical gel capsule . . . . .	133
6.6	Relationship between the thicknesses of a capsule shell and the tensile strength in each iteration during the optimisation process . . . . .	136

# **Chapter 1**

## **Introduction**

This chapter outlines the research motivation, aims and objectives of this work in order to give the reader a glimpse of what inspired this line of research. The original contributions, publications and the thesis structure are also covered in this chapter.

### **1.1 Motivation**

Pharmaceutical tablets have been the most dominant form for drug delivery and most are used in the oral administration of drugs. These tablets need to be strong enough to tolerate external stresses. Quality tablets are those that have consistent hardness, uniform content and accurate mass and height. The quality of the produced tablets depends on the compaction properties of pharmaceuti-

cal powders, which are characterised by their compressibility and compactibility, and consequently, these properties require investigation. Both mechanical behaviours can be determined through the powder compaction stage, which is one of the stages in the tableting process. Additionally, the shape and size of a tablet are two important features in determining the tablet properties apart from enhancing its aesthetic appearance.

Recently, the use of computer vision has been applied widely in medical applications, especially in medical image processing (Peiró et al. 2007), designing drugs (Song et al. 2009), pharmaceutical tablet formulations (Yu et al. 2009) and simulations of various tablet processing techniques (Cunningham et al. 2004; Fu et al. 2006; Siiriä and Yliruusi 2007). A number of methods have been proposed to simulate powder compression, such as finite element (FE) (Wu et al. 2008) and discrete element (DE) (Hassanpour et al. 2004) methods. However, it has been reported by Frenning (2008) that the implementation of the FE method is quite complicated and cannot distribute information on the particle range. Meanwhile, the DE method fails to give an accurate result if the particle deformation is extensive and it is hard to obtain stresses within individual particles (Frenning 2008). Thus, a combined FE/DE method has been introduced to overcome these problems (Frenning 2010). However, no report has been found in the literature regarding any work related to the geometric modelling of phar-

maceutical tablets, either interactively or based on the use of parametric surface representations.

At present, there exists a variety of methods that can be utilised to generate the geometry of pharmaceutical tablets, such as Bézier surfaces (Shang et al. 2008), B-spline (Pungotra et al. 2008), Non-uniform rational B-splines (NURBS) (Sánchez et al. 2004) and also a surface representation technique based on the use of Partial Differential Equations (PDEs), known as the PDE method (Ugail and Wilson 2005). Of all these methods, the PDE method is the most suitable for representing any given shape of tablet and its components since it can generate surfaces of complex geometries from a small number of parameters. The PDE method has been introduced in Computer-aided Design (CAD) as a solution of a particular type of elliptic PDE to generate smooth parametric surfaces (Ugail 2006). The shape of the surfaces generated by this method is based on a boundary representation and can easily be modified since it is characterised by data distributed around the boundaries.

The PDE method is compatible with other well established spline-based surface designs, such as B-spline (Du and Qin 2005). Thus, PDE surfaces can be effectively integrated into existing commercial design systems. Furthermore, the use of the PDE method can significantly reduce the computational cost associated

with the process of designing pharmaceutical tablets since PDE-based surfaces can be generated in any CAD package such as Autodesk Maya Plug-in, Microsoft Visual Studio C<sup>++</sup> and MATLAB. Moreover, this technique offers modelling tools to manipulate the shape of a PDE surface by altering the values of its design parameters (Ugail and Wilson 2005). Thus, a PDE-based model preserves its geometric nature when the values of its design parameters are changed. In the present context, this means that PDE surfaces can adapt to physical changes in the tablet when the tablet has been compressed axially or diametrically.

Before the produced tablet comes onto the market, the compactness of the tablet will have to be determined. This is usually done via physical prototypes and that process is often quite expensive and time consuming. Therefore, an alternative computer based simulation tool needs to be developed in order to determine the compactness of tablets before they can be mass produced. Based on the aspects discussed here, the intention of this thesis is to develop a surface representation model to simulate the tablet compaction process, which is a fundamental problem in the pharmaceutical industry.

## **1.2 Objectives**

The aim of this research is to adopt the PDE method for use in the pharmaceutical industry, focusing on the shape characterisation of tablets. The scope of the

research relates specially to the design and mechanical properties of tablets. The aim is to develop a parametric representation, and eventually a computer based simulation algorithm, for pharmaceutical use. This platform may prove useful for minimising the cost and time taken during the powder compaction process. The aim can be achieved by following these objectives.

The objectives of this research are:

- I. To model various shapes of pharmaceutical tablets based on the use of Partial Differential Equations.
- II. To generate solid objects by extending the mathematical formulation of the PDE method to a higher dimension and integrating it in a CAD environment for designing solid pharmaceutical tablets.
- III. To exploit the formulation of the PDE method in order to find simple expressions characterising the height and radius of the generated solid tablet. These simple expressions can be used to manipulate tablet configurations.
- IV. To develop an axial displacement model for a compressed pharmaceutical powder in a cylindrical die during the Single Ended Compression (SEC) process.
- V. To make use of the contact law of a granule, as found in the literature, to measure the displacement of a spherical tablet and hence relate the physics of the law to the parametric shape of the tablet in question.

- VI. To construct computer based simulations to determine the compressibility of tablets in cylindrical and spherical shapes.
- VII. To construct automatic shape optimisation of pharmaceutical tablets based on the PDE method in order to find optimal shapes of tablets with maximum strength and specific volume.

### **1.3 Research Contributions**

The contributions for this research are:

- I. The PDE-based geometric modelling has been introduced into the shape design of pharmaceutical tablets (Chapter 4).
- II. The PDE method has been extended to a higher dimensional space in order to generate a volumetric object (Chapter 4).
- III. Simple expressions characterising the height and radius of a PDE-based representation of a tablet (Chapter 4). Particularly, expressions for a tablet generated using the extended PDE method together with circular-shaped boundary conditions and the spine of the tablet parallel to the  $z$ -axis have been obtained.
- IV. A mathematical model for measuring the axial displacement of an axially compressed pharmaceutical powder in a cylindrical die (Chapter 5).

- V. Simulation based on the use of a parametric surface representation as a tool to predict compaction properties of cylindrical and spherical tablets (Chapter 5 and Chapter 6).
- VI. Simulation results as a benchmark for modelling the powder compaction process in the future.
- VII. Several optimal shapes of tablet, which are obtained by carrying out an optimisation analysis (Chapter 6).

## 1.4 Publications

In order to support the contributions listed above, a number of publications have been submitted internationally recognised conferences and publishers. The comments given by the reviewers to such submissions have been taken into consideration and improvements have been made to ensure the quality of the research so that it can make a significant contribution. A list of the publications related to this research is outlined in this section. They are divided as follows:

- List of journals and conference publications already published:
  - I. Ahmat, N., González Castro, G. & Ugail, H. (2012) Automatic design optimisation of pharmaceutical tablets using PDEs. *Proceedings of the 2<sup>nd</sup> International Conference on Simulation and Modeling Methodologies*,

- Technologies and Applications*, Rome, 28 – 31 July 2012, SciTePress, pp. 125-130.
- II. Ahmat, N., Ugail, H. & González Castro, G. (2012) Modelling the mechanical behaviour of a pharmaceutical tablet using PDEs. In: Günther, M., Bartel, A., Brunk, M., Schöps, S. & Striebel, M., eds. *Progress in Industrial Mathematics at ECMI 2010*. Germany: Springer-Verlag Berlin Heidelberg, pp. 505-511.
- III. Ahmat, N., Ugail, H. & González Castro, G. (2012) Elastic-plastic contact law for simulation of tablet crushing using the Biharmonic equation. *International Journal of Pharmaceutics*, 427(2), pp. 170-176.
- IV. Ahmat, N., Ugail, H. & González Castro, G. (2011) Method of modelling the compaction behaviour of cylindrical pharmaceutical tablets. *International Journal of Pharmaceutics*, 405(1-2), pp. 113-121.
- V. Ahmat, N., Ugail, H. & González Castro, G. (2011) Shape parameterisation of tablet shapes using Partial Differential Equations. Paper presented at 2<sup>nd</sup> World Conference on Information Technology (WCIT) in Antalya, Turkey (23 - 26 November 2011).
- List of works accepted to be published:
- VI. Ahmat, N., González Castro, G. & Ugail, H. Geometric modeling and parametric characterization for virtual design of pharmaceutical tablets. Submit-

ted to the *International Conference on CyberWorlds 2012* in Darmstadt, Germany (25 – 27 September 2012).

- List of work in review:

VII. Ahmat, N., González Castro, G. & Ugail, H. Automatic shape optimisation of pharmaceutical tablets using Partial Differential Equations. Submitted to the *Journal of Computers and Structures*.

## 1.5 Structure of the Thesis

The rest of the thesis is structured as follows:

**Chapter 2: On the Compaction of Pharmaceutical Tablets** contains a literature review related to the compaction properties of pharmaceutical tablets in terms of compressibility and compactibility. It also explains the Heckel model which is used to analyse the compressibility of a powder bed, as well as some mathematical models used to measure the tensile strength of a tablet.

**Chapter 3: Techniques for Geometric Modelling** discusses the history of the development of surfaces in Computer Aided Geometric Design (CAGD), including a brief overview of spline-based surfaces. The mathematical theory associated with the PDE method, together with some graphical examples of PDE surfaces, is also discussed. This method is used as the surface generation technique

throughout this thesis. The last section in this chapter lists methods for numerical optimisation and explains how design optimisation can be carried out using the MATLAB Optimisation ToolBox.

**Chapter 4: The PDE Method for Tablet Shape Modelling** shows various shapes of pharmaceutical tablets that have been created using the PDE method. Formulae for measuring the surface area and volume of a parametric surface are also presented in this chapter. A new parameter has been introduced to the formulation of the PDE method in order to generate a solid object. Furthermore, a subroutine has been coded in a MATLAB file to generate the cuboid mesh for solid PDE-based representation of pharmaceutical tablets. The final part of this chapter presents some simple mathematical expressions which can be used for shape manipulation of the PDE-based object.

**Chapter 5: Modelling the Mechanical Behaviour of Pharmaceutical Tablets.**

This chapter is divided into two main sections. The first section presents a mathematical model for measuring an axial displacement of a compressed powder bed in a cylindrical die. This model is developed by utilising the analytic solution of the Love's stress function together with a particular set of boundary conditions. The second section shows the PDE-based simulation of a compressed spherical tablet and the result is compared with the theoretical one.

**Chapter 6: Automatic Design Optimisation** explains the methodology for shape optimisation. The initial parametric shape of the tablets, which has been created in Chapter 4, along with constraints are supplied to an optimisation routine. The Active Set method is used to perform such an optimisation process. Different shapes such as flat-faced circular and spherical tablets as well as a soft-shell spherical capsule have been used.

**Chapter 7: Conclusions** summarises the research and discusses the contributions made. It also discusses ideas for future work.

## 1.6 Summary

The mechanisms involved in the compaction of pharmaceutical powders have become a crucial step in the development cycle for robust tablet design with required properties. Given that the shape and size of tablets also play an important role in determining their mechanical properties, this work proposes a method to model various solid shapes of pharmaceutical tablets, incorporating the use of parametric surface representations. The motivation to pursue research in this area is to encourage the future development of pharmaceutical technologies through computer generated simulations. Based on the objectives and contributions to the field, this thesis can be used as a guide and for further exploration by other researchers who have the same interests.

## **Chapter 2**

### **On the Compaction of Pharmaceutical Tablets**

#### **2.1 Introduction**

Tablets are the most widely used dosage forms for drug delivery in the pharmaceutical industry, occupying two-thirds of the global market (Wu and Seville 2009). A tablet is usually taken orally, but can be administered sublingually, rectally or intravaginally to deliver an accurate dosage to a specific site. This type of dosage form has many advantages over other dosage forms: they are convenient to use by patients, have long term storage stability and have good tolerance to changes in temperature and humidity. Additionally, tablets can be designed to protect unstable medications or disguise unpalatable ingredients (Dey et al. 2008).

Tablets have been made in many shapes, sizes and consistencies. This helps to distinguish between different medicines and is also useful for product branding. The most common shapes for tablets are round, oval and caplet. The dosage form varies in size from a few millimetres to about a centimetre, a range that is regarded as ideal for easy swallowing. The quality of such tablets can be described by several parameters, such as hardness, accurate mass and height, as well as content uniformity (Belic et al. 2009).

The shape and geometry of a tablet play an important role in determining the strength of the object where the selection of a specific shape may improve the mechanical properties of the tablet (Santos and Sousa 2008). It has also been reported that the shape, size and surface area of the tablet can affect drug release profiles (Reynolds et al. 2002). The latter work has demonstrated that round and oval tablets have the same drug release profile if the surface area,  $S$ , to the volume,  $V$ , ratio is set as constant. Furthermore, the effect of size of round tablets on drug release has been investigated in work by Siepmann et al. (2000). This work found that larger round tablets have a slower release profile compared to those of smaller dimensions.

In this chapter the properties of pharmaceutical tablets are discussed in detail. This includes the mechanical properties of tablets, which can be influenced by their components and the manufacturing process. Section 2.2 describes the

compaction properties of pharmaceutical powders in terms of compressibility and compactibility. These two mechanical behaviours are important in this study because they can affect the strength of the produced tablets.

## **2.2 Compaction Properties of Pharmaceutical Powders**

Most pharmaceutical tablets are initially presented in powder form or granules. A granule is composed of several powder particles, which bond together by the adhesion force at the contact area (Antonyuk et al. 2005). Many tablets are constituted by granules since they have better flow behaviour and can compress well even at a low pressure (Antonyuk et al. 2010). A tablet formed from granules will have good characteristics, such as consistent hardness, uniform content and ease of controlling drug release (Tousey 2002).

Tablets are produced through a tableting process, which is divided into three stages (Wu et al. 2008). First, the powders or granules are filled into the die cavity which is responsible for determining the diameter and shape of the tablet. Secondly, a compaction process takes place, which involves compression and decompression of the powder or granular bed. Finally, the compacted powder is ejected from the die in the form of a tablet after the required height is obtained. It has been found that the relative densities of pharmaceutical powders increase as they transform into solid dosage forms (Hancock et al. 2003).

However, some common defects can occur during the tableting process, such as sticking, capping and laminating. Sticking refers to the tablet materials adhering to the die walls instead of locking together to create a uniform tablet, resulting in breakage of the tablet edges (Waimier et al. 1999). Capping is the term used to describe a phenomenon involving the horizontal separation of the upper part of the tablet, either partially or completely from the tablet body, while laminating refers to the separation of a tablet into two or more distinct layers (Cox Gad 2008). All mechanical failures mentioned above may affect the mechanical strength of the tablet and its quality (Belic et al. 2009).

Recently, there has been increased interest in the study of the effect of granular properties on the mechanical properties of tablets. Work by Eichie and Kudehinbu (2009) has shown that a tablet formed from larger granules has a higher degree of consolidation than a tablet formed from smaller ones. The same result was obtained by Spaniol et al. (2009) who found that the bulk density of granules can affect the compression properties, in which low density granules give harder tablets. Moreover, fast-dissolving tablets have been formed by highly plastic granules, which allow fast absorption of water into the compressed tablet and hence provide a soft paste for easy swallowing (Fu et al. 2005). This type of granule is produced by a wet granulation process and maintains its porosity even after it has been compressed as a tablet (Fu et al. 2005).

Details of the mechanical properties of granular materials will be presented in Chapter 5.

It has been reported in Coube et al. (2005) that the mechanical strength or disintegration of the tablet also depends significantly upon the behaviour of the powder during all stages of the tableting process. Through this process, the compressibility and compactibility of the pharmaceutical powder bed are determined. The most important stage in the tableting process is the powder compaction stage. The compression and compaction processes occur during this stage and are two inseparable and dependent sequences (Bacher et al. 2007). Although compaction usually occurs when the powder bed is compressed, this is not necessarily the case since it requires the formation of interparticulate bonding in order to generate a coherent compact (Bacher et al. 2007).

Some authors have investigated the radial and axial powder movements during the tableting process, using flat and curved faced punches for single-ended axial strain applications (Eiliazadeh et al. 2003). They found that flat faced tablets are non homogeneous with high density regions near the moving punch surface and at the middle of the bottom half, while the low density regions are found at the bottom edges of the tablet. A year later, these researchers developed further experimental methods to gain a better understanding of the movement of

the powder during the compaction process. The results showed that the radial powder movement in flat faced tablets takes place away from the die wall (Eiliazadeh et al. 2004).

It is therefore very important to understand the mechanical behaviour of the powder during each stage for successful formulation processing. Furthermore, the quality of the produced tablets depends on the compaction properties of pharmaceutical powders, which are characterised by their compressibility and compactibility. These properties must be investigated since the produced tablets have to be strong enough to sustain any possible load after the tableting process, such as film coating, packing and handling (Wu et al. 2005).

### **2.2.1 Compressibility of Pharmaceutical Powders**

Many studies have investigated the compressibility of different types of excipients, such as Microcrystalline cellulose (Zhang et al. 2003; Hassanpour et al. 2004) and Lactose (Zhang et al. 2003; Hassanpour et al. 2004; Ilić et al. 2009). Compressibility refers to the ability of the powder to change in volume when subjected to pressure (Ilić et al. 2009), which explains mechanical properties of the bed in terms of elasticity and plasticity. Elasticity is the ability of a solid to recover its original shape and volume once the applied load is removed

(Owolabi et al. 2010), while plasticity contrasts with elasticity. In other words, a high plasticity object is capable of being shaped or moulded.

Finite element (FE) methods have been widely used to model the compressibility of elastic-plastic powder in both tableting and roller compaction operations (Sinha et al. 2010). This method depends very much on the accuracy of the constitutive model used to describe powder's deformation behaviour as well as the quality of the parameters set (Chtourou et al. 2002). It has been reported in the literature that the Drucker-Prager Cap (DPC) model is the most commonly used constitutive model for simulation of the compaction process (Han et al. 2008). This model is governed by elliptical caps, which determine the densification yield loci, and is able to capture the shearing phenomenon in powders during the decompression and ejection phases (Sinha et al. 2010). Furthermore, the DPC model requires some parameters related to the unloading and ejection phases of the tableting process.

However, this model is unsuitable in some cases, such as experiments in which researchers or scientists are not taking the physics of the tableting process or the effect of tooling geometry into consideration. To that purpose, a mathematical model of axial displacement of a compressed powder in a cylindrical die is proposed in this thesis. The model is developed by using the solution of Love's stress function together with a particular set of boundary conditions.

Only the initial dimensions of the powder bed, together with its material properties, are considered in this simple model. This model is explained in detail in Chapter 5, section 5.2.1.

Most deformation models discussed in the literature are designed for a group of powders or a powder bed of cylindrical shape. Therefore, in order to measure the compressibility of a powder bed of spherical shape, it is assumed that the mechanical behaviour of the powder in this particular bed is similar to the behaviour of a spherical granule. Recently, a force-displacement model for an elastic-plastic granule with radius,  $r_s$ , has been developed by Antonyuk et al. (2010)

$$F_{ep} = \frac{\pi s_y r_s \omega_z}{2} \left( 1 - \frac{1}{3} \sqrt[3]{\frac{\omega'_z}{\omega_z}} \right), \quad (2.1)$$

where  $F_{ep}$  is the axial force applied on the elastic-plastic granule,  $s_y$  represents the micro-yield strength,  $\omega_z$  denotes the full axial displacement and  $\omega'_z$  is the displacement at the yield point. The details of the mechanical behaviour of elastic-plastic granules are presented by Antonyuk et al. (2005) and Antonyuk et al. (2010), and will be discussed in detail in Chapter 5.

Several approaches can be used to analyse the compressibility of a powder bed, such as the Heckel (Zhang et al. 2003; Hassanpour et al. 2004; Ilić et al. 2009), Kawakita (Zhang et al. 2003) and modified Walker models (Ilić et al. 2009). The

Heckel model has been the most popular model among pharmaceutical scientists. This model is used to measure the values of apparent yield pressure and mean yield pressure of active substances and tableting excipients (Sonnergaard 1999). It has been developed on the assumption that powder compression follows a first-order chemical reaction, where the pores are the reactant (Zhang et al. 2003), and it is based on force-displacement data, which is converted to a relative density-pressure relationship (Heckel 1961). The Heckel equation is written as

$$\ln\left(\frac{1}{1-\rho_{\text{rel}}}\right) = PK + A, \quad (2.2)$$

where  $\rho_{\text{rel}}$  represents a relative density,  $P$  is a pressure, and  $K$  and  $A$  are constants. The relative density is the bulk density proportional to the true density

$$\rho_{\text{rel}} = \frac{\rho_{\text{bulk}}}{\rho_{\text{true}}}, \quad (2.3)$$

and the term  $(1 - \rho_{\text{rel}})$  represents the porosity. The slope,  $K$ , and  $y$ -intercept,  $A$ , of the linear graph are obtained when plotting the value of  $\ln\left(\frac{1}{1-\rho_{\text{rel}}}\right)$  against the applied axial pressure,  $P$ . The constant,  $K$ , gives the value of the plasticity of a compressed powder and  $A$  is associated with the particle rearrangement before deformation (Zhang et al. 2003). The reciprocal of  $K$  is a measure of the yield pressure,  $P_y$ , of the particles, which gives the value of the hardness of pow-

ders (Hassanpour et al. 2004). Low values of  $P_y$  usually indicate harder tablets (Nokhodchi 2005).

The Heckel model is suitable for materials that strengthen by plastic deformation (Yap et al. 2008). Plastic deformation refers to the reduction in bulk volume of the powder bed when the applied external load has been removed from the bed (Owolabi et al. 2010). However, it has been reported that the Heckel analysis also has some drawbacks. Heckels' parameters are very sensitive to small errors associated with experimental conditions (maximum pressure, punch displacement measurements and weight of the compact) and variations in the true density measurement (Hassanpour et al. 2004; Ilić et al. 2009). Furthermore, the Heckel plot can be influenced by the particle size (Hassanpour et al. 2004), die size, the degree of lubrication and the overall time of compression (Sovány et al. 2009). Therefore, the effects of these variables should be taken into consideration when designing tablet formulations.

In this work, the practical and theoretical results of a compressed powder in cylindrical and spherical shapes are analysed using the Heckel model. However, not all of the factors mentioned above are considered when performing the compression process in order to obtain the experimental data.

### 2.2.2 Compactibility of Tablets

Compactibility is the ability of powders to convert from small particles into a coherent solid dosage form (Yap et al. 2008). The compactibility of a powder compact is estimated by measuring its mechanical strength (Sonnergaard 2006), which can be assessed using a combination of simple failure and erosion tests together with more sophisticated engineering tests (Swaminathan and Kildsig 2000). The mechanical strength of round tablets is characterised by the measurement of tensile strength (Wu et al. 2005; Wu and Seville 2009).

Tensile strength is a measure of the ability of a given material to resist forces that tend to pull it apart. In other words, the tablets must possess at least a minimum mechanical strength to uphold any potential load encountered during post-compaction processes (Wu et al. 2005). Generally, the tensile strength of pharmaceutical tablets in a round shape is determined by the diametrical (Wu and Seville 2009) or axial compression tests (Han et al. 2008). This is done by placing the tablet between two platens and compressing it until the tablet breaks or crushes, as illustrated in Figure 2.1. In Figure 2.1(a), the tablet is crushed along its central line, whereas Figure 2.1(b) shows the tablet being compressed axially. These tests have been applied to both single component tablets and matrix tablets made from various components (Wu and Seville 2009).

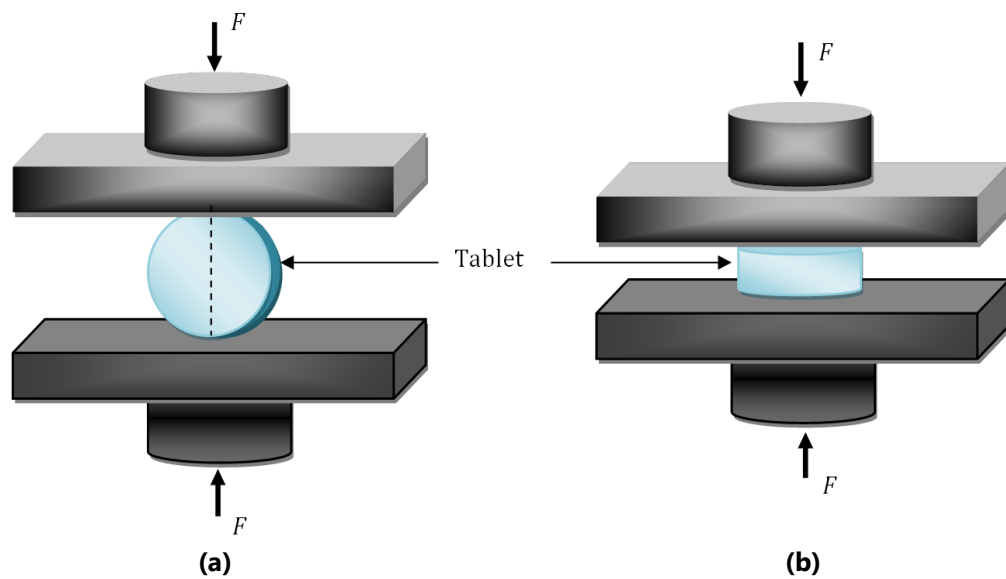


Figure 2.1: Tablet strength measurement in (a) diametrical test and (b) axial compressive strength. This figure is reproduced from Han et al. (2008).

Since an understanding of tablet tensile strength is vital, there has been increased interest in developing mathematical models of tensile strength. The measured force,  $F$ , obtained from the test together with the diameter,  $D$ , and thickness,  $t$ , of a flat-faced round tablet are used to calculate the tensile strength. The diametrical tensile strength of such a tablet is calculated from

$$\sigma_T^d = \frac{2F_{\max}}{\pi Dt}, \quad (2.4)$$

where  $F_{\max}$  is the maximum crushing force while the axial compression strength of that particular tablet shape is determined from the following equation (Han et al. 2008)

$$\sigma_T^a = \frac{4F_y}{\pi D^2}, \quad (2.5)$$

where  $F_y$  is the force at the yield point. The tensile strength of round tablets of single or mixture components can also be measured at various relative densities. It is found that the logarithm of tensile strength is proportional to the relative density as shown in the Ryshkewitch-Duckworth equation (Wu and Seville 2009)

$$\ln\left(\frac{\sigma_T}{\sigma_T^*}\right) = k(\rho_{rel} - 1), \quad (2.6)$$

where  $\sigma_T^*$  represents the tensile strength of the components with zero porosity ( $\rho_{rel} = 1$ ) and  $k$  denotes a material constant of bonding capacity.

More than two decades ago, some researchers developed a model for the tensile strength of a convex-faced round tablet (Pitt et al. 1988). They generated a model that not only considers the force,  $F$ , and tablet's diameter,  $D$ , but also the total thickness,  $t$ , and central cylindrical thickness,  $W$ , of the tablet

$$\sigma_T^d = \frac{50F_{\max}}{\pi D^2 \left( \frac{71t}{5D} - \frac{63t}{100W} + \frac{63W}{4D} + \frac{1}{20} \right)}. \quad (2.7)$$

Then, in 2011, the same author and his colleague proposed a new model to calculate the tensile strength of elongated tablets (extended standard flat-faced and convex-faced round tablets). From this model, which is derived from the existing models (Equations (2.4) and (2.7)), it was concluded that, as the tablet was

elongated from the standard round tablet, the peak principal tensile strength reached approximately  $\frac{2}{3}$  of that calculated for round tablets (Pitt and Heasley 2011). Therefore, the calculation for the tensile strength of a flat-faced elongated tablet is

$$\sigma_T^d = \frac{4F_{\max}}{3\pi Dt}, \quad (2.8)$$

and a convex-faced elongated tablet is

$$\sigma_T^d = \frac{100F_{\max}}{3\pi D^2 \left( \frac{71t}{5D} - \frac{63t}{100W} + \frac{63W}{4D} + \frac{1}{20} \right)}. \quad (2.9)$$

The dimensions of the tablet shapes discussed above can be seen in Figure 2.2.

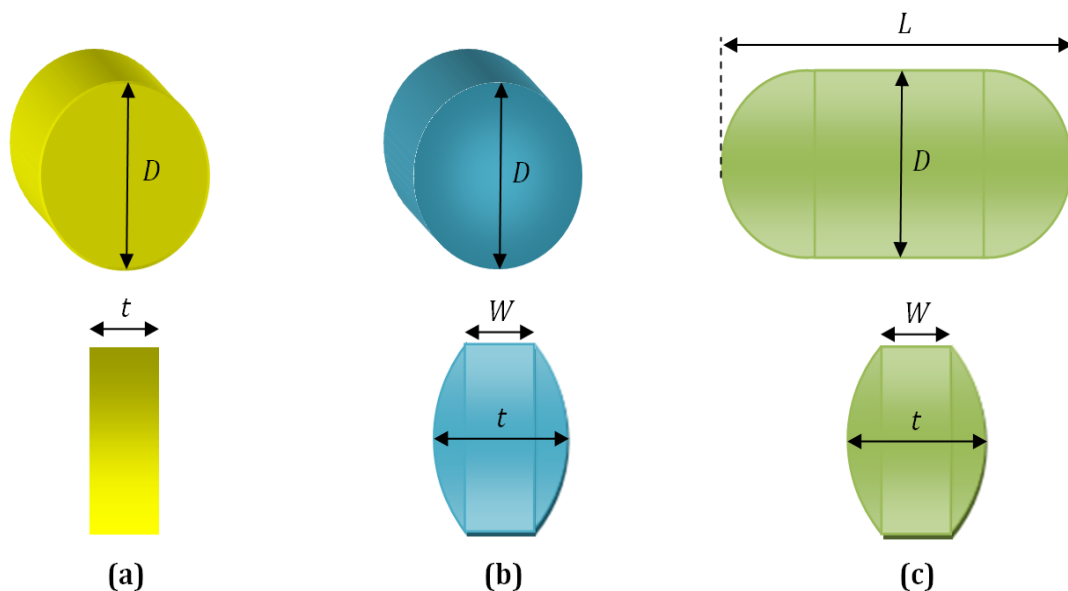


Figure 2.2: Front and side elevation of a (a) flat-faced round, (b) convex-faced round and (c) convex-faced elongated tablet. Figure adapted from Pitt and Heasley (2011).

Again, for a compacted powder in a spherical shape, it is assumed that both tablets and elastic-plastic granules in this particular shape have similar compaction behaviour. According to Antonyuk et al. (2010), the tensile strength of a spherical granule follows the Hertz law, which is given by

$$\sigma_T^s = \frac{F_{ep}(1 - 2\gamma)}{2\pi r_c^2}, \quad (2.10)$$

where  $\gamma$  represents the Poisson's ratio and  $r_c$  is the contact radius

$$r_c = \frac{\pi s_y r_s (1 - \gamma^2)}{2E}, \quad (2.11)$$

where  $E$  denotes the Young's modulus.

Many studies have been conducted to explore the dependence of tensile strength on the tablets' properties, such as density and surface area. It has been shown by Elkhider et al. (2007) that the density variation may affect the compact properties. The former work reported that the tensile strength of a tablet decreases as the density decreases. Furthermore, Adolfsson et al. (1999) have shown that a tablet with a large surface area has a high tensile strength. This is achieved by adjusting the tablet's surface area and the average distance between particles in compacts of different materials.

In this thesis, the design of tablets possessing the maximum tensile strength subject to the required volume and mass is considered. This is because all produced tablets need to be mechanically strong enough to uphold any potential load encountered during post-compaction processes whilst also dissolving easily in the mouth for easy administration of active pharmaceutical ingredients. Therefore, some of the equations of tensile strength will be used in the work discussed in Chapter 6.

### **2.3 Summary**

This chapter presented the literature reviews of the underlying fundamental knowledge required to undertake this research study involving pharmaceutical tablets. The literature review began with an introduction to pharmaceutical tablets, considering their physical properties such as sizes, shapes and components. This was followed by a discussion of the compaction properties of pharmaceutical powders, which are characterised by their compressibility and compactibility. The Heckel model is the most popular model for analysis of the compressibility of the powder, while its compactibility is determined by the measurement of tensile strength.

## **Chapter 3**

### **Techniques for Geometric Modelling**

#### **3.1 Introduction**

This chapter comprises several aspects of the research study. It starts by outlining the state of the art of CAD, along with its history and use for other applications. Then, a summarisation of spline-based techniques for surface generation will be presented in Section 3.3. Later, the mathematical details behind the PDE method and its applications are also discussed, together with some related works. It is worth mentioning that special emphasis is made on this technique because the PDE method will be used throughout the thesis for generating the parametric shape of pharmaceutical tablets. Also, an overview of several numerical techniques used in MATLAB Optimisation ToolBox will also be discussed

and briefly explained. The summary of this chapter will be given in the last section.

## 3.2 History

Computer-aided Design (CAD) refers to the use of computer software and systems to design and create two-dimensional (2D) and three-dimensional (3D) virtual objects. CAD is widely used in many applications, including the automotive and aerospace industries, architecture design and computer animation, as well as medical applications. The history of CAD starts in the 1950s. In the year 1957, Dr. Patrick Hanratty developed the first numerical control program called Pronto (Coons 1963). However, Ivan Sutherland was considered to be the father of CAD since he invented Sketchpad in 1963 as part of his thesis (Harris and Meyers 2007). The software used a light pen to create engineering drawings directly on a large CRT monitor.

Then, in the 1960s, applications of CAD systems continued to be developed by manufacturers' internal groups in collaboration with university researchers. CAD software was first utilised by large automotive and space companies. Throughout that decade, large companies such as General Motors produced Design Automated by Computer (DAC) (Krull 1994); Ford made a Product Design Graphic System (FDGS); McDonnell-Douglas created Computer Aided Design

and Drafting (CADD) (Harris and Meyers 2007), whilst Lockheed developed Computer Augmented Design and Manufacturing (CADAM) (Kasik et al. 2005). Such developments continued until the early 1970s, when Mercedes-Benz produced SYRICO, Nissan released CAD-I and Toyota created TINCA (Patra 2010).

CAD software has evolved dramatically since the 1980s. Autodesk was the first vendor to offer a PC based CAD system called AUTOCAD (Bilalis 2000). Over the decade, Diehl Graphsoft released MINICAD for MAC users, which became the bestselling CAD software (Tornincasa and Monaco 2010). Then, in the late 1980s, the Parametric Technology Corporation released Computer Aided Three Dimensional Interactive Application (CATIA) and Unigraphics for UNIX Workstation (Tornincasa and Monaco 2010). In the 1990s, the market for CAD systems became more popular and grew widely. In 1995, SolidWorks, a 3D CAD software, was released for desktop PCs by Dassault Systèmes SolidWorks Corporation. Then, SolidEdge which had software similar to SolidWorks, was produced by Intergraph in 1996 (Tornincasa and Monaco 2010).

Early in the year 2000, Autodesk released an internet edition of AUTOCAD 2000i, that has the capability to publish data on the web. Ford also produced the Ford Mondeo, an integration of 3D CAD software and the Internet enabled Product Data Management (Tornincasa and Monaco 2010). NX and Solid Edge inte-

grated a new tool called Synchronous Technology in 2008. In the same year, Instant 3D was introduced in SolidWorks (Tornincasa and Monaco 2010). In 2009, Autodesk launched its Inventor Fusion Technology that provides direct manipulation capabilities.

The term CAGD refers to Computer Aided Geometric Design, a mathematical application of CAD that is concerned with the representation, construction and deformation of designing curves, surfaces and volumes. The evolution of CAGD began in the early 20<sup>th</sup> century, when the catalogues of functionality and application of particular families of curves to classify airfoil shapes were generated by the National Advisory Committee for Aeronautics (NACA) (Kasik et al. 2005). The first parametric curve was created in 1962 by Pierre Bézier, an engineer at Renault, for designing mechanical parts of automobile body (Farin 2002). Later, surface patch systems were introduced by Ferguson in 1963 (Farin 2002). In patch systems, several curvilinear patches are smoothly joined together to create the surface.

With the ability of powerful computers and sophisticated graphics software, CAD packages offer several tools for designing complex geometries and surfaces in general. Surface modelling techniques are fundamental to many visual computing applications in CAD and interactive graphics (Du and Qin 2005). The

most common representation for curves and surfaces is the parametric representation, as in Bézier, B-spline, NURBS and PDE (González Castro et al. 2008). Each of these representations is discussed in the next sections.

### 3.3 Spline-Based Surface

Most of the methods used in CAGD for surface generation are commonly based on polynomial surfaces. Polynomial-based techniques such as Bézier surfaces, B-spline and Non-uniform Rational Basis Spline (NURBS) have become industrial standards for modelling and data exchange in CAD. This is due to the ability of these techniques to generate complex geometries, where the shape of the surface is controlled by a set of control points. These techniques also offer a unified mathematical formulation for free-form curves, surfaces and solids.

#### I. Bézier Surfaces

A Bézier surface is defined by a set of control points and is transformed in the same way as its control points under all linear transformations and translations (Shang et al. 2008). Two-dimensional Bézier surfaces of order  $(m, n)$  are determined by

$$\mathbf{X}(u, v) = \sum_{i=0}^m \sum_{j=0}^n \mathbf{k}_{ij} B_i^m(u) B_j^n(v), \quad u, v \in [1, 0], \quad (3.1)$$

where  $\mathbf{k}_{ij}$  denotes the  $(m + 1)(n + 1)$  array of control points and  $B_i^m$  and  $B_j^n$  are known as Bernstein polynomial functions, which are defined by

$$B_i^m(u) = \binom{m}{i} u^i (1 - u)^{m-i}, \quad (3.2)$$

and

$$B_j^n(v) = \binom{n}{j} v^j (1 - v)^{n-j}, \quad (3.3)$$

respectively.

Generally, the most common use of Bézier surfaces is as nets of bicubic patches, which are defined by 16 control points ( $m = n = 3$ ), as shown in Figure 3.1 (Lavoué 2008). However, constructing a composite Bézier surface can be quite complex since particular smoothness constraints need to be satisfied (Loop 1994).

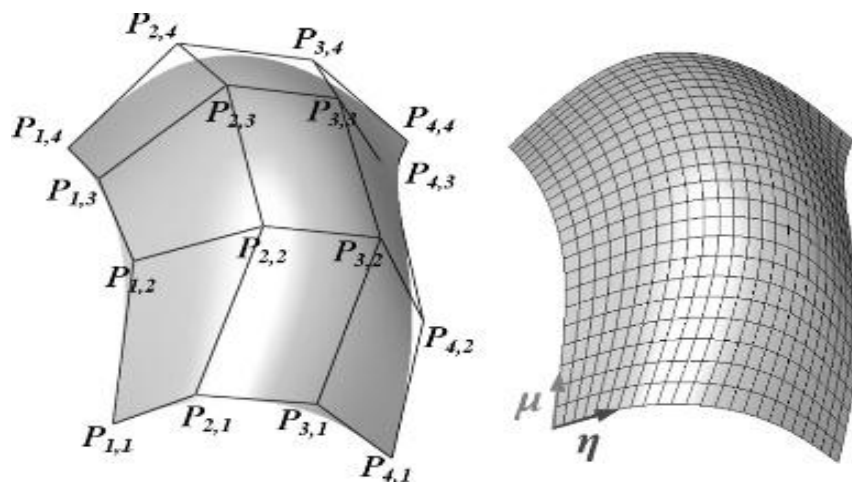


Figure 3.1: Bicubic Bézier surface. Figure extracted from Lavoué (2008).

## II. B-spline Surfaces

Over the past few decades, the B-spline representation has become the standard for CAD systems. This method is based on polynomial interpolation through the complete set of points. A B-spline surface is a generalisation of a Bézier curve, where the shape of the basic functions is determined by the position of the knots. The surface is obtained by replacing the Bernstein polynomial functions in Equation (3.1) by the B-spline basis functions,  $N_i^p$  and  $N_j^q$ , thus

$$\mathbf{X}(u, v) = \sum_{i=0}^p \sum_{j=0}^q \mathbf{k}_{ij} N_i^p(u) N_j^q(v), \quad (3.4)$$

where

$$N_i^1(u) = \begin{cases} 1 & (u_i \leq u < u_{i+1}) \\ 0 & (\text{otherwise}) \end{cases}, \quad (3.5a)$$

$$N_i^p(u) = \frac{u - u_i}{u_{i+p-1} - u_i} N_i^{p-1} + \frac{u_{i+p} - u}{u_{i+p} - u_{i+1}} N_{i+1}^{p-1}, \quad (3.5b)$$

and similarly for  $N_j^q(v)$ . The degree of resulting polynomials in  $u$  and  $v$  are  $(p - 1)$  and  $(q - 1)$  respectively. The knot values,  $u_i$  and  $v_j$ , relate to the parametric variables,  $u$  and  $v$ , to the control points,  $\mathbf{k}_{ij}$ . Local modifications to B-spline surfaces can be achieved by transforming the control points, and only the neighbouring area will be affected by the change of any modified point (Xie and Farin 2004). The functions  $N_i^p(u)$  and  $N_j^q(v)$  depend upon whether the surface

is periodic or non-periodic, have uniform or non-uniform knot vector, the degree of surface and the number of control points in  $u$  and  $v$  directions (Chuang and Pan 1998).

B-spline surfaces have been widely used in an interactive modelling environment since the formulation is capable of preserving arbitrarily high degrees of continuity over the complex surface consisting of multiple patches (González Castro et al. 2008). However, B-spline surfaces face a major problem when representing a deformable model because of the absence of an efficient algorithm to detect collision between two or more complex B-spline surfaces. Thus, Pungotra et al. (2008) proposed an efficient method for precise collision detection between two or more B-spline surfaces, whereby both model and tool are represented as B-spline surfaces and can have complex shape, elastic or plastic properties and multiple contacts. The authors also stated that the proposed method could potentially be used as a sculpting technique.

### **III. NURBS**

The NURBS formulation has been formed by extending the formulation of the B-spline, which is mathematically described by the ratio of two B-spline functions

$$\mathbf{X}(u, v) = \frac{\sum_{i=0}^m \sum_{j=0}^n \mathbf{k}_{ij} w_{ij} N_i^p(u) N_j^q(v)}{\sum_{i=0}^m \sum_{j=0}^n w_{ij} N_i^p(u) N_j^q(v)}, \quad (3.6)$$

where  $w_{ij}$  represents the weight of every control point associated with knot vectors in order to generate and represent curves and surfaces. For a surface with  $(p - 1)$  and  $(q - 1)$  degrees of basis functions along  $u$  and  $v$  axes respectively, the parameter domain is in the range of  $u_{p-1} \leq u \leq u_{n+1}$  and  $v_{q-1} \leq v \leq v_{m+1}$ . These surfaces are evaluated using three different representations: B-spline, Bézier and power basis representation, where each representation has its own set of points and normal vectors evaluation algorithms (Sánchez et al. 2004).

NURBS are the most popular of the spline-based modelling techniques, and have been incorporated into a number of modelling packages (Zhang and You 2002). This method offers great flexibility and precision for handling both analytic and freeform shapes. It offers advantages which make it attractive for design applications (Dimas and Briassoulis 1999):

- The evaluation is straightforward, fast and computationally stable.
- It offers a common mathematical representation for free-form surfaces and the shape is easily changed through the manipulation of control points, weights and knots.

- The degree of elevation, splitting, and knot insertion, deletion and refinement offers a wide range of tools to design and analyse shape information.

Although spline-based methods are commonly used in CAD, they still have a few drawbacks. The manipulation of spline-based surfaces is not straightforward since the relationship between the changes in geometry and the manipulation of the control points is not intuitive (Monterde and Ugail 2006). This is because the associated control points and weights are often unevenly distributed across the surface (Monterde and Ugail 2006). Besides that, the traditional polynomial-based modelling techniques can be difficult, time-consuming, less natural, and require strong mathematical expertise from the users (Du and Qin 2005).

### **3.4 Parametric Surfaces Based on the Use of Partial Differential Equations**

As mentioned in Section 3.3, spline-based surface generation techniques are not capable of promising global smoothness. A few decades ago, Partial Differential Equations were introduced as a tool for surface generation to overcome that problem. In this section, a brief description of the mathematical details concerning Partial Differential Equations of relevance to this work is presented.

A differential equation is an equation that relates to the derivatives of a function depending on one or more variables. Partial Differential Equations are equations which involve an unknown function of several independent variables and its partial derivatives with respect to those variables. For instance

$$A \frac{\partial^2 u}{\partial x^2} + B \frac{\partial^2 u}{\partial x \partial y} + C \frac{\partial^2 u}{\partial y^2} + D \frac{\partial u}{\partial y} - Eu = T(x, y), \quad (3.7)$$

where  $u(x, y)$  is an unknown function depending on two variables,  $x$  and  $y$ , while  $A, B, C, D$  and  $E$  may be functions of  $x, y$  and even  $u$ . There are two common notations for partial derivatives; the first one is the familiar Leibniz notation,  $\partial$ , whereas the other one uses subscripts. For example,  $u_{xxy}$  can be used to

represent  $\frac{\partial^3 u}{\partial x^2 \partial y}$ . Thus, Equation (3.7) can be written as

$$Au_{xx} + Bu_{xy} + Cu_{yy} + Du_y - Eu = T(x, y). \quad (3.8)$$

PDEs are classified according to certain criteria, such as order, linearity and homogeneity. Again, if Equations (3.7) and (3.8) are considered, PDEs are classified as follows:

- If  $A = B = C = 0$ , then the PDE is first-order.
- If functions  $A, B, C, D$  and  $E$  do not depend on dependent variable  $u$ , then the PDE is linear; otherwise it is non-linear.

- If  $T(x, y) = 0$ , then the PDE is said to be homogeneous, and otherwise if this term has a different value.

A linear PDE can also be classified in three categories: elliptic, parabolic and hyperbolic, according to the type of coefficients or specifically the discriminant,  $B^2 - AC$ . For instance, Equation (3.8) can fall into any of these categories:

- Elliptic if  $B^2 - AC < 0$ .
- Parabolic if  $B^2 - AC = 0$ .
- Hyperbolic if  $B^2 - AC > 0$ .

PDEs are notably difficult and therefore, continuous active research is being carried out to find solutions to some of these PDEs. So far, several methods have been developed to find their solutions, varying from purely analytical to fully numerical ones (González Castro et al. 2008). This type of differential equation arises in almost every physical phenomenon: in physics, engineering, medicine and within biology itself. Third order PDEs arise when modelling waves in dispersive media, such as water or plasma waves (Benkhaldoun and Seaid 2008). Fourth order PDEs appear in elasticity, particularly involving plate and beam mechanics (Engel et al. 2002). Nowadays, their application has been extended to areas such as finance, computer graphics and animation (González Castro et al. 2008).

### 3.4.1 Introduction to the PDE Method

In this section, the essential information concerning the theoretical modelling of a particular shape parameterisation technique is provided. This technique is referred to as the PDE method. The geometries of the tablets displayed throughout this work are designed by employing the analytic solution to elliptic PDEs of the form

$$\left( \frac{\partial^2}{\partial u^2} + \alpha^2 \frac{\partial^2}{\partial v^2} \right)^\ell \boldsymbol{\chi}(u, v) = 0, \quad (3.9)$$

where  $\boldsymbol{\chi}(u, v)$  is the function representing a parametric surface in 3D space defined within a parametric domain,  $\Omega$ , described by  $u$  and  $v$  where  $0 \leq u \leq 1$  and  $0 \leq v \leq 2\pi$ , and boundary data around the edge region of  $\partial\Omega$ , as shown in Figure 3.2 The intrinsic parameter,  $\alpha$ , controls the relative smoothness of the surface in the  $u$  direction, while  $\ell$  defines the order of the PDE and these are restricted to  $\alpha \geq 1$  and  $\ell \geq 2$  (Ugail 2006). The full three-dimensional representation of  $\boldsymbol{\chi}(u, v)$  is written in the form of

$$\boldsymbol{\chi}(u, v) = \left( \chi_x(u, v), \chi_y(u, v), \chi_z(u, v) \right). \quad (3.10)$$

Note that Equation (3.9) transforms to the general form of a fourth-order elliptic PDE by taking  $\ell = 2$  and this equation is known as the Biharmonic equation if  $\alpha$  is equal to one.

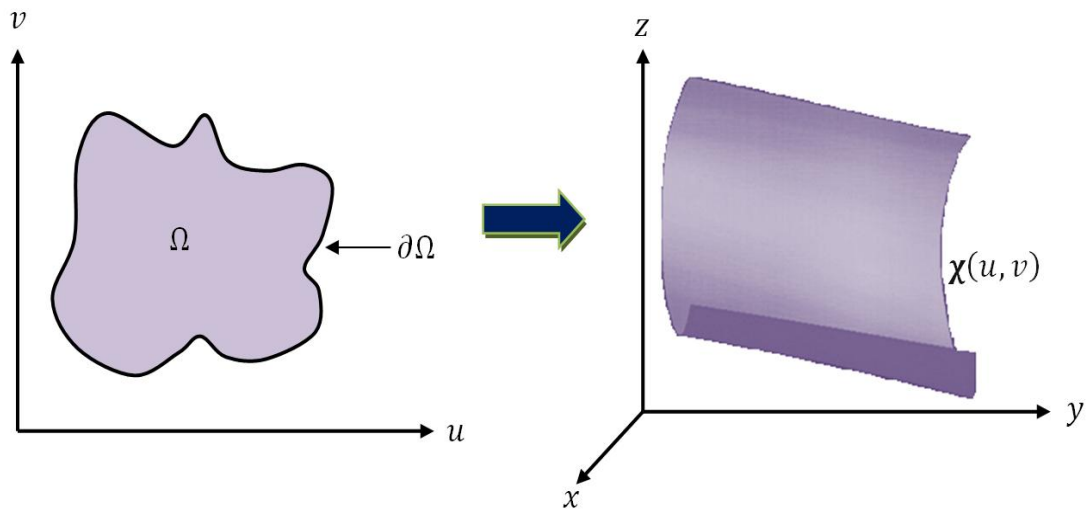


Figure 3.2: The boundary  $\partial\Omega$  in the  $(u, v)$  space is mapped to the three-dimensional space,  $(x, y, z)$ .

Elliptic PDEs similar to the equation shown in Equation (3.9) can be solved by using different methods, such as Separation of Variables, Green's Function, Integral Transform and the Finite Element Method (Ugail and Sourin 2008). The Separation of Variables method together with a set of four periodic boundary conditions has been used to find the solution to the Biharmonic equation (Ugail and Wilson 2005). The boundary conditions on the solution are of the form

$$\boldsymbol{\chi}(0, v) = \mathbf{P}_1(v), \quad (3.11a)$$

$$\boldsymbol{\chi}(u_1, v) = \mathbf{d}_1(v), \quad (3.11b)$$

$$\boldsymbol{\chi}(u_2, v) = \mathbf{d}_2(v), \quad (3.11c)$$

$$\boldsymbol{\chi}(1, v) = \mathbf{P}_2(v), \quad (3.11d)$$

where  $\mathbf{P}_1(v)$  and  $\mathbf{P}_2(v)$  determine the position at the edges of the surface patch at  $u = 0$  and  $u = 1$  respectively.  $\mathbf{d}_1(v)$  and  $\mathbf{d}_2(v)$  define the values of the second and third functions where  $u_1$  and  $u_2$  are positions in the interior curves such that,  $0 < u_1 < u_2 < 1$ . The interior conditions are important to determine the shape of the surface (Ugail 2006).

The analytic solution to the Biharmonic equation can be written as

$$\chi(u, v) = \mathbf{A}_0 + \sum_{n=1}^{\infty} [\mathbf{A}_n(u) \cos(nv) + \mathbf{B}_n(u) \sin(nv)], \quad (3.12)$$

where

$$\mathbf{A}_0 = \sum_{m=1}^4 \mathbf{a}_{0m} u^{m-1}, \quad (3.13)$$

$$\mathbf{A}_n = (\mathbf{a}_{n1} + \mathbf{a}_{n3}u)e^{nu} + (\mathbf{a}_{n2} + \mathbf{a}_{n4}u)e^{-nu}, \quad (3.14)$$

$$\mathbf{B}_n = (\mathbf{b}_{n1} + \mathbf{b}_{n3}u)e^{nu} + (\mathbf{b}_{n2} + \mathbf{b}_{n4}u)e^{-nu}. \quad (3.15)$$

The term  $\mathbf{A}_0$  in Equation (3.12) is a cubic polynomial on the parameter  $u$ , tracing the spine of a PDE surface that brings out the symmetries of the surface, while the remaining terms in the mentioned equation represent the radial position of a point in the surface relative to the spine. The vector-valued constants  $\mathbf{a}_{01}$ ,  $\mathbf{a}_{02}$ ,  $\mathbf{a}_{03}$ ,  $\mathbf{a}_{04}$ ,  $\mathbf{a}_{n1}$ ,  $\mathbf{a}_{n2}$ ,  $\mathbf{a}_{n3}$ ,  $\mathbf{a}_{n4}$ ,  $\mathbf{b}_{n1}$ ,  $\mathbf{b}_{n2}$ ,  $\mathbf{b}_{n3}$  and  $\mathbf{b}_{n4}$  are determined by the imposed boundary conditions at  $u = 0$  and  $u = 1$  (Ugail 2006).

The spine of an object possesses many geometric properties, one of which is that it constitutes the medial axis (or skeleton) of the shape. Furthermore, the spine also represents more topologies than that of the object from which it is obtained (Ugail 2004). A notable work has been carried out by Ugail (2004) to investigate how the spine of the PDE surface can be utilised in parameterising complex shapes. The former work has shown that the spine of the PDE surface can be used as a powerful tool for shape manipulation. Furthermore, a technique for cyclic animation has been achieved by exploiting the mathematical expression associated with the spine of the PDE surface as a driving mechanism (González Castro et al. 2010).

In order to define the different constants in the solution for a general set of boundary conditions, it is necessary to express the boundary conditions as Fourier series so that the corresponding coefficients are identified. Since Equation (3.12) gives infinite solutions, the approximation to this series needs to be found. This is based on the sum of the first Fourier modes (typically  $N = 6$ ) and a remainder function,  $\mathbf{R}(u, v)$ , which represents an error term, since  $N$  is a finite value

$$\boldsymbol{\chi}(u, v) \cong \mathbf{F}(u, v) + \mathbf{R}(u, v), \quad (3.16)$$

where

$$\mathbf{F}(u, v) = \mathbf{A}_0 + \sum_{n=1}^N [\mathbf{A}_n(u) \cos(nv) + \mathbf{B}_n(u) \sin(nv)], \quad (3.17)$$

and

$$\mathbf{R} = (\mathbf{r}_1(v) + \mathbf{r}_3(v)u)e^{\beta u} + (\mathbf{r}_2(v) + \mathbf{r}_4(v)u)e^{-\beta u}, \quad (3.18)$$

where  $\beta = N(\alpha + 1)$  while  $\mathbf{r}_1, \mathbf{r}_2, \mathbf{r}_3$  and  $\mathbf{r}_4$  are obtained by considering the difference between the original boundary conditions and the boundary conditions satisfied by Equation (3.17).

As mentioned earlier in this section, a set of four boundary conditions needs to be defined to solve the Biharmonic equation. In this thesis, all parametric surfaces are generated by specifying the boundary conditions in terms of curves. Figure 3.3 presents the effect of the interior conditions on the shape of the surface, where all the PDE surfaces have the same positional conditions whereas the interior conditions have been varied. Figure 3.3(a) shows a set of boundary conditions and the resulting shape of the fourth-order PDE surface is illustrated in Figure 3.3(b). The shape of a surface can be manipulated by changing the size and direction of the interior curves. It has been reported by Ugail (2006) that the interior conditions are crucial in determining the overall shape of the surface. Figures 3.3(d) and 3.3(f) illustrate the effect of changing the interior curves originally shown in Figure 3.3(a), where all of these PDE surfaces have the same  $P_1$  and  $P_2$  curves. These interior curves have been resized (Figure 3.3(c)) and ver-

tically translated from the corresponding positional boundary curves (Figure 3.3(e)). It is worth emphasising that the shape of the surface can be controlled solely by the shape of its boundary curves. Therefore, the boundary conditions have to be defined appropriately in order to create the wanted surface using the PDE method.

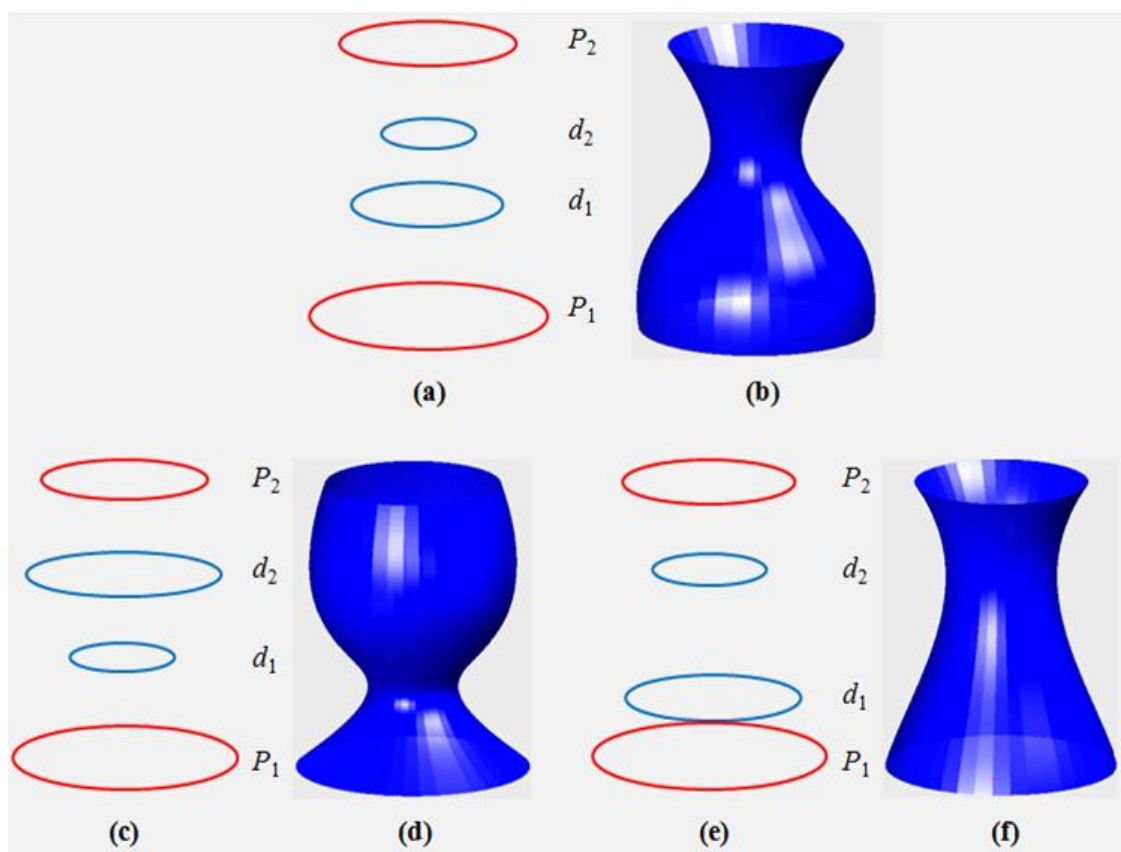


Figure 3.3: Shape of PDE surfaces generated by the Biharmonic equation. (a) The boundary curves and (b) the corresponding surface shape. The effect on the shape of the surface by (c) resizing and (e) translating the interior curves. The resulting manipulated surface shape in (d) and (f).

In the real world, many objects are considered as complex geometries. To generate a complex geometry using this method, more than one PDE is needed. The graphic representation of such PDE is referred as patch and therefore, complex geometries are represented by several surface patches. Each of the patches comprises four boundary curves,  $c_{jk}$  where  $c$  indicates the type of curve, with the letter  $P$  denoting the positional curves and  $d$  denoting the interior curves. The index  $j$  ( $j = 1, \dots, n$ ) represents the order of the patch:  $j = 1$  for the first patch,  $j = 2$  for the second patch and  $j = n$  for the  $n^{\text{th}}$  patch. The subscript  $k$  ( $k = 1, 2$ ) corresponds to the boundary edges of the surface.

The adjacent surface patch is created by evaluating the boundary conditions using the next set of curves. Adjacent patches need to be blended together by sharing one boundary curve with either one or two different patches to ensure the positional continuity along the generated surface. For example, the PDE-based representation of an ice cream cone, shown in Figure 3.4, is generated from a surface composed of two patches. As it can be seen in Figure 3.4(a), the second positional boundary curve of the first patch, which corresponds to  $u = 1$  (marked as  $P_{12}$ ), is used as the first positional curve of the second patch ( $P_{21}$ ). Hence, only seven curves are required to generate this particular shape.

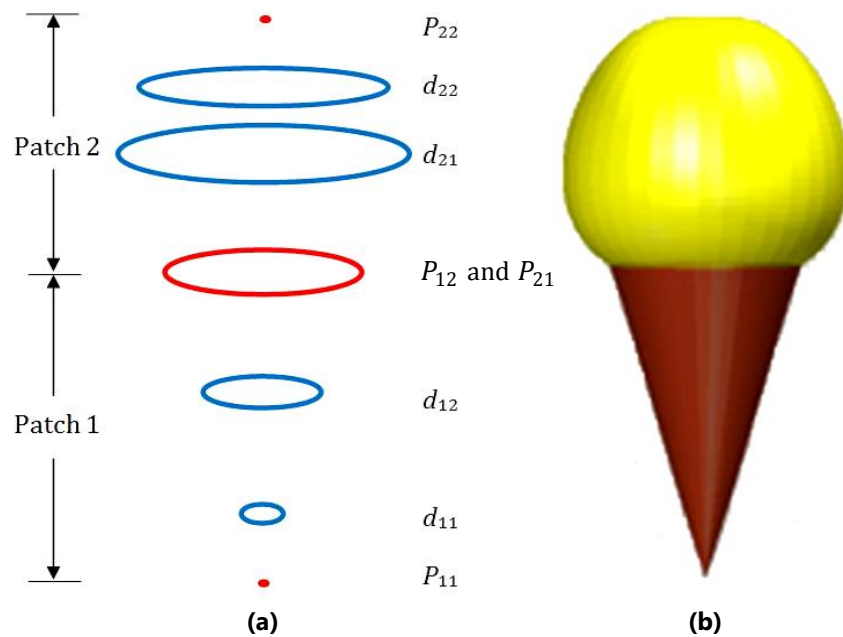


Figure 3.4: Example of a two-patch PDE surface subject to a specific set of boundary conditions outlined in (a).

PDE surfaces offer many advantages over other types of surface. Most of all, a PDE surface is generated from a small number of design parameters since it is characterised by data distributed around the boundaries, instead of data distributed over the surface area, e.g. control points. Additionally, they are a natural representation and offer a close representation of the real world because they are controlled by physical laws and can integrate geometric attributes with functional constraints for surface modelling, design and analysis. Furthermore, PDE surfaces can be easily associated with the physical world. For example, the parameters in the PDE can give a physical meaning, such as elasticity and stiff-

ness, if they are formulated properly (Zhang and You 2004). Moreover, smooth surfaces with high-order continuity requirements can be defined through PDEs since the formulation is well-conditioned and technically sound. This technique is also capable of blending surfaces (González Castro et al. 2008) and it offers modelling tools to manipulate the shape of a PDE surface by altering the values of its design parameters (Ugail 2006). Thus, a PDE-based model remains continuous when the values of its design parameters are changed.

### **3.4.2 Applications of PDE Surfaces**

The PDE method was initially introduced into the area of blend shape generation in CAD by Bloor and Wilson (1989). In recent years, the use of the PDE method has been broadened into many areas of computer graphics, including 3D data modelling and processing, shape morphing and animation (González Castro et al. 2010). This is due to the fact that a PDE surface is generated by blending several surface patches and its shape can easily be manipulated or trimmed.

The work by Ugail and Wilson (2005) has shown that the PDE method can be used in medical applications. The authors created a set of boundary curves, which has been acquired from 3D medical scanning data for reconstructing ulcer-affected human limbs. This method proves that a variety of geometries of

limbs affected by ulcers can be generated by extracting 3D scan data; this geometry can be manipulated to provide a shape that is a good representation of the limb and associated ulcer for any given patient. However, this method is unable to preserve irregular and sharp features appearing on the scan, due to its smoothing nature. Therefore, Sheng et al. (2010) have proposed a patchwise PDE method to address this problem. They have proved that the patchwise PDE method has successfully reconstructed a 3D human femur bone, which obviously has an irregular geometry. In this approach, the shape of the object is represented by patches with a localised  $uv$  coordinate system, with the irregular or sharp details on the surface of the object preserved by matching the respective patches. These patches have various sizes and orientations to the surface.

The PDE method has also appeared to be very useful in animation, including facial expressions (Sheng et al. 2008) and cyclic animation (González Castro et al. 2010). This method offers a natural mechanism for generating cyclic motions and thus developing real-time dynamic animation. The simulation of the animation process is performed by making the shape parameters time-dependent and this enables the re-generating of the geometry. Using this technique, the keyframing in the animation process is controlled by the animator via the time dependent shape parameters. Furthermore, Athanasopoulos et al. (2010) have developed a computer-based interactive talking head system based on the ani-

mation of facial expressions developed by Sheng et al. (2008). The user can interact with this system by using an AIML chatterbot, which generates responses from input text.

In addition to the uses mentioned above, this method has been proved to be useful in addressing optimisation problems (Ugail 2003; Ugail and Wilson 2003). Several works have successfully utilised the PDE method for automatic design functioning in a variety of design scenarios. These include: minimising the thickness of a yogurt container subject to a given strength and volume (Ugail 2003), and predicting stable structures of biological vesicles by minimising the surface energy (Ugail and Wilson 2003). This is achieved by combining engineering design criteria as constraints into the geometric design of PDE surfaces. Furthermore, the PDE-based optimisation is completed within a reasonable computational time (Ugail 2003).

PDEs have been used to deal with some problems related to the graphical modelling of natural phenomena, such as smoke and fire, since modelling these phenomena in the real world is very complicated (González Castro et al. 2008). However, these phenomena are modelled using a different type of PDEs. Therefore, further investigation on the mathematical properties of PDEs is desirable to exploit their full potential in CAGD. Moreover, a solid modelling method has

been developed by You et al. (2008) by using a solution of a non-homogeneous fourth order PDE, which had previously been used for free-form surface generation. This model involves three parametric parameters:  $u$ ,  $v$  and  $w$ , together with three vector-valued shape control parameters. Although this model seems quite promising in generating a solid object, the work in this thesis has proved that the solution proposed by Bloor and Wilson (1989) also can be implemented in solid modelling.

Later in this thesis, the application of the Bloor-Wilson PDE method in pharmaceutical area will be discussed. The analytic solution of the particular Biharmonic equation has been extended to a higher dimension in order to generate various solid geometries of tablets. This work also involves manipulation of the PDE-based representation of a solid tablet, which is done by taking advantage of a mathematical characteristic related to the extended PDE method. In addition, a methodology for automatic design optimisation of the parametric shape of tablets is also carried out in this thesis by using a similar approach to that used by Ugail (2003) and Ugail and Wilson (2003).

### 3.5 Design Optimisation

Optimisation problems arise in many areas, including the physical sciences, computer science, economics and engineering. For example, in engineering design problems, design optimisation is performed practically in order to improve or to achieve the most efficient design of an object with particular properties and requirements without violating the nature of the problem (Van der Velden and Koch 2010). Mostly, this type of problem is solved by integrating the optimisation method and CAD. This is achieved through various steps of the design process involving model creation using the CAD technique, physical analyses and shape optimisation (Ugail 2003).

An optimisation problem involves a set of design variables, a group of constraints and an objective function that measures the desirable value. The most important aspect of optimisation is the definition of a suitable objective function, which has to be minimised or maximised. The selection of the function strongly depends on the specific situation and requires considerable expertise. The general mathematical formulation of an optimisation problem to minimise a given objective function under equality and inequality constraints is written as

$$\begin{aligned} & \text{minimise} && f(\mathbf{x}) \\ & \text{subject to} && g_i(\mathbf{x}) \leq 0, \quad i = 1, \dots, m \\ & && h_i(\mathbf{x}) = 0, \quad i = 1, \dots, p \\ & && \mathbf{x}_l \leq \mathbf{x} \leq \mathbf{x}_u; \quad \mathbf{x} \in \mathbb{R}^n \end{aligned} \tag{3.19}$$

where  $f(\mathbf{x})$  is the objective function,  $\mathbf{x}$  is a vector of  $n$  design variables with sets of lower,  $\mathbf{x}_l$ , and upper,  $\mathbf{x}_u$ , bounds, while  $g_i(\mathbf{x})$  and  $h_i(\mathbf{x})$  represent inequality and equality constraints respectively. These constraints define the scope of design variables as well as specifying relationships between those variables.

A remarkable development in software tools for solving optimisation problems occurred several decades ago. One of these is MATLAB, which offers Optimisation Toolbox. This toolbox provides algorithms for solving standard and large-scale optimisation involving constrained and unconstrained problems. These algorithms can also solve continuous and discrete problems since the toolbox's software contains functions for linear, quadratic and nonlinear, as well as multiobjective optimisation problems. The toolbox functions and solver options can be accessed with Optimisation Tool or at the command line. The Optimisation Tool can be called by typing the syntax 'optimtool' on the command window or by clicking on the Optimisation Tool's tab from the main MATLAB window.

There are various methods for numerical optimisation which can be divided into two categories. The first category includes methods that require only the evaluation of the objective function, while the other category includes methods that not only require the evaluation of the objective function but also its derivative, with respect to the design variables (Enciu et al. 2010). The Interior-point, Simplex and Active Set method are examples of methods that are included in the first category, whereas the Gradient-based optimisation method belongs to the second one. Table 3.1 lists some methods used in Optimisation Toolbox to solve linear and nonlinear programming problems. In Mathematics, the term 'programming' refers to optimisation. Linear programming is a technique to solve an optimisation problem when the objective function and constraint equations are represented in linear relationships to the variables. However, if the objective function and some or all constraints are nonlinear, then the problem is known as nonlinear programming.

The Interior-point and Active Set methods are common methods used to solve both linear and nonlinear programming problems. In the MATLAB Optimisation ToolBox, the Interior-point method handles large-scale problems, while the Active Set method is classified as a medium-scale algorithm. According to Shahat et al. (2011), a large scale algorithm uses linear algebra, whereas this algebra neither needs to store nor operate on full matrices. Additionally, no sparse matrices need to be specified when using this algorithm. On the other hand, the

Table 3.1: Algorithms offered by the MATLAB Optimisation Toolbox for solving linear and nonlinear programming problems.

Linear Programming	Nonlinear Programming	
	Unconstrained	Constrained
<p><b>Interior-Point</b></p> <ul style="list-style-type: none"> <li>• Based on primal-dual predictor-corrector algorithm.</li> <li>• Useful for a problem that can be defined by sparse matrices.</li> </ul>	<p><b>Quasi-Newton</b></p> <ul style="list-style-type: none"> <li>• Uses mixed quadratic and cubic line search procedure and Fletcher-Goldfard-Shanno (BFGS) formula.</li> </ul>	<p><b>Interior-Point</b></p> <ul style="list-style-type: none"> <li>• For general nonlinear optimisation.</li> <li>• Useful for large-scale problems.</li> <li>• Based on a barrier function.</li> <li>• All iterations remain feasible with respect to bounds during the optimisation process.</li> </ul>
<p><b>Active Set</b></p> <ul style="list-style-type: none"> <li>• Works over the active set or locally active constraints to minimise the objective function at each iteration.</li> </ul>	<p><b>Nelder-Mead</b></p> <ul style="list-style-type: none"> <li>• Can handle non-smooth objective functions.</li> </ul>	<p><b>Active Set</b></p> <ul style="list-style-type: none"> <li>• For general nonlinear optimisation.</li> </ul>
<p><b>Simplex</b></p> <ul style="list-style-type: none"> <li>• Most widely used algorithm for linear programming.</li> <li>• Generates and tests candidate vertex solutions to a linear program.</li> </ul>	<p><b>Trust-Region</b></p> <ul style="list-style-type: none"> <li>• Useful for large-scale problems.</li> </ul>	<p><b>SQP</b></p> <ul style="list-style-type: none"> <li>• For general nonlinear optimisation.</li> <li>• Compromises with user-defined objective function and constraint equations evaluation failures.</li> </ul>
		<p><b>Trust-Region Reflective</b></p> <ul style="list-style-type: none"> <li>• Only for bound constrained problems or linear equalities.</li> <li>• Useful for large-scale problems.</li> </ul>

medium-scale algorithm uses dense linear algebra and internally creates full matrices (Shahat et al. 2011). Although the Interior-point method can solve large-scale problems efficiently with many inequality constraints, the Active Set method is sometimes more stable than the Interior-point method since it is less sensitive to the choice of starting point and the scaling of the problem (Byrd and Waltz 2009). Therefore, the design optimisation problems included in this work, which will be discussed in Chapter 6, are performed using the Active Set method and MATLAB Optimisation ToolBox.

### **3.6 Summary**

The literature review in this chapter starts with the history of CAD including CAGD, which was briefly discussed. Surfaces are commonly represented in terms of polynomial functions of two parameters in CAGD. There are different types of polynomial based methods for surface generation in CAGD, such as Bézier surfaces, B-spline, and Non-uniform rational B-splines (NURBS). The polynomial based methods generate a surface patch using a set of control points and change the surface shape by manipulating these points. However, it is very difficult to manipulate these kinds of surfaces since they involve too many control points and weights. Furthermore, the techniques can be time-consuming, less natural and counter-intuitive.

By contrast, the PDE method has been introduced by Bloor and Wilson as a solution to a particular type of elliptic PDE to generate smooth parametric surfaces. Generally, PDE surfaces are easier to manipulate than polynomial surfaces since it is necessary to modify some of the parameters to change the surface shape. This technique generates surfaces of complex geometries from a small number of parameters since it is characterised by data distributed around the boundaries. The PDE method has been applied in many disciplines, including medical applications, animation and optimisation analysis.

The choice of a particular algorithm for numerical optimisation, together with an appropriate objective function and the number of design variables to be used, may reduce the computing time to obtain the optimal result. MATLAB offers a toolbox to solve standard and large-scale optimisation problems numerically.

## **Chapter 4**

### **The PDE Method for Tablet Shape Modelling**

#### **4.1 Introduction**

This chapter provides details on the methodology used in this research. It presents a technique for shape modelling of pharmaceutical tablets based on the use of Partial Differential Equations (PDEs), and explains how to measure their volume and surface area. It also describes in detail how solid pharmaceutical tablets are created by utilising the PDE method. The final section in this chapter shows how the shape and size of the PDE-based representation of pharmaceutical tablets can be manipulated intuitively by changing the boundary curves or design parameters. This is done by exploiting the mathematical properties of the analytic solution to the Biharmonic equation.

## 4.2 Modelling Parametric Representation of Tablet Shapes

This section discusses how to use the PDE method to design various shapes of pharmaceutical tablets: flat-faced round, shallow convex round, shallow convex oval, oblong and sphere. The geometric models representing the tablet shapes used in this study have been obtained by using a specific number of generating curves, according to the specific needs of each shape. These curves are closed ones, as presented in Figure 4.1. The shape of pharmaceutical tablets is considered as complex geometry. Therefore, several patches are required to generate these tablets. The number of patches and boundary curves used to generate each tablet shape can be found in Table 4.1, together with the size of the corresponding tablet. Table 4.1 also outlines which of the geometric representations in Figure 4.2 corresponds to each respective tablet configuration.

The geometric model representing the flat-faced round tablet has been obtained using ten generating curves to produce a surface composed of three patches, since each surface patch requires four curves. Each of these curves represents a circle of a given radius at a particular height. The  $\nu$  parametric coordinate represents the domain from 0 to  $2\pi$ , which after the polar transformation is applied guarantees the use of closed curves. In order to use the PDE method to design a flat-faced round tablet, the whole design procedure is split

into several steps. First, the base of the tablet (Patch 1) is generated, followed by the body of that tablet (Patch 2) and finally, the top surface (Patch 3) is designed. As can be seen in Figure 4.1, the last curve of Patch 1,  $P_{12}$ , is used as the first curve of Patch 2,  $P_{21}$ , in order to ensure  $C^0$  continuity between patches.

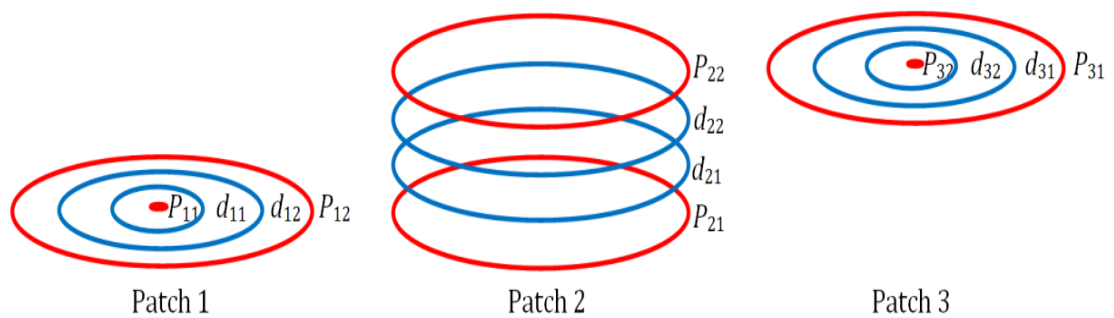


Figure 4.1: Generating curves for a flat-faced round tablet.

Table 4.1: Parameters and properties of each PDE-based representation of tablet configurations used in this project.

Shape of the tablet	Dimension (mm) Diameter $\times$ height	Num. of patches	Num. of boundary curves	Figure 4.2
Flat-faced round	10 $\times$ 6	3	10	(a)-(c)
Spherical shaped	5 $\times$ 5	2	7	(d)-(f)
Shallow convex round	10 $\times$ 3	3	10	(g)-(i)
Shallow convex oval	6 $\times$ 12 $\times$ 3	3	10	(j)-(l)
Oblong	5 $\times$ 15	3	10	(m)-(o)

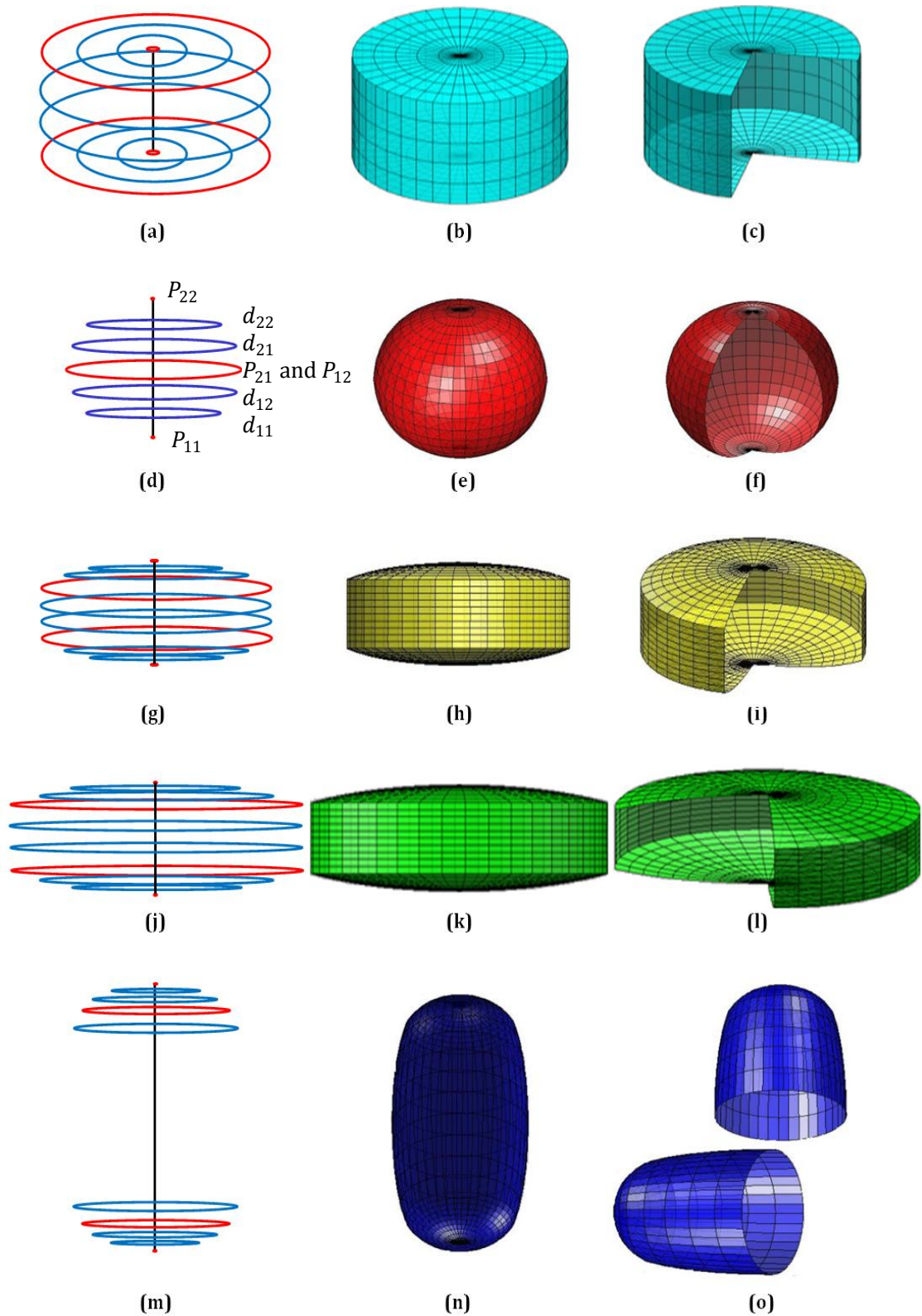


Figure 4.2: Different shapes of pharmaceutical tablets created using either two or three PDE surface patches accordingly. The boundary curves for each shape are shown together with the corresponding spine in (a), (d), (g), (j) and (m). The interior part of each generated parametric tablet is illustrated in (c), (f), (i) (l) and (o).

This work considers a spherical tablet that is regarded as a surface composed of two patches representing the surface of its upper and lower hemispheres. Given that this object has symmetry, only the upper hemisphere is considered. The radius,  $r_{c_{jk}}$ , and height,  $z_{c_{jk}}$ , for each boundary curve representing the upper hemisphere are determined by

$$r_{c_{jk}} = r_s \cos(\psi_{c_{jk}}) \text{ and } z_{c_{jk}} = r_s \sin(\psi_{c_{jk}}), \quad (4.1)$$

where  $r_s$  is the radius of the sphere,  $c_{jk}$  represents the type of curve (refer to Section 3.4.1) and  $\psi_{c_{jk}} = \{\psi_{P_{21}}, \psi_{d_{21}}, \psi_{d_{22}}, \psi_{P_{22}}\} = \{0, \frac{\pi}{6}, \frac{\pi}{3}, \frac{\pi}{2}\}$ . Generally, the position of each point on the boundary curves can be written as

$$(x_0 + r_{c_{jk}} \cos v, y_0 + r_{c_{jk}} \sin v, z_0 + z_{c_{jk}}), \quad (4.2)$$

where  $0 \leq v \leq 2\pi$  and  $(x_0, y_0, z_0)$  is the centre of the sphere. Consider a sphere with radius,  $r_s = 2.5$  mm, as shown in Figure 4.2(e), with the coordinates of these points such that the curves representing the upper hemisphere are given by

$$P_{21}: (x_0 + 2.5 \cos v, y_0 + 2.5 \sin v, z_0), \quad (4.3a)$$

$$d_{21}: (x_0 + 2.17 \cos v, y_0 + 2.17 \sin v, z_0 + 1.25), \quad (4.3b)$$

$$d_{22}: (x_0 + 1.25 \cos v, y_0 + 1.25 \sin v, z_0 + 2.17), \quad (4.3c)$$

$$P_{22}: (x_0, y_0, z_0 + 2.5). \quad (4.3d)$$

The curves in Equations (4.3a) - (4.3d) can be reflected to obtain the boundary curves corresponding to the lower hemisphere. As displayed in Figure 4.2(d), the curve  $P_{21}$  is chosen to be the common boundary where both surface patches meet.

Once all the necessary curves have been created, these curves are saved in external .OBJ files. The PDE method is implemented in C<sup>++</sup> to read the boundary curves that define the shape of the tablet and produce the solution for each set of curves. A MEX file has been created as an interface between MATLAB and Visual C<sup>++</sup>. When the MATLAB file is compiled, the MEX file is dynamically loaded and allows calling the pertaining C<sup>++</sup> subroutine within MATLAB as if it were a built-in function. A subroutine has been developed in MATLAB to display the resulting shape of the tablets.

The surface representations produced in this work have been obtained using three different set of boundary conditions to solve the Biharmonic equation, which has been solved using five Fourier modes for flat-faced round, convex round, convex oval and oblong tablets. The only exception to this consists of the surface for the spherical shaped tablet, which has been generated by solving two different PDEs. The output shape of the generated flat-faced round tablet with radius,  $c = 5$  mm and thickness,  $t = 6$  mm is shown in Figure 4.2(b). All

sets of curves in Figure 4.2(a) lay on in the resulting surface. The shape of other tablets with specific radii and heights are presented in Figures 4.2(b), 4.2(e), 4.2(h), 4.2(k) and 4.2(n) respectively. Note that the shape of each surface patch can easily be controlled by the shape of the boundary curves.

For many practical designs, a portion of the original surface sometimes needs to be removed. Thus, Ugail (2006) has proposed a method for trimming surfaces as solutions to PDEs and has proved that the proposed method can be used to trim other types of parametric surfaces. Here, the surface is trimmed by determining the new region of parameter space  $(u, v)$ , where all points which do not belong to this region will be discarded from the resulting surface. For the purpose of showing the interior part of the generated tablets, the domain of the parameter  $v$  is set from  $\frac{\pi}{2}$  to  $2\pi$ . The trimmed PDE surfaces for the convex round and convex oval tablets are shown in Figures 4.2(i) and 4.2(l) respectively.

#### **4.2.1 The Surface Area and Volume of a Parametric Tablet**

As mentioned in Chapter 2, the surface area and volume of tablets play an important role in characterising pharmaceutical compaction properties. Thus, it is necessary to measure the area and volume of PDE surfaces. The remaining part of this section shows the formulae used to calculate both area and volume of parametric surfaces.

Equation (3.12) has a vectorial representation of the form

$$\boldsymbol{\chi}(u, v) = \chi_x(u, v)\mathbf{i} + \chi_y(u, v)\mathbf{j} + \chi_z(u, v)\mathbf{k}, \quad (4.4)$$

where  $\mathbf{i}$ ,  $\mathbf{j}$  and  $\mathbf{k}$  are the Cartesian basis vectors, known as unit vectors along  $x$ -,  $y$ - and  $z$ -axis respectively while  $\chi_x$ ,  $\chi_y$  and  $\chi_z$  represent the coordinates of a given point on the surface. Given that the boundary curves of the tablets generated in Section 4.2 represent circles, the approximated solution of the elliptic PDE fits the original boundary conditions perfectly. Hence, the vector  $\mathbf{R}$  is equal to zero at these particular positions and  $\chi_x$ ,  $\chi_y$  and  $\chi_z$  can be written as

$$\chi_x = A_{0x} + \sum_{n=1}^N [A_{nx} \cos(nv) + B_{nx} \sin(nv)], \quad (4.5)$$

$$\chi_y = A_{0y} + \sum_{n=1}^N [A_{ny} \cos(nv) + B_{ny} \sin(nv)], \quad (4.6)$$

$$\chi_z = A_{0z} + \sum_{n=1}^N [A_{nz} \cos(nv) + B_{nz} \sin(nv)]. \quad (4.7)$$

The area of a parametric surface is determined by

$$S = \iint_{\Omega} |\boldsymbol{\chi}_u \times \boldsymbol{\chi}_v| d\Omega, \quad (4.8)$$

and the volume can be found by using

$$V = \frac{1}{3} \iint_{\Omega} \boldsymbol{\chi} \cdot (\boldsymbol{\chi}_u \times \boldsymbol{\chi}_v) d\Omega, \quad (4.9)$$

where

$$\mathbf{x}_u = \frac{\partial \chi_x}{\partial u} \mathbf{i} + \frac{\partial \chi_y}{\partial u} \mathbf{j} + \frac{\partial \chi_z}{\partial u} \mathbf{k}, \quad (4.10)$$

$$\mathbf{x}_v = \frac{\partial \chi_x}{\partial v} \mathbf{i} + \frac{\partial \chi_y}{\partial v} \mathbf{j} + \frac{\partial \chi_z}{\partial v} \mathbf{k}. \quad (4.11)$$

These derivatives (Equations (4.10) and (4.11)) can be found by differentiating the analytic expression of the solution to the Biharmonic equation given in Equations (4.5) – (4.7), with respect to  $u$  and  $v$  respectively.

The area and the volume of the generated parametric surface can be calculated numerically using MATLAB. This software has a command '*dblquad*' for integrating the functions of two variables. A vectorization technique is used in this process to ensure that the algorithm is executed properly. This strategy improves the speed of the MATLAB code by replacing the loop calculations by equivalent matrix and vector operations (Birkbeck et al. 2007). The significance of this is that MATLAB is an array-based language (Joisha and Banerjee 2003). Therefore, the area of the PDE surface patch is calculated by writing the last two command lines as

```
S = inline(vectorize('|\mathbf{x}_u \text{ cross } \mathbf{x}_v|'), 'u', 'v');
SurfaceArea = dblquad(S, lower limit u, upper limit u, lower limit v, upper limit v);
```

The estimated area and volume of each patch of the PDE-based representation of flat-faced round and spherical tablets calculated by Equations (4.8) and (4.9) are given in Tables 4.2(a) and 4.2(b) respectively. The surface area of a paramet-

ric tablet is the sum of the area of each patch comprising the surface, and similarly for the volume. These estimated values for round and spherical tablets are compared with the respective values obtained from the accurate models (parametric and standard formulae).

Table 4.2(a): Comparison between estimated and theoretical values of surface area and volume of a flat-faced round tablet.

<b>Flat-faced Round Tablet: <math>c = 5 \text{ mm}</math>, <math>t = 6 \text{ mm}</math></b>		
PDE-based Representation of Tablet	Parametric Cylinder $x = c \cos \theta, y = c \sin \theta, z = z$	Cylinder (Standard formulae)
<p><b>Surface Area</b></p> <p>= Area Patch 1 + Area Patch 2 + Area Patch 3</p> <p>= (78.361 + 188.340 + 78.361) mm<sup>2</sup></p> <p>= 345.062 mm<sup>2</sup></p>	<p><b>Surface Area</b></p> <p>= Area Patch 1 + Area Patch 2 + Area Patch 3</p> <p>= (78.539 + 188.500 + 78.539) mm<sup>2</sup></p> <p>= 345.578 mm<sup>2</sup></p>	<p><b>Surface Area</b></p> <p>= <math>2\pi c(c + t)</math></p> <p>= 345.575 mm<sup>2</sup></p>
<p><b>Volume</b></p> <p>= Vol Patch 1 + Vol Patch 2 + Vol Patch 3</p> <p>= (0 + 313.597 + 156.723) mm<sup>3</sup></p> <p>= 470.320 mm<sup>3</sup></p>	<p><b>Volume</b></p> <p>= Vol Patch 1 + Vol Patch 2 + Vol Patch 3</p> <p>= (0 + 314.160 + 157.081) mm<sup>3</sup></p> <p>= 471.241 mm<sup>3</sup></p>	<p><b>Volume</b></p> <p>= <math>2\pi c^2 t</math></p> <p>= 471.239 mm<sup>3</sup></p>

Table 4.2(b): Comparison between estimated and theoretical values of surface area and volume of a spherical tablet.

<b>Spherical Tablet: <math>r_s = 2.5</math> mm</b>		
PDE-based Representation of Tablet	Parametric Sphere $x = r_s \cos \theta \sin \phi$ $y = r_s \sin \theta \sin \phi, z = r_s \cos \phi$	Sphere (Standard formulae)
<p><b>Surface Area</b></p> <p>= Area Patch 1 + Area Patch 2</p> <p>= (38.957 + 38.957) mm<sup>2</sup></p> <p>= 77.913 mm<sup>2</sup></p>	<p><b>Surface Area</b></p> <p>= Area Patch1 + Area Patch2</p> <p>= (39.270 + 39.270) mm<sup>2</sup></p> <p>= 78.540 mm<sup>2</sup></p>	<p><b>Surface Area</b></p> <p>= <math>4\pi r_s^2</math></p> <p>= 78.540 mm<sup>2</sup></p>
<p><b>Volume</b></p> <p>= Volume Patch 1 + Volume Patch 2</p> <p>= (15.941 + 48.523) mm<sup>3</sup></p> <p>= 64.464 mm<sup>3</sup></p>	<p><b>Volume</b></p> <p>= Volume Patch 1 + Volume Patch 2</p> <p>= (16.465 + 48.984) mm<sup>3</sup></p> <p>= 65.449 mm<sup>3</sup></p>	<p><b>Volume</b></p> <p>= <math>\frac{4}{3}\pi r_s^3</math></p> <p>= 65.450 mm<sup>3</sup></p>

Notice that the volume of Patch 3 of the round tablet is different from that of Patch 1. This is because Equation (4.9) satisfies the Divergence Theorem of a closed surface, whereby the unit normal vector,  $\mathbf{n}$ , of Patch 1 points along the negative direction of the  $z$ -axis and the  $\mathbf{n}$  of Patch 3 points along the positive direction of the  $z$ -axis. As can be seen in Tables 4.2(a) and 4.2(b), the surface area and volume of a parametric cylinder and sphere measured using Equations (4.8) and (4.9) are very similar to the values obtained from the standard formu-

lae. However, these physical properties of the PDE-based representation of tablets are slightly different from values obtained from the accurate models. This difference is attributed to the fact that both tablet shapes generated using the PDE method is not exact. This is due to the limitation of the PDE method, which can only approximate the shape of the surface of any given object. The measured surface area and volume of other PDE-based tablets can be seen in Table 4.3.

Table 4.3: Surface area and volume of shallow convex round, shallow convex oval and oblong tablets.

<b>Shallow convex round</b>			<b>Shallow convex oval</b>		<b>Oblong</b>	
Patch	S. Area (mm <sup>2</sup> )	Volume (mm <sup>3</sup> )	S. Area (mm <sup>2</sup> )	Volume (mm <sup>3</sup> )	S. Area (mm <sup>2</sup> )	Volume (mm <sup>3</sup> )
1	79.129	7.827	57.382	5.316	23.491	5.856
2	62.780	104.344	58.082	75.127	203.050	204.915
3	79.129	86.044	57.382	61.632	23.491	87.892
<b>Total</b>	<b>221.038</b>	<b>198.215</b>	<b>172.846</b>	<b>142.075</b>	<b>250.032</b>	<b>298.663</b>

### 4.3 Three-Dimensional Mesh Generation Using the PDE Method

This section shows a methodology for generating a cuboid solid mesh for pharmaceutical tablets using the PDE method. This cuboid mesh represents the inner part of the tablet, since the PDE method's formulation used in Section 3.4.1 only generates the tablet's shell. The mesh generation algorithm is based on a simple mechanical analogy between a cuboid mesh and the PDE coefficients. Equation (3.16) has been extended to a higher-dimensional space by introducing a new parameter,  $w$ , in order to generate a solid PDE-based representation of a tablet

$$\mathbf{X}(u, v, w) = \mathbf{A}_0 + w \left[ \sum_{n=1}^N [\mathbf{A}_n(u) \cos(nv) + \mathbf{B}_n(u) \sin(nv)] + \mathbf{R}(u, v) \right], \quad (4.12)$$

where  $0 \leq w \leq 1$ . As mentioned before,  $u$  and  $v$  define the parametric region while  $\mathbf{A}_0$  and  $\sum_{n=1}^{\infty} [\mathbf{A}_n(u) \cos(nv) + \mathbf{B}_n(u) \sin(nv)]$  describe the spine and a radial distance from the spine to the surface patch respectively. This new parameter generates points for the interior of the object, from the spine towards its surface. The direction of each parameter in Equation (4.12) is illustrated in Figure 4.3.

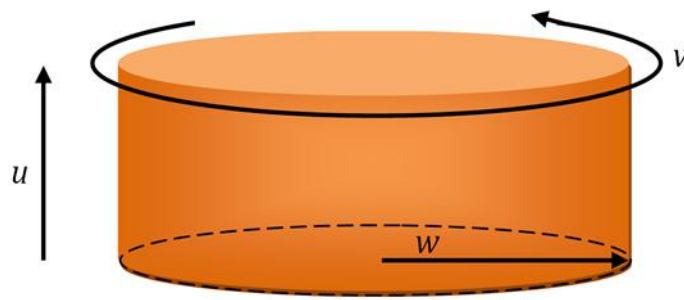


Figure 4.3: Independent variables in the extended PDE Method.

Figure 4.4 shows a schematic diagram describing the process by which the cuboid mesh is generated. The number of nodes and cuboids used to generate the solid object depend on parameters  $s_x$ ,  $s_y$  and  $s_z$ . Let parameters  $s_x$ ,  $s_y$  and  $s_z$  represent the number of nodes on  $x$ -,  $y$ - and  $z$ -axis respectively. In particular, the cube shown in Figure 4.4 is produced by defining parameters  $s_x$ ,  $s_y$  and  $s_z$  equal to 4, 5 and 3 respectively, giving rise to 60 nodes ( $4 \times 5 \times 3$ ) and 24 cuboids ( $3 \times 4 \times 2$ ). All six faces of the cuboid are grouped into three sets of opposite faces: Face1 (parallel to  $yz$  plane), Face2 (parallel to  $xy$  plane) and Face3 (parallel to  $zx$  plane). Each Face1, Face2 and Face3 of a cuboid is generated by connecting four vertices. For a smooth mesh generation, Face1, Face2 and Face3 of all cuboids are generated layer by layer starting from Face1's layers, followed by those of Face2 and ending with those of Face3. The cuboid mesh generation is complete when all nodes have been connected to the neighbouring nodes and several cuboids are linked into one polyhedron with a defined shape.

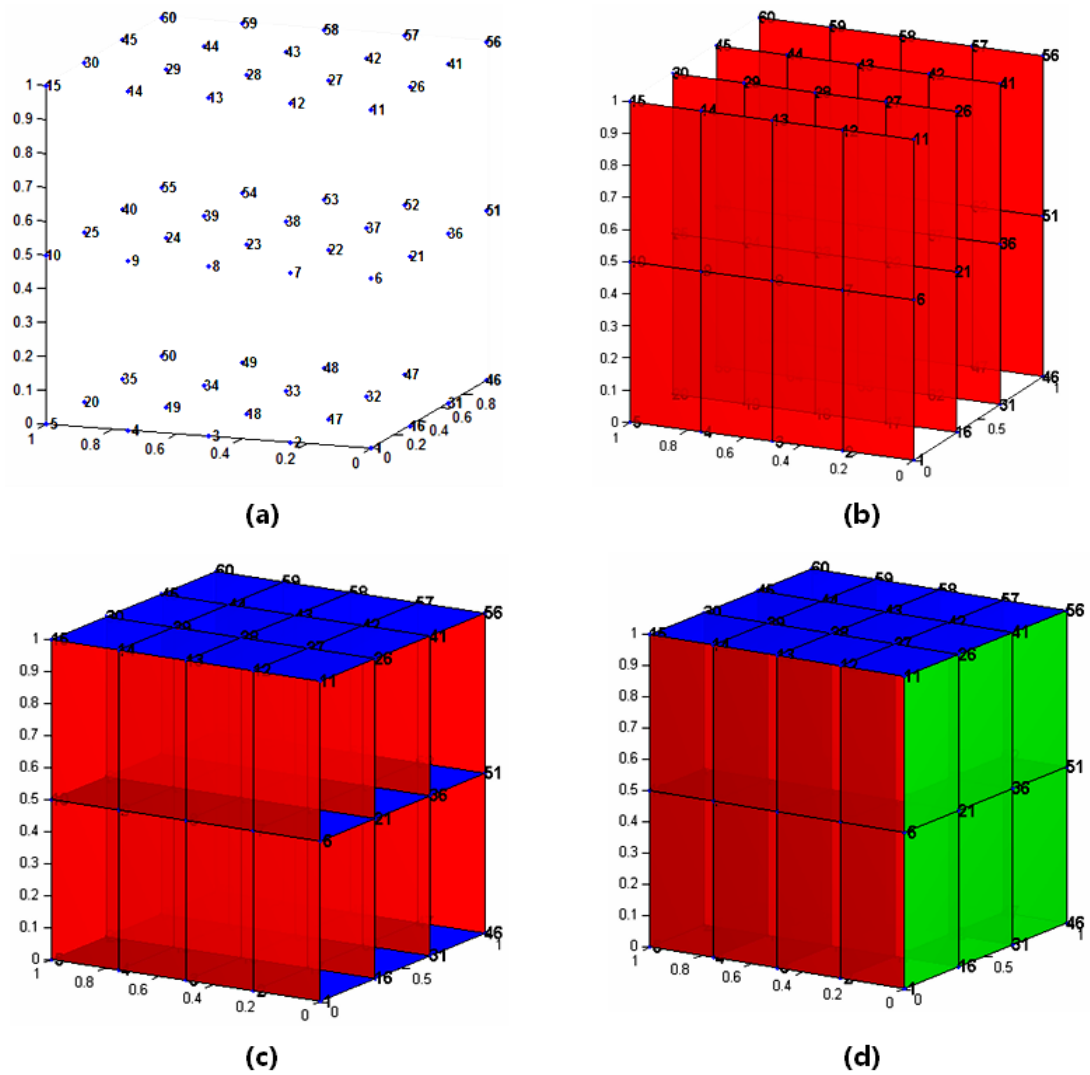


Figure 4.4: Cuboid mesh generation process. (a) Generated nodes. (b) Generating Face1 faces parallel to  $yz$ -plane from front layer to  $s_x$ -layer. (c) Generating Face2 faces parallel to  $xy$ -plane from bottom layer to  $s_z$ -layer. (d) Generating Face3 faces parallel to  $zx$ -plane from right layer to  $s_y$ -layer.

A subroutine has been coded in MATLAB to generate the cuboid mesh for a PDE-based representation of an object. The process for mesh generation is divided into the following steps:

- Firstly, the boundary curves are created and the subroutine which produced the coefficients of the solution to the Biharmonic PDE in  $C^{++}$  is called.

- Then, a uniform rectangular grid given by three vectors  $\mathbf{u}$ ,  $\mathbf{v}$  and  $\mathbf{w}$  is created using the '*meshgrid*' function. Next, nodes are produced by connecting the vectors  $\mathbf{u}$ ,  $\mathbf{v}$  and  $\mathbf{w}$  with the PDE coefficients. The distance between each node depends on both the coefficients and the grid. The coordinates of all nodes are stored in an array.
- All faces (Face1, Face2, Face3) of each cuboid are produced through an algorithm that iterates through the 3D array of nodes and join set of four nodes. Finally, the cuboid meshes are generated from the nodes, as shown in Figure 4.4(d).

The pseudocode for the cuboid mesh generation algorithm presented here is shown in **Appendix A**.

As mentioned earlier in this section, the number of cuboids in the mesh generation process depends on the selection of  $s_x$ ,  $s_y$  and  $s_z$ . These parameters influence the resolution of the mesh describing the object and consequently, the smoothness is intrinsically related to them. Figure 4.5 illustrates the sequence of shapes resulting in changes of the values of  $s_x$ ,  $s_y$  and  $s_z$  which have been run on MATLAB R2008a with a 2.20 GHz Intel Core 2 Duo T7500 processor. The particular values of these variables are shown in Table 4.4 together with the time taken to complete the meshing process. As can be seen in Figure 4.5, the small flat faces almost disappear in a reasonable time as the values of  $s_x$ ,  $s_y$  and  $s_z$  increase.

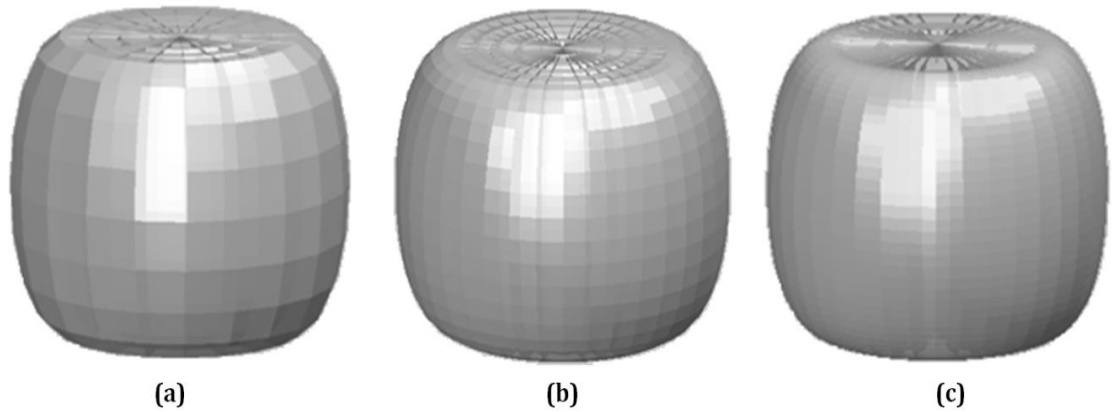


Figure 4.5: Cuboid mesh of a spheroid; (a) 800, (b) 3800 and (c) 7600 cuboids.

Table 4.4: Number of nodes and time required to create the geometries shown in Figure 4.5.

$s_x$	$s_y$	$s_z$	Time (s)	Figure 4.5
11	21	5	8	(a)
21	39	6	88	(b)
41	39	6	195	(c)

The generated solid pharmaceutical tablets obtained by using the PDE method are shown in Figure 4.6. These tablets have been trimmed by defining both parameters  $u$  and  $w$  from 0 to 1 respectively and the domain of the parameter  $v$  is  $\left[\frac{\pi}{2}, 2\pi\right]$ . The parameters  $s_x$ ,  $s_y$  and  $s_z$  have been set as 11, 41 and 6 respectively. Therefore, the number of cuboids in a spherical tablet is 3000, while the other tablets are produced using 4500 cuboids.

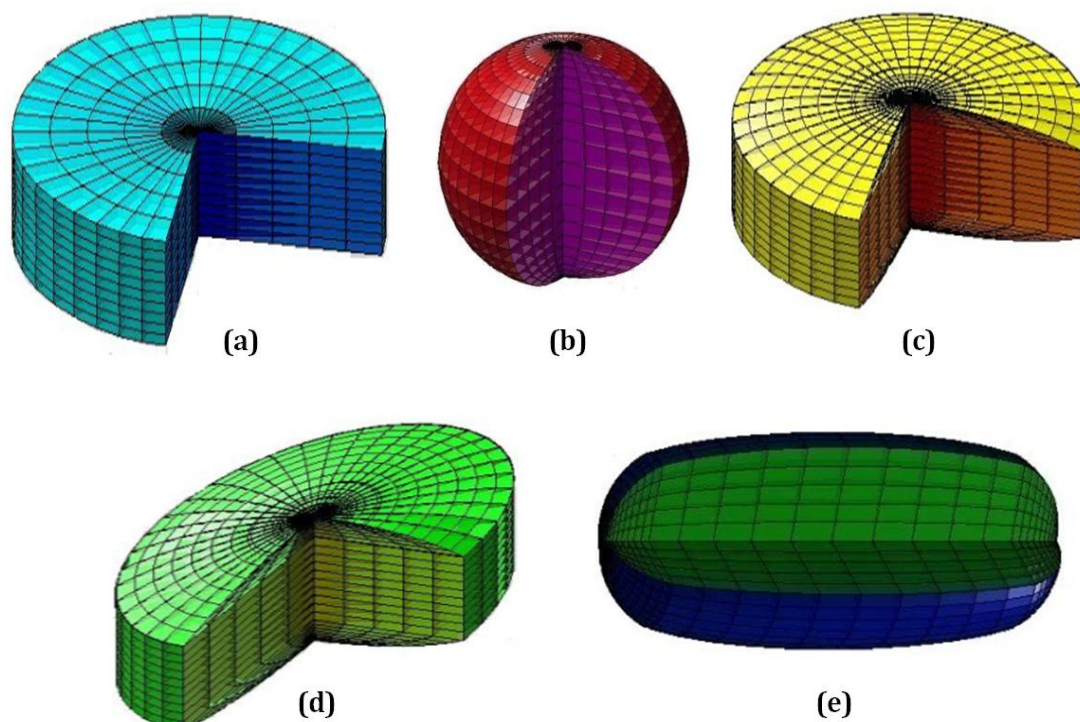


Figure 4.6: Solid PDE-based representation of tablets; (a) Flat-faced round, (b) Spherical, (c) Convex round, (d) Convex oval and (e) Oblong tablets.

#### 4.4 Manipulation of PDE-Based Objects

This section describes the application of the extended PDE method (Equation (4.12)) to modify the shape of pharmaceutical tablets, as discussed in the previous section. The modification involves changing the height and radius of the tablet. For the purpose of finding simple relationships between the PDE coefficients and physical properties of a tablet (height and radius), the analytic solution of the PDE and a circle are considered.

The analytic solution of the PDE can be written in the form

$$(\chi_x, \chi_y, \chi_z) = \begin{pmatrix} A_{0x} + w \left[ \sum_{n=1}^N [A_{nx} \cos(nv) + B_{nx} \sin(nv)] + R_x \right], \\ A_{0y} + w \left[ \sum_{n=1}^N [A_{ny} \cos(nv) + B_{ny} \sin(nv)] + R_y \right], \\ A_{0z} + w \left[ \sum_{n=1}^N [A_{nz} \cos(nv) + B_{nz} \sin(nv)] + R_z \right] \end{pmatrix}. \quad (4.13)$$

Again, the vector  $\mathbf{R}$  in Equation (4.13) is equal to zero since the boundary conditions of these generated tablets represent circles of different radii. Therefore, only the terms  $\mathbf{A}_0$ ,  $\mathbf{A}_n$  and  $\mathbf{B}_n$  will be considered to generate the new shape of the tablet. Given that the term  $\mathbf{A}_0$  represents the spine of the solid PDE-based representation of an object, the height of the generated tablets depends on this term.

Equation (4.13) is compared to a circle with a centre  $(x_0, y_0, z)$  and radius,  $r$ , which can be written in a parametric form

$$(x, y, z) = (x_0 + r \cos v, y_0 + r \sin v, z). \quad (4.14)$$

Therefore, the centre of the boundary curve is found at  $(A_{0x}, A_{0y}, A_{0z})$ . As can be seen in Figures 4.2(a), 4.2(d), 4.2(g), 4.2(j) and 4.2(m), the  $z$ -axis has been chosen to represent the axis of symmetry (and consequently the height) of the tablets. Thus, only  $A_{0z}$  is used to represent the height of the PDE-based

representation of pharmaceutical tablets. The mathematical expression found for such a purpose is

$$A_{0z} = a_{00z} + a_{01z}u. \quad (4.15)$$

The height of the generated PDE-based tablets can be measured from the length of the spine

$$h = A_{0z}|_{u=1} - A_{0z}|_{u=0} = a_{01z}. \quad (4.16)$$

Next, the analytic expression for the radius associated with the PDE surface is used to find the relation between  $\mathbf{A}_n$  and  $\mathbf{B}_n$ , thus obtaining the simplified equation of the radius. By simple comparison between Equations (4.13) and (4.14) when  $w = 1$ , it is noticed that

$$\begin{aligned} r \cos(v) &= \sum_{n=1}^N [A_{nx} \cos(nv) + B_{nx} \sin(nv)] \\ &= A_{1x} \cos(v) + B_{1x} \sin(v) + A_{2x} \cos(2v) + B_{2x} \sin(2v) \\ &\quad \dots + A_{Nx} \cos(Nv) + B_{Nx} \sin(Nv), \end{aligned} \quad (4.17)$$

and

$$\begin{aligned} r \sin(v) &= \sum_{n=1}^N [A_{ny} \cos(nv) + B_{ny} \sin(nv)] \\ &= A_{1y} \cos(v) + B_{1y} \sin(v) + A_{2y} \cos(2v) + B_{2y} \sin(2v) \\ &\quad \dots + A_{Ny} \cos(Nv) + B_{Ny} \sin(Nv). \end{aligned} \quad (4.18)$$

From Equations (4.17) and (4.18), it is found that  $A_{nx}$ ,  $B_{nx}$ ,  $A_{ny}$  and  $B_{ny}$  for  $n > 1$  are zero. Thus, the above equations can be re-written as

$$r \cos(v) = A_{1x} \cos(v) + B_{1x} \sin(v) \quad (4.19a)$$

and

$$r \sin(v) = A_{1y} \cos(v) + B_{1y} \sin(v). \quad (4.19b)$$

As a result, it is observed that  $A_{1x} = B_{1y}$ . Another relationship can be found from the basic equation of a circle

$$r^2 = x^2 + y^2 = (r \cos v)^2 + (r \sin v)^2. \quad (4.20)$$

By substituting Equations (4.19a) and (4.19b) into Equation (4.20), it is found that

$$\begin{aligned} (r \cos v)^2 + (r \sin v)^2 &= (A_{1x} \cos(v) + B_{1x} \sin(v))^2 + (A_{1y} \cos(v) + B_{1y} \sin(v))^2, \\ r^2(\cos v)^2 + r^2(\sin v)^2 &= (A_{1x}^2 + A_{1y}^2)(\cos v)^2 + (B_{1x}^2 + B_{1y}^2)(\sin v)^2 \\ &\quad + 2(A_{1x}B_{1x} + A_{1y}B_{1y}) \sin v \cos v. \end{aligned} \quad (4.21)$$

By comparing the left hand side (LHS) and right hand side (RHS) of Equation (4.21), the radius of the PDE-based tablet is then given by

$$r = \sqrt{A_{1x}^2 + A_{1y}^2} = \sqrt{B_{1x}^2 + B_{1y}^2}, \quad (4.22)$$

and the relationship between  $A_{1y}$  and  $B_{1x}$  is

$$A_{1y} = -B_{1x} . \quad (4.23)$$

Therefore, Equations (4.16) and (4.22) can be used for the simulation corresponding to the heights and radii of the PDE-based representations of the pharmaceutical tablets respectively.

#### 4.4.1 Examples of Tablet Shape and Size Manipulation

The new shapes of solid pharmaceutical tablets are generated by changing the values of the height and radius of the original tablet shapes shown in the previous section. Ring-shaped, deep convex round and oval, oblate and prolate spheroid, rod and caplet tablets have been created using the PDE Method and these tablets are illustrated in Figure 4.7. The detailed description of these shapes can be found in Table 4.5.

As shown in Figure 4.7(a), a ring-shaped tablet with a 6 mm hole and a thickness of 4.5 mm is created by multiplying the spine of the body (Patch 2) of the flat-faced round tablet by 0.75, while the parameter  $w$  is set from 0.5 to 1. In addition, an oblate spheroid shaped tablet of diameter 10 mm and a thickness of 2.5 mm, as shown in Figure 4.7(c), is produced by doubling the original radius of the spherical tablet whilst compressing both the upper and lower hemispheres. The prolate spheroid shaped tablet (Figure 4.7(d)) is generated by doubling the height of the spherical tablet. Furthermore, a PDE-based representation of a

caplet, which is illustrated in Figure 4.7(f), has been created by increasing the height of the shallow convex oval tablet and also reducing its radius.

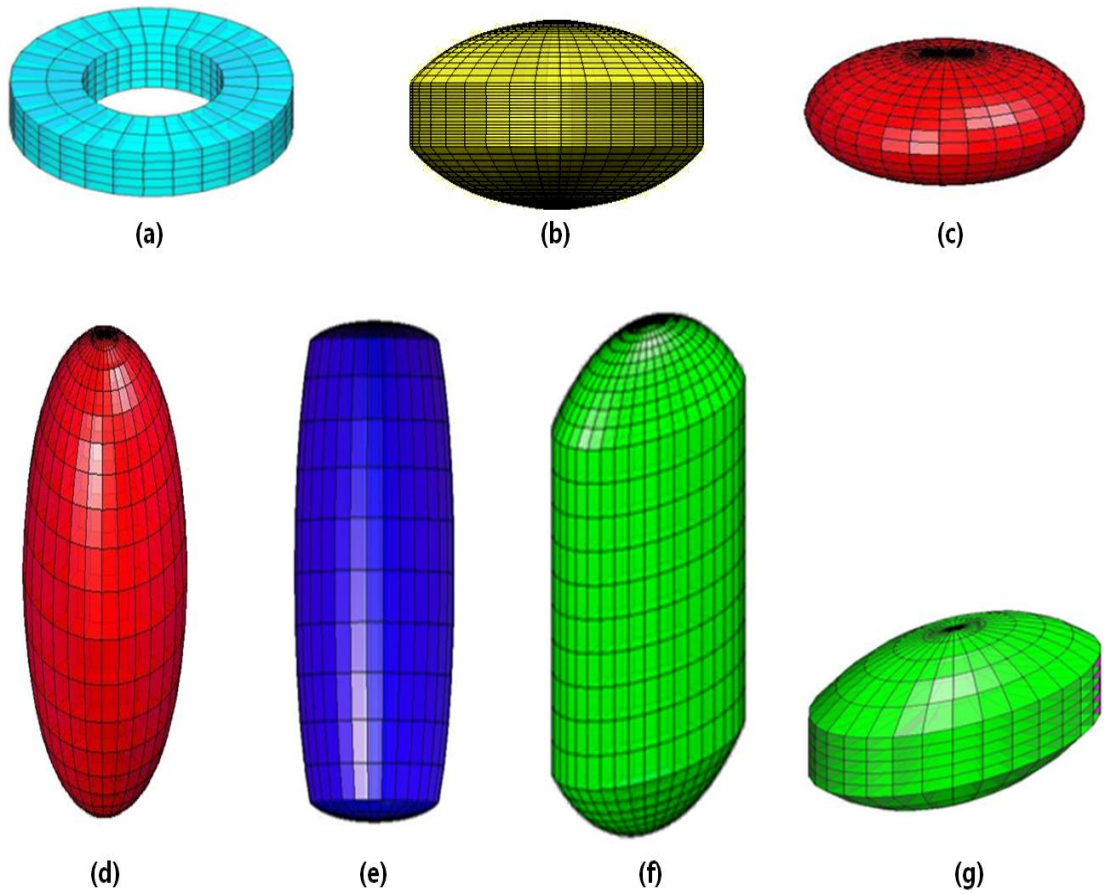


Figure 4.7: Different tablet shapes obtained by changing the design parameters.

Table 4.5: Changes made to the design parameters of the original tablet shape.

Original Shape	New Shape	Dimension (mm) $D \times h$	Changes to Coefficients	Figure 4.7
Flat-faced round	Ring-shaped	$12 \times 4.5$	<ul style="list-style-type: none"> <li>• <math>0.75A_{0z2}</math></li> <li>• <math>1.2 r</math></li> <li>• <math>w = [0.5, 1]</math></li> </ul>	(a)
Shallow convex round	Deep convex round	$10 \times 4$	<ul style="list-style-type: none"> <li>• <math>3A_{0z1}</math></li> <li>• <math>0.5A_{0z2}</math></li> <li>• <math>3A_{0z3}</math></li> </ul>	(b)
Spherical shaped	Oblate spheroid	$10 \times 2.5$	<ul style="list-style-type: none"> <li>• <math>0.5A_{0z1}</math></li> <li>• <math>0.5A_{0z2}</math></li> <li>• <math>2 r</math></li> </ul>	(c)
Spherical shaped	Prolate spheroid	$5 \times 10$	<ul style="list-style-type: none"> <li>• <math>2A_{0z1}</math></li> <li>• <math>2A_{0z2}</math></li> </ul>	(d)
Oblong	Rod	$3 \times 7.5$	<ul style="list-style-type: none"> <li>• <math>0.2A_{0z1}</math></li> <li>• <math>0.6A_{0z2}</math></li> <li>• <math>0.2A_{0z3}</math></li> <li>• <math>0.6 r</math></li> </ul>	(e)
Shallow convex oval	Caplet	$3.5 \times 7 \times 15$ (Length $\times$ width $\times$ height)	<ul style="list-style-type: none"> <li>• <math>5A_{0z1}</math></li> <li>• <math>5A_{0z2}</math></li> <li>• <math>5A_{0z3}</math></li> <li>• <math>0.585 r</math></li> </ul>	(f)
Shallow convex oval	Deep convex oval	$6 \times 12 \times 3.1$ (Length $\times$ width $\times$ height)	<ul style="list-style-type: none"> <li>• <math>2A_{0z1}</math></li> <li>• <math>0.55A_{0z2}</math></li> <li>• <math>2A_{0z3}</math></li> </ul>	(g)

## 4.5 Summary

The work presented in this chapter focuses on the application of the PDE method for designing parametric representations of pharmaceutical tablets. Generally, three smooth surface patches generated by a fourth order PDE have been blended together to construct hollow flat-faced round, shallow convex round, shallow convex oval and oblong tablets. However, a spherical shaped tablet is produced by solving two PDEs. The volume and surface area of the generic tablets have been determined by using the formulae of the volume and surface area of a parametric surface respectively, and the values can be obtained numerically using MATLAB.

A solid PDE-based representation of a tablet is generated by extending the PDE method to a higher dimension with the introduction of an additional parameter,  $w$ , into the analytical solution of the elliptic PDE. This variable generates points from the centreline or spine of the patch towards its surface. All generated points are used as vertices of rectangular faces so that uniform cuboids are created to form the shape of the tablet. Additionally, the generated solid tablet can be trimmed by changing the region defined by independent variables  $u$ ,  $v$  or  $w$ . Finally, the analytic solution of the Biharmonic equation can be exploited to achieve simple mathematical expressions characterising the height and radius of

a tablet. Therefore, these mathematical expressions can be used as a tool for changing the shape and size of the generated PDE-based representation of tablets.

## **Chapter 5**

# **Modelling the Mechanical Behaviour of Pharmaceutical Tablets**

### **5.1 Introduction**

Chapter 5 outlines the stress functions for compressed round and spherical-shaped tablets. Section 5.2 discusses the solution to an axisymmetric boundary value problem for a finite cylinder with assigned stresses previously used for compressing cylindrical objects, together with details of the axial compression process used to characterise the displacement behaviour of pharmaceutical powders and the PDE-based representation of a tablet. The contact model for elastic-plastic granules by slow compression is described in Section 5.3. The

theoretical and PDE-based results for a compressed tablet of spherical shape are also presented and discussed.

## 5.2 Solution of the Love's Stress Function in Cylindrical Coordinates

Axisymmetric or axisymmetrical are adjectives which refer to an object with only one axis of rotation, known as cylindrical symmetry (Sekula 2010). There exist a large number of practical problems involving geometrical features with a natural axis of symmetry, such as a solid cylinder. For instance, the problem of equilibrium on an elastic cylinder of finite length subject to a surface load is one of the most discussed problems in the theory of elasticity (Liang et al. 2008; Sburlati 2009). According to Sburlati (2009), the use of a Love's stress function may reduce the three-dimensional axisymmetric elastic problem into a two-dimensional one.

In order to find a solution for this problem, a circular, finite, homogeneous and isotropic elastic cylinder of thickness,  $t$ , and radius,  $c$ , with the origin at the centre of the top plane subject to an axisymmetric load,  $F$ , has been considered (Ding et al. 2005; Sburlati 2009). Figure 5.1 shows the stress components acting on each face of the loaded cylinder. The stress components acting on each face of the wedge from the loaded cylinder are visualised in Figure 5.1(b).

The normal stress components,  $\sigma_z$ ,  $\sigma_\theta$  and  $\sigma_r$ , are known respectively as the axial, hoop and radial stresses and are the principal stresses at a given stressed point,  $B$ . Each component has double subscripts (except for the normal stress components), where the first subscript defines the face on which the stress component acts and the second subscript denotes the direction in which the stress component acts. For instance,  $\sigma_z$ ,  $\tau_{zr}$  and  $\tau_{z\theta}$  are stress components on the  $z$  surface and acting in the  $z$ ,  $r$  and  $\theta$  directions respectively.

The state of stress at point  $B$  is written as an array of nine stress components comprising three normal stresses and six shear stresses

$$\zeta = \begin{pmatrix} \sigma_z & \tau_{z\theta} & \tau_{zr} \\ \tau_{\theta z} & \sigma_\theta & \tau_{\theta r} \\ \tau_{rz} & \tau_{r\theta} & \sigma_r \end{pmatrix}, \quad (5.1)$$

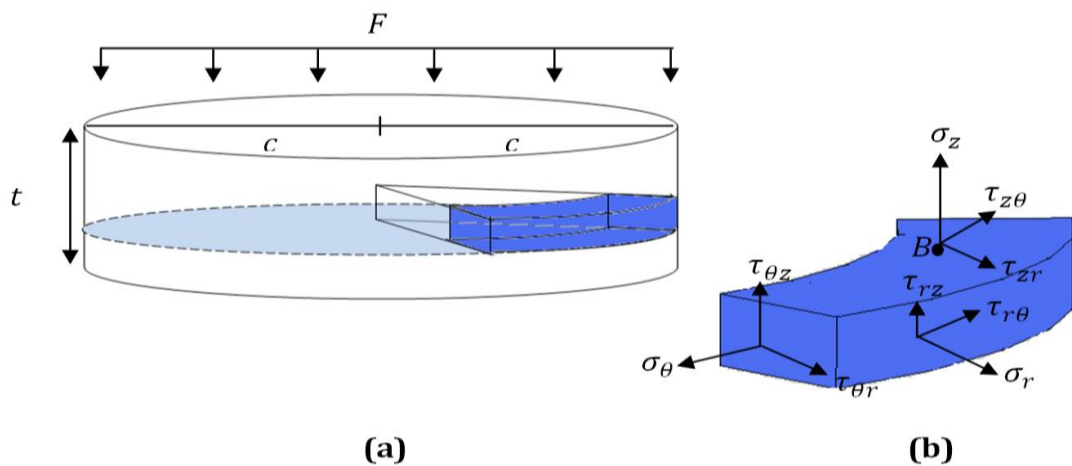


Figure 5.1: Stresses in cylindrical coordinates where  $\sigma_z$ ,  $\sigma_\theta$  and  $\sigma_r$  are the normal stress components in the  $z$ ,  $\theta$  and  $r$  directions respectively.

where each row represents the stress components acting on a particular set of surfaces ( $z, \theta, r$ ) and on the other hand, each column consists of the stress components acting in a particular coordinate direction. A stress component on a surface is considered positive if it acts parallel to the direction of the corresponding axis.

The displacement of a solid cylinder due to external loads is completely described when the displacement of all its parts are defined respectively. In cylindrical coordinates,  $\omega_z, \varepsilon_\theta$  and  $\mu_r$  are axial, hoop and radial displacements, parallel to the  $z, \theta$  and  $r$  directions respectively. Any point originally at  $(z, \theta, r)$  is displaced to  $(z + \omega_z, \theta + \varepsilon_\theta, r + \mu_r)$  after the compression process is completed (Baxter Brown 1973). The components  $\varepsilon_\theta, \tau_{z\theta}$  and  $\tau_{r\theta}$  vanish if the compression of the cylinder is due to torsionless axisymmetry.

In the case of the axisymmetric problem in the absence of body forces, the stress and displacement components can be expressed in terms of a Love's stress function,  $\phi(r, z)$ , as (Timoshenko and Goodier 1970)

$$\sigma_z = (2 - \gamma) \frac{\partial}{\partial z} \nabla^2 \phi - \frac{\partial^3 \phi}{\partial z^3}, \quad (5.2)$$

$$\sigma_r = \gamma \frac{\partial}{\partial z} \nabla^2 \phi - \frac{\partial^3 \phi}{\partial z \partial r^2}, \quad (5.3)$$

$$\sigma_{\theta} = \gamma \frac{\partial}{\partial z} \nabla^2 \phi - \frac{1}{r} \frac{\partial^2 \phi}{\partial z \partial r}, \quad (5.4)$$

$$\tau_{rz} = (1 - \gamma) \frac{\partial}{\partial r} \nabla^2 \phi - \frac{\partial^3 \phi}{\partial r \partial z^2}, \quad (5.5)$$

$$\mu_r = -\frac{1}{2G} \frac{\partial^2 \phi}{\partial z \partial r}, \quad (5.6)$$

$$\omega_z = \frac{1}{2G} \left[ 2(1 - \gamma) \nabla^2 \phi - \frac{\partial^2 \phi}{\partial z^2} \right], \quad (5.7)$$

where  $G$  is the shear modulus and  $\gamma$  is the Poisson's ratio. The function  $\phi(\mathbf{r}, \mathbf{z})$  in Equations (5.2) – (5.7) is Biharmonic and satisfies the following Partial Differential Equation (Love 1892)

$$\nabla^2 \nabla^2 \phi = \left( \frac{\partial^2}{\partial r^2} + \frac{1}{r} \frac{\partial}{\partial r} + \frac{\partial^2}{\partial z^2} \right)^2 \phi = 0, \quad (5.8)$$

where  $\nabla^2$  is the three-dimensional Laplace's operator.

The development of analytical approaches to the solution of boundary value problems is important in many areas such as in engineering (Grinchenko 2003) and physics (Liang and Jeffrey 2009), not only for theoretical motivations but also as benchmarks for solutions obtained by numerical methods. A number of models have been developed and modified to find solutions of a symmetrically loaded cylinder that rigorously satisfies all the boundary conditions on the side surface or on both ends of the cylinder.

The work presented by Liang et al. (2008) proposes an analytical solution of a thick-walled cylinder subjected to a uniform pressure at two ends, with different inner and outer surface pressures that are constant circumferentially but vary linearly along the axis by applying a Love's stress function. The solution is obtained by assuming that the condition of constraint and the external loads are all symmetrical with respect to any plane passing through the  $z$ -axis, and that the stress and displacement components will have the same symmetry in the functions of two coordinates,  $r$  and  $z$ . More recently, another method has been proposed to solve of an axisymmetric boundary value problem for a compressed finite elastic cylinder by utilising the Love's stress function with a Bessel expansion (Sburlati 2009). The solution provides a full description of the local behaviour of the radial and shear stresses at the sides of the plate and long cylinder, particularly those near the corner points.

However, the solutions proposed by Liang et al. (2008) and Sburlati (2009) seem complicated and difficult to modify. Moreover, the solution obtained by Liang et al. (2008) for a compressed thick-walled cylinder is not practical to apply to a compressed round tablet. A simple solution has been found in work done by Ding et al. (2005). They found a three-dimensional analytical solution for a uniformly loaded isotropic circular plate by making use of the Love's stress function subject to two different types of clamped edges. The solution is obtained by utilising the Biharmonic polynomial potential functions with eight terms

$$\begin{aligned}
\phi = & \frac{1}{3}a_6(16z^6 - 120z^4r^2 + 90z^2r^4 - 5r^6) + b_6(8z^6 - 16z^4r^2 - 21z^2r^4 + 3r^6) \\
& + a_4(8z^4 - 24z^2r^2 + 3r^4) + b_4(2z^4 + z^2r^2 - r^4) + a_3(2z^3 - 3zr^2) + b_3(z^3 + zr^2) \\
& + a_2(2z^2 - r^2) + b_2(z^2 + r^2), \tag{5.9}
\end{aligned}$$

where  $a_i, b_i$  ( $i = 2,3,4,6$ ) are unknown constants to be determined from the boundary conditions. Ding et al. (2005) employed two different types of boundary conditions and the results showed that different boundary conditions exert no influence on  $\sigma_z$  and  $\tau_{rz}$ .

In order to model the mechanical behaviour of an axially compressed PDE-based representation of a round tablet, Equation (5.9) together with a particular set of boundary conditions will be used. The results obtained from this model will be compared with the experimental results of the compressed pharmaceutical powder.

### 5.2.1 Simulation of Axial Compression on the PDE-based Tablets

Tablets of thickness 3mm were prepared at the Institute of Pharmaceutical Innovation (IPI), University of Bradford and were composed of 300 mg of  $\alpha$ -lactose monohydrate (Pharmatose 200 M, DMV International, The Netherlands). Tablets were made by uni-axial compression using circular flat faced punches in a die with a diameter of 10 mm where the lower punch remains stationary, as shown

in Figure 5.2. This process is known as Single Ended Compression (SEC) (Wu et al. 2008). The  $\alpha$ -lactose monohydrate is a common excipient in a pharmaceutical tablet production. This is due to its stability, low hygroscopicity and hardness (Ilić et al. 2009), being capable of supporting external loads such a packaging, but at the same time being easy to dissolve for rapid assimilation. Particle size for the powder was measured by Laser Diffractometer, Mastersizer 2000 Ver. 2.00 (Malvern Instruments, Malvern, UK), with values ranging from 63 – 90  $\mu\text{m}$ . The values of the Young's modulus and Poisson's ratio of  $\alpha$ -lactose monohydrate are  $E = [2550, 4350] \text{ N/mm}^2$  and  $\gamma = [0.12, 0.5]$  respectively (Perkins et al. 2007).

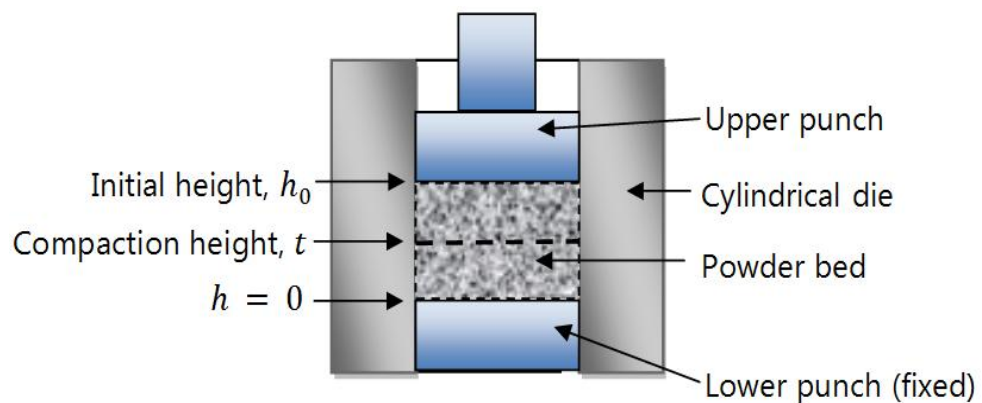


Figure 5.2: Schematic representation of the powder compaction process.

The  $\alpha$ -lactose monohydrate, with true density,  $\rho_{\text{true}} = 1.3 \text{ mg/mm}^3$ , was poured into a cylindrical die. The true density of the powder had been measured using an Accupyc 1330 helium pycnometer (Micromeritics Ltd.). The density-pressure profile was obtained by using the "in-die" method, whereby the compact's dimensions were measured from the punch displacements. The powder was compressed and decompressed by the upper punch at 100 mm/s. The values of the load and displacement were taken only after the load has started to increase and until it became linear. When the punch reaches the height of approximately 6 mm, it starts receiving resistance from the powder as it rearrange itself and the load starts increasing from  $0.05 \text{ N/mm}^2$ . The load continues to increase linearly until a compact is formed and, once the compact with maximum strength is formed, the load and displacement relation is no longer linear. The powder compression process involves only an axial displacement: that is, the radius is fixed and only the height of the compressed powder is changed.

From the experimental procedure explained above, the axial displacement of a compressed PDE-based tablet can be obtained by setting up appropriate boundary conditions as follows

$$\sigma_z = 0, \quad \tau_{rz} = 0 \quad \text{when } z = 0, \quad (5.10a)$$

$$\sigma_z = -P, \quad \tau_{rz} = 0 \quad \text{when } z = h_0, \quad (5.10b)$$

$$\omega_z = 0, \quad \frac{\partial \omega_z}{\partial r} = 0 \quad \text{when } z = 0, \quad (5.10c)$$

$$\mu_r = 0, \quad \text{when } r = c, \quad (5.10d)$$

where  $P$  is the axial pressure,  $c$  is the radius of the die or tablet and  $h_0$  is the initial height of the powder bed. As can be seen in Equation (5.10c), there is no axial displacement at the bottom plane of the powder bed near the lower punch as well as the radial displacement at the die wall (Equation (5.10d)), since there is no movement occurring near these areas. Additionally, it is assumed that the shear stress is zero at the bottom and upper plane of the powder bed. The stress and displacement components,  $\sigma_z, \tau_{rz}, \mu_r$  and  $\omega_z$ , can be expressed in terms of unknown constants by substituting Equation (5.9) into Equations (5.2) – (5.7), therefore

$$\begin{aligned} \sigma_z = & a_6(960r^2z - 640z^3) + b_6[(448 - 704\gamma)z^3 - (1728 - 1056\gamma)zr^2] \\ & - 192a_4z + 4b_4(16 - 14\gamma)z - 12a_3 + b_3(14 - 10\gamma), \end{aligned} \quad (5.11)$$

$$\begin{aligned} \tau_{rz} = & a_6(960z^2r - 240r^3) + b_6[(432 - 264\gamma)r^3 + (-672 + 1056\gamma)rz^2] \\ & + 96a_4r - 2b_4(16 - 14\gamma)r, \end{aligned} \quad (5.12)$$

$$\begin{aligned} \mu_r = & \frac{1}{2G} [a_6(320z^3r - 240r^3z) + b_6(128z^3r + 168zr^3) + 96a_4rz \\ & - 4b_4rz + 6a_3r - 2b_3r], \end{aligned} \quad (5.13)$$

$$\begin{aligned} \omega_z = \frac{1}{2G} \{ & b_6[(174 - 132\gamma)r^4 - (864 - 1056\gamma)r^2z^2 + (112 - 352\gamma)z^4] \\ & - a_6(160z^4 - 480r^2z^2 + 60r^4) + b_4[(32 - 56\gamma)z^2 - (30 - 28\gamma)r^2] \\ & - a_4(96z^2 - 48r^2) + (14 - 20\gamma)b_3z - 12a_3z + (10 - 12\gamma)b_2 - 4a_2 \}. \end{aligned} \quad (5.14)$$

Since  $a_2$  and  $b_2$  appear only in Equation (5.14) and the simulation involved only seven boundary conditions, these unknowns are replaced by  $c_2$  where  $c_2 = (10 - 12\gamma)b_2 - 4a_2$ .

Equations (5.11) – (5.14) are substituted into the boundary conditions to determine the seven unknown constants

$$c_2 = \frac{-Pr^2(\gamma - 2)}{8h_0}, \quad (5.15a)$$

$$a_3 = \frac{-Pz(4z^2 - 4z^2\gamma + 3c^2\gamma - 3r^2\gamma)(5\gamma - 7)}{180h_0r^2(\gamma - 1)}, \quad (5.15b)$$

$$b_3 = \frac{Pz(4z^2 - 4z^2\gamma + 3c^2\gamma - 3r^2\gamma)}{30h_0r^2(\gamma - 1)}, \quad (5.15c)$$

$$a_4 = \frac{-P(-1 + 7\gamma)}{1344h_0}, \quad b_4 = \frac{P}{56h_0}, \quad (5.15d)$$

$$a_6 = \frac{-P(-7 + 11\gamma)}{5280h_0r^2}, \quad b_6 = \frac{P}{528h_0r^2}. \quad (5.15e)$$

This leads to the expression of the axial displacement

$$\omega_z = \frac{50Pz^2}{Gh_0} \left[ \frac{z^2\gamma}{r^2} - \frac{(1-\gamma)}{2} + \frac{\gamma^2}{\gamma-1} \left( 1 - \frac{c^2}{r^2} \right) \right], r > 0 \quad (5.16)$$

where  $z$  and  $r$  are any points in  $z$  and  $r$  directions respectively, while  $G$  is given by

$$G = \frac{E}{2(1+\gamma)}. \quad (5.17)$$

### 5.2.2 Results and Discussion

The experimental data (a set of forces and displacements of compressed  $\alpha$ -lactose monohydrate, as shown in **Appendix B**), together with the fixed true density and compacted mass value, were analysed using the Heckel model from which powder deformation mechanisms are determined using the apparent yield pressure. However, experimental data are commonly not linear, as can be seen in Figure 5.3. Nonlinear curves exist at regions with both very low pressure (Zone A) and high pressure (Zone C), whilst linearity is shown only in the centre pressure range (Zone B). The curvature at Zone A is due to particle rearrangement and fragmentation, while it is agreed that the linear part represents particle plastic deformation (Gabaude et al. 1999). For the Heckel analysis, only data varying from 10 N/mm<sup>2</sup> up to 50 N/mm<sup>2</sup> in pressure (Zone B) are used because this range showed the best linearity.

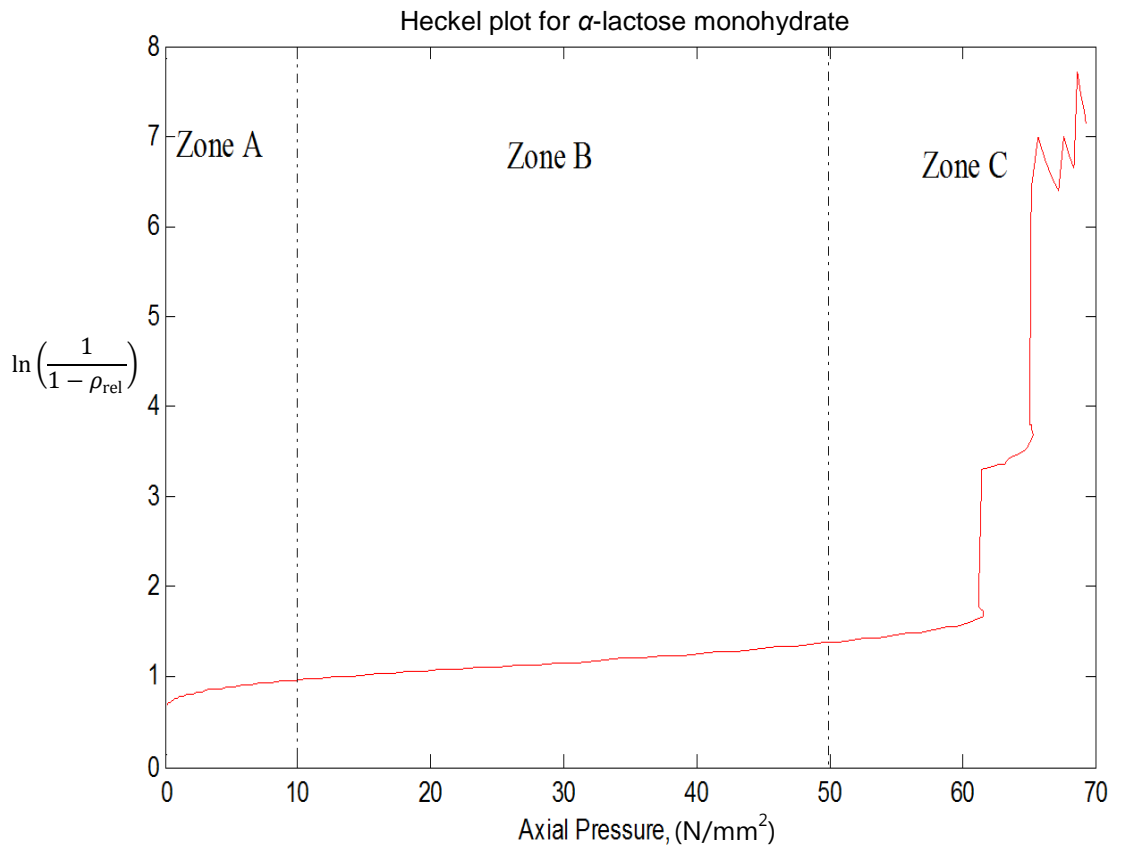


Figure 5.3: Heckel plot of compressed  $\alpha$ -lactose monohydrate using experimental data.

Due to the different initial porosity of the particles used in the experiment and simulation based on the PDE-based formulation proposed in this work, Equation (5.16) has been modified by adding an adjustment constant,  $\omega_{z0}$ . This leads to

$$\omega_z = \omega_{z0} + \frac{100Pz^2(1+\gamma)}{Eh_0} \left[ \frac{z^2\gamma}{r^2} - \frac{(1-\gamma)}{2} + \frac{\gamma^2}{\gamma-1} \left( 1 - \frac{c^2}{r^2} \right) \right]. \quad (5.18)$$

This constant is obtained from the difference between the initial axial displacement (after the particle rearrangement - Zone A) of the experiment and the

simulation (PDE-based model). For example, in the case of  $\alpha$ -lactose monohydrate, the axial displacement of the powder bed at pressure  $10 \text{ N/mm}^2$  is  $-1.2935 \text{ mm}$ . Meanwhile, the axial displacement of the PDE-based representation of a round tablet at the same pressure, which is measured using Equation (5.16) with the value of  $E = 2640 \text{ N/mm}^2$  and  $\gamma = 0.21$ , is  $-0.2155 \text{ mm}$ . Therefore, in order to ensure that both the powder and the parametric tablet have the same height at the beginning of plastic deformation in Heckel analysis (Zone B), the value of  $\omega_{z0}$  is set as  $-1.078 \text{ mm}$ .

The change in height of the PDE-based tablet due to axial pressure ranging from  $10 \text{ N/mm}^2$  to  $50 \text{ N/mm}^2$  is measured using Equation (5.18) with the material properties as previously described. The density-pressure relationship for the  $\alpha$ -lactose powder is plotted as a best linear regression line, as shown in Figure 5.4, and the trend is compared with the simulation prediction. It is observed that the slope of the simulation is steeper than the slope of the experimental one. Additionally, both lines have a slightly different  $y$ -intercept. Table 5.1 summarises the estimated data obtained from the Heckel diagram for both simulation and experiment. From the graphs, it is found that the yield pressure of experimentally compressed  $\alpha$ -lactose is higher than that obtained from the developed model, where the values are  $102.04 \text{ N/mm}^2$  and  $93.458 \text{ N/mm}^2$  respectively. It can be concluded that the plasticity of  $\alpha$ -lactose is very low since it has a low value of  $K$  (or high yield pressure).

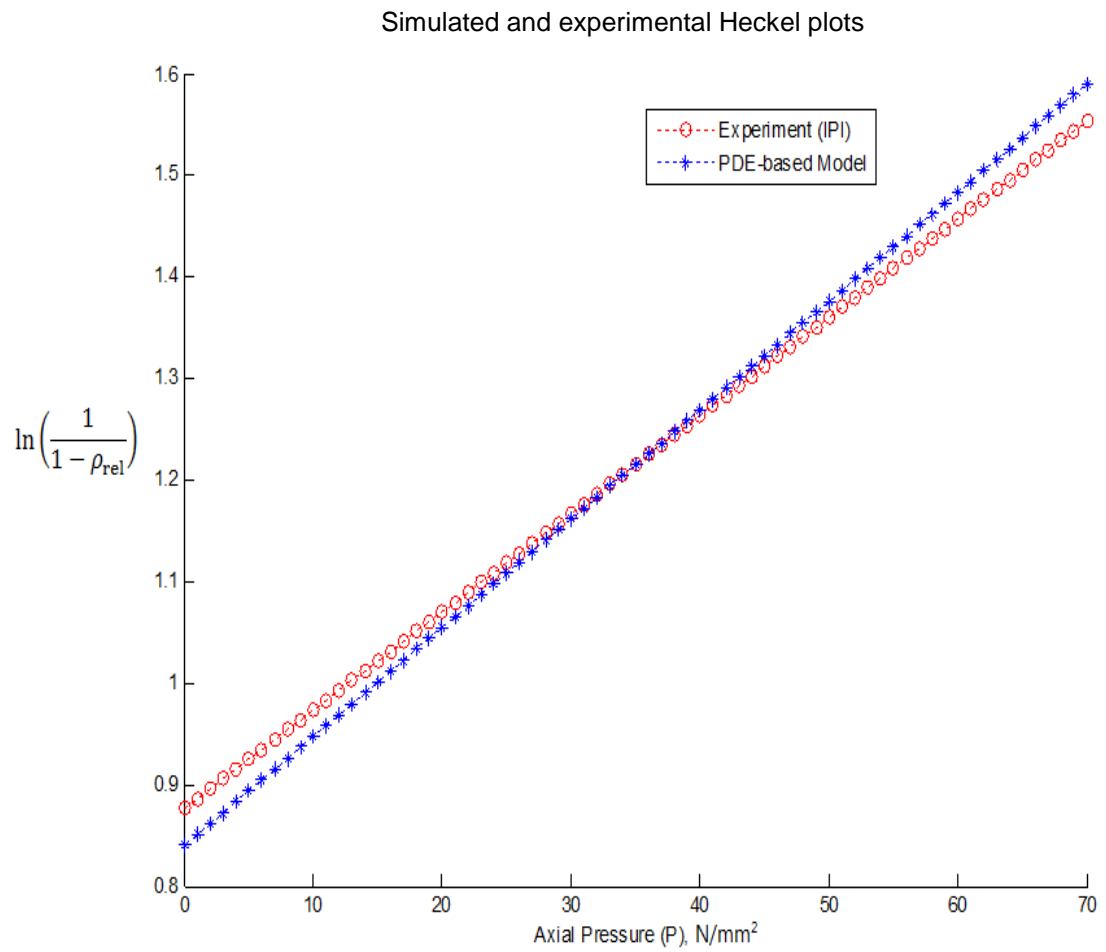


Figure 5.4: Comparison between the Heckel plot of the simulated compression and the experimental result on  $\alpha$ -lactose powder.

Table 5.1: Heckel's parameters for  $\alpha$ -lactose from experiment and simulation.

Heckel Parameter	Experiment	PDE-based	FEM	PDE-based
	(IPI)	Model	Simulation	Model
Slope, $K$ ( $\text{mm}^2/\text{N}$ )	0.0098	0.0107	0.0031	0.0041
y-intercept, $A$	0.8738	0.8402	0.8663	0.6420
Yield Pressure, $P_y$ ( $\text{N}/\text{mm}^2$ )	102.04	93.4579	322.5806	243.902

Another set of force-displacement data of compressed Lactose in a cylindrical die of radius 4 mm has been found in Wu et al. (2008). The data was generated from the Finite Element Method (FEM) simulation with the value of the true density, Young's modulus and Poisson's ratio of Lactose are  $1.548 \text{ mg/mm}^3$ ,  $3.57 \text{ N/mm}^2$  and 0.12 respectively. This data has been converted to the relative density-pressure relationship with the linear part starting from  $60 \text{ N/mm}^2$  to  $230 \text{ N/mm}^2$ . The graph is presented in Figure 5.5 together with a Heckel plot of the PDE-based tablet. It shows that both lines are not in very good agreement because there is a large difference between their slopes and  $y$ -intercepts. The calculated  $P_y$  of Lactose in FEM and PDE-based simulations are  $322.581 \text{ N/mm}^2$  and  $243.902 \text{ N/mm}^2$  respectively, as shown in Table 5.1.

The results shown in Figure 5.4 prove that the solution of Love's stress function can be utilised to measure the axial displacement of the compressed solid PDE-based representation of a tablet. The difference between the  $y$ -intercept of the experiment and the simulation is very small. This is expected because the simulation's axial displacement values are calculated from the parametric representation of the pharmaceutical tablet. Furthermore, the PDE-based tablet does not take the particle size and the degree of porosity into account. For the results illustrated in Figure 5.5, the difference occurs because the FEM simulation has been carried out using the DPC model, which considers the hardening or plasticity of the powder as well as the interparticle friction (Wu et al. 2008). On the

other hand, the result obtained from the developed model shown in Equation (5.18) is fully based on the elasticity and does not consider the unloading behaviour of the powder.

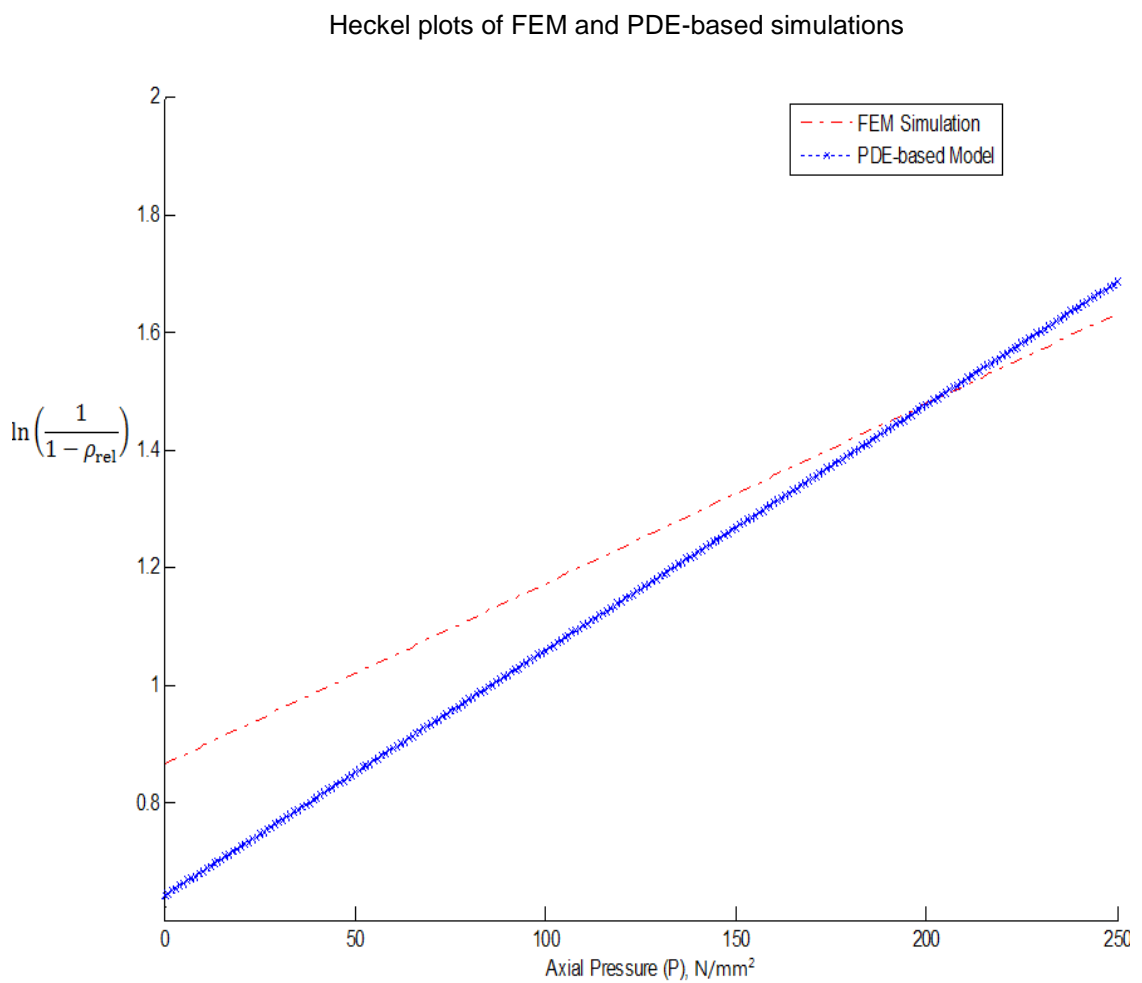


Figure 5.5: Density-pressure linear regression lines of FEM versus PDE simulations on Lactose powder.

However, the validity of the developed model is only verified at the lower pressure, where the deformation of the powder is indicated. Furthermore, this model can be applied only to a round tablet defined by a set of boundary conditions that depend on the chosen tableting process. Consequently, a more general model for characterising the stress distribution should be developed.

### **5.3 Elastic-Plastic Contact Deformation of a Spherical Granule**

In this section, the mechanical properties of spherical granules are discussed in detail. According to the pharmaceutical definition, granules are produced through a granulation process which involves either wet or dry granulation. During this process, several powder particles are collected and bonds between them are created to make a larger form. Compared to powders, granules have better flow behaviour and can compress well, even at a low pressure (Antonyuk et al. 2005). The work by Fu et al. (2005) has reported that fast-dissolving tablets are formed from highly plastic granules, which are produced by a wet granulation process.

Many studies have been carried out to investigate the mechanical behaviour of elastic-plastic granules in compression tests by varying the size and shape of the granules. For dry granular materials, the mechanical behaviour is measured by several methods, such as ring-shear tests, grain characterisation and simple ana-

logue experiments (Panien et al. 2006). By contrast, the mechanical behaviour of wet granules needs to be conducted numerically since they have more complicated behaviour compared to that of dry granules (Schulz and Schulz 2006). It has been reported by Herbold et al. (2008) that the crushing strength of the granule decreases as the granule size increases. Furthermore, researchers have shown that a spherical granule has lower flow stresses than the non-spherical counterpart (Iveson and Page 2005). According to them, both shapes exhibit transformation from brittle to plastic failure during the uniaxial compression test.

The Hertzian contact law has been widely used for a few decades in discrete (Wellmann et al. 2008) and finite element (Kabir et al. 2008) simulations to study the flow and compression behaviours of elastic granules. Recently, a new force-displacement model for an elastic-plastic granule has been developed (Antonyuk et al. 2010). This model is derived by extending the model of Tomas (2001), whereby the adhesion in the contact has been disregarded. Elastic and elastic-plastic laws are used in continuum mechanics studies since the properties of granules can be either elastic or elastic-plastic. An elastic object is capable of recovering its original shape and volume after being compressed or stretched (Owolabi et al. 2010), while plastic behaviour is in contrast to elastic behaviour. An elastic-plastic granule is a granule that has both elastic and plas-

tic properties. Therefore, it is necessary to understand the mechanical behaviour of granules across the elastic, elastic-plastic and plastic range.

When a soft spherical granule is compressed by two flat surface punches, as shown in Figure 5.6(a), two contact areas are formed. The contact area deforms as a circle with radius,  $r_c$ , which depends on the granule radius,  $r_s$ . According to the existing literature, the radius of the contact area is smaller than that of the deformed area (Antonyuk et al. 2010). The shape of the compressed granule is illustrated in Figure 5.6(b), where the small spheres in the granule (before and after compression) represent the group of powder particles. For an elastic-plastic granule, the plastic deformation starts when the pressure reaches the micro-yield strength,  $s_y$ . However, some authors have reported that plastic deformation begins when the maximum contact pressure reaches at 1.6 times of the uniaxial yield stress (Li et al. 2009). Before the yield point,  $p_p$ , is reached, the force-displacement curve of the loaded spherical granule shows a nonlinear elastic deformation. It has been reported by Tomas (2001) that the force,  $F_e$ , during the elastic deformation of a spherical granule follows Hertz law, as below

$$F_e = \frac{E}{3(1-\nu^2)} \sqrt{2r_s \omega_z^3}, \quad (5.19)$$

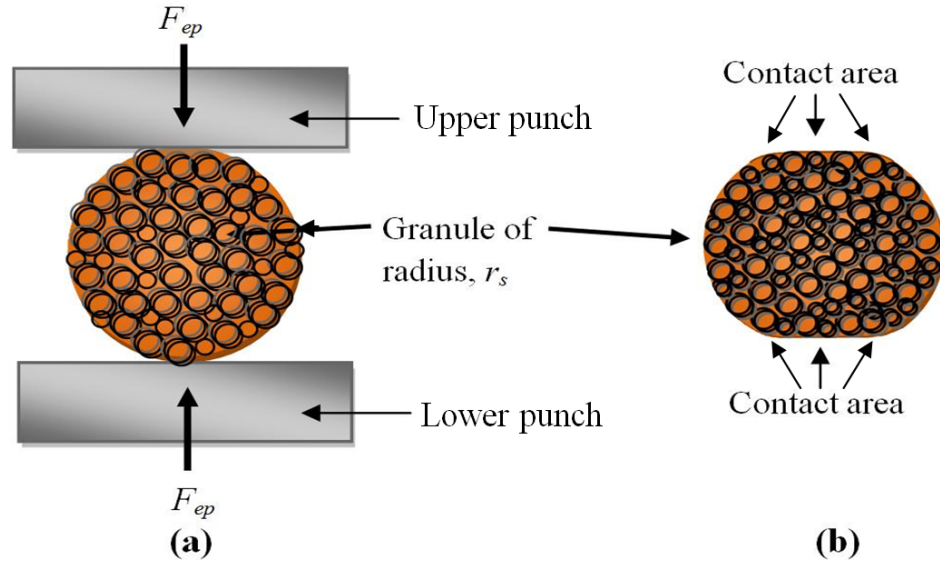


Figure 5.6: Compression of a spherical granule. (a) The slow compression of a spherical granule with two contact points. (b) The shape of a granule after the elastic-plastic deformation.

where  $\omega_z$  is the full axial displacement. The material behaviour changes from elastic to elastic-plastic at the yield point, as shown in Figure 5.7. When the pressure exceeds the yield pressure,  $P_y$ , the total axial displacement of the compressed elastic-plastic granule at force  $F_{ep}$ , is given by (Antonyuk et al. 2010)

$$\omega_z = \frac{1}{81r_s s_y} \left[ \frac{J^{1/3}}{\pi} + \frac{\omega'_z s_y r_s (\omega'_z \pi s_y r_s + 324 F_{ep})}{J^{1/3}} + \frac{\omega'_z \pi s_y r_s + 162 F_{ep}}{\pi} \right], \quad (5.20)$$

where

$$J = \omega'_z \pi s_y r_s \left( 1458 F_{ep} \sqrt{F_{ep} (2\omega'_z \pi s_y r_s + 729 F_{ep}) + 39366 F_{ep}^2} + (\omega'_z \pi s_y r_s)^2 + 486 \omega'_z \pi s_y r_s F_{ep} \right), \quad (5.21)$$

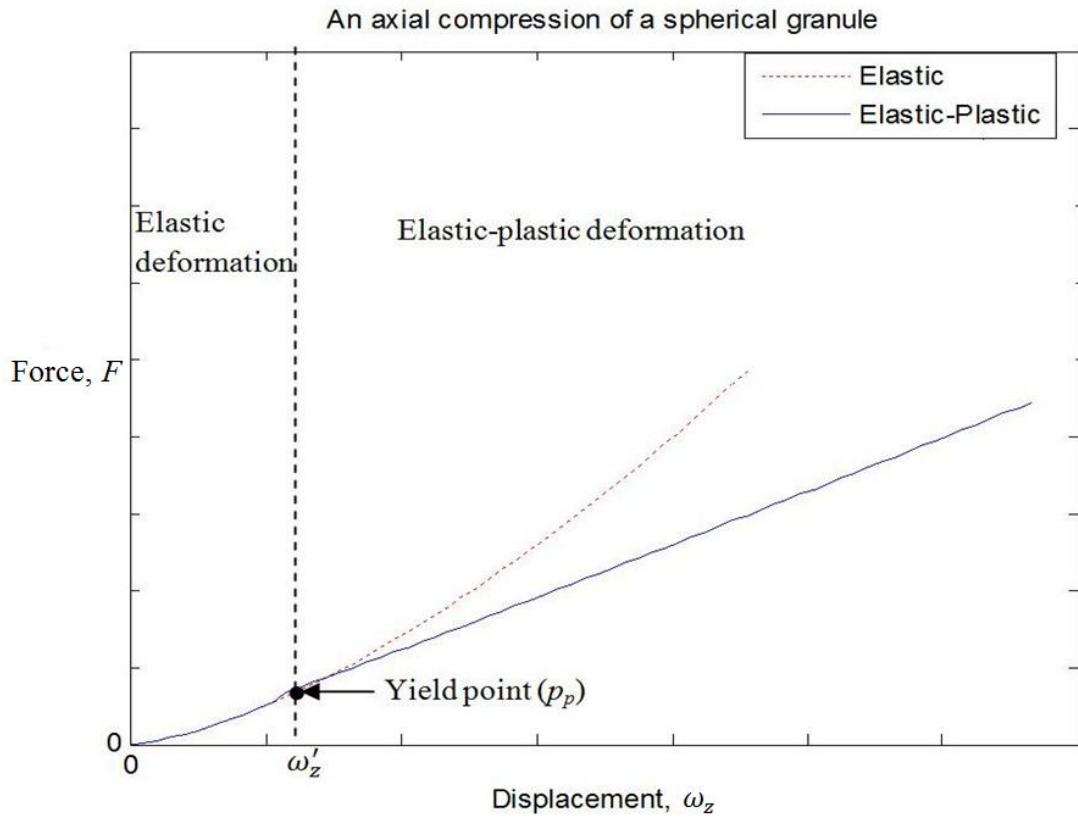


Figure 5.7: Force-displacement curve of a spherical granule during compression. This graph has been reproduced from Antonyuk et al. (2010).

and  $\omega'_z$  is the displacement at the yield point and the micro-yield strength is derived as

$$s_y = \frac{2E}{\pi(1-\gamma^2)} \sqrt{\frac{\omega'_z}{r_s}}. \quad (5.22)$$

Furthermore, the radius of the contact area of the granule during the elastic-plastic deformation is given by

$$r_c = \sqrt{r_s \omega_z}. \quad (5.23)$$

In this study, the mechanical behaviour of a spherical tablet is assumed to be similar to the behaviour of a spherical granule. This is because some authors have reported that many tablets are formed from granules, and these tablets have consistent hardness and uniform content. Therefore, the contact law of a granule, as found in the literature, is used to measure the displacement of a compressed spherical tablet, hence relating the physics of the law to the parametric shape of the tablet in question.

### 5.3.1 Deformation of a PDE-Based Spherical Tablet

The original shape of the solid PDE-based representation of a spherical tablet has been shown in Figure 4.6(b). In order to study the mechanical behaviour of a compressed spherical tablet using the PDE method, the mathematical properties of the Biharmonic equation have been exploited to achieve simple mathematical expressions characterising the shape of the tablet. The height and radius of this parametric tablet have been presented in Equations (4.16) and (4.22)

$$h = a_{01z} \quad \text{and} \quad r_s = \sqrt{A_{1x}^2 + A_{1y}^2}, \quad (5.24)$$

respectively. The shape of the compressed spherical tablet can be obtained by relating Equations (5.20) – (5.23) with Equation (5.24). The new height of the PDE-based tablet after it has been compressed is given by

$$a_{01z(\text{after})} = a_{01z(\text{before})} - \omega_z, \quad (5.25)$$

and its contact radius can be written as

$$A_{1x}^2|_{u=1} + A_{1y}^2|_{u=1} = \sqrt{A_{1x}^2 + A_{1y}^2} \omega_z. \quad (5.26)$$

Thus, the height, radius and contact area of the tablet in this particular shape due to uniaxial compression, are represented by analytic expressions relating the coefficients associated with the solution to the Biharmonic equation. The theoretical results obtained from the model proposed by Antonyuk et al. (2010) will be compared with the simulation results generated from the PDE method.

### 5.3.2 Results and Discussion

Simulations of the compressed spherical tablet have been carried out on two different elastic-plastic industrial materials. Only the upper hemisphere is considered in the simulation due to the geometrical and loading symmetries. It is assumed that the contact between the pharmaceutical tablet and the punches is frictionless. The details of corresponding material properties have been obtained from the literature and are listed in Table 5.2.

Table 5.2: Mechanical characteristics of the examined materials by compression.

<b>Material</b>	<b>Radius (mm)</b>	<b><math>E</math> (N/mm<sup>2</sup>)</b>	<b><math>\gamma</math></b>	<b><math>s_y</math> (N/mm<sup>2</sup>)</b>
Lactose (Wu et al. 2003)	0.1	2080	0.30	616.6
Köstrolith (Antonyuk et al. 2005)	0.7	820	0.28	71.007

Figure 5.8 shows two graphs of PDE coefficients,  $a_{01z}$ ,  $a_{11x}$ ,  $a_{12x}$ ,  $a_{13x}$  and  $a_{14x}$ , obtained from Equations (5.25) and (5.26). It is found from the simulation that the value of  $A_{1y}$  is zero. These coefficients are responsible for creating the shape of distorted spherical tablets made of Lactose and Köstrolith. All plots are displayed as best linear regression lines and, as can be seen in both graphs, each coefficient shows the same pattern, except  $a_{11x}$ . The slope and  $y$ -intercept of each line are given in Table 5.3. The data from this table can be used to estimate the height and contact area of the compressed spherical tablet. For instance, the values of  $a_{01z}$ ,  $a_{11x}$ ,  $a_{12x}$ ,  $a_{13x}$  and  $a_{14x}$  at a force equal to 3.5 N for Köstrolith are 0.672, -0.0656, 0.766, -0.1 and 0.826 respectively. Therefore, the estimated height of the deformed tablet in spherical shape is 1.3440 mm and its contact area is 0.1355 mm<sup>2</sup>. Meanwhile, the theoretical values of these variables at the same force are 1.3444 mm and 0.1395 mm<sup>2</sup> respectively. It is interesting to note that the simulated values show little difference from those obtained theoretically.

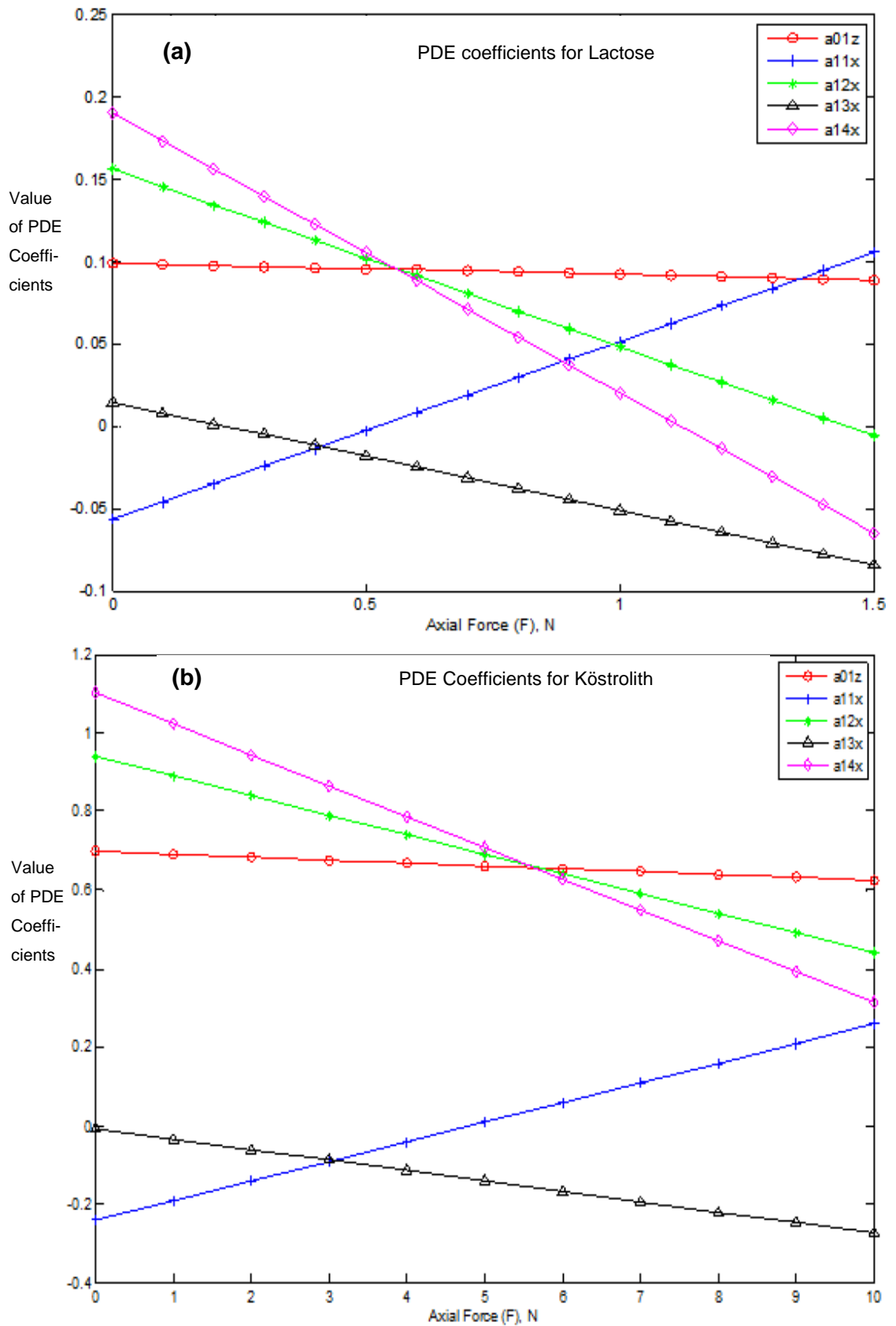


Figure 5.8: PDE coefficients representing the height and contact area of the compressed spherical (a) Lactose and (b) Köstrolith.

Table 5.3: The parameters of best-fit linear regression line for PDE coefficients.

PDE coefficients	Lactose		Köstrolith	
	Slope	y-intercept	Slope	y-intercept
$a_{01z}$	-0.0066	0.0993	-0.0073	0.6978
$a_{11x}$	0.1081	-0.0565	0.0490	-0.2402
$a_{12x}$	-0.1081	0.15651	-0.0490	0.9402
$a_{13x}$	-0.0660	0.0149	-0.0265	-0.0076
$a_{14x}$	-0.1704	0.1909	-0.0789	1.1021

The comparison between the theoretical and simulated contact radius as a function of the axial force is shown in Figure 5.9. Given that this work focuses on the elastic-plastic deformation behaviour, both graphs start after the load reaches the yield point, with Lactose at force 0.58 N and Köstrolith at force 0.46 N. It is observed that the contact radius of spherical Lactose and Köstrolith, as measured by Equation (5.23), differ slightly from those generated by Equation (5.26) at lower forces. However, as the contact force is increased, the curve generated by the PDE method fits the theoretical ones. The shapes of the solid PDE-based representation of a spherical Köstrolith tablet at different forces are illustrated in Figure 5.10. The generated object consists of 5082 nodes and 4000 cuboids, which is produced by defining the parameter  $s_x = s_z = 11$  and  $s_y$  equal to 21.

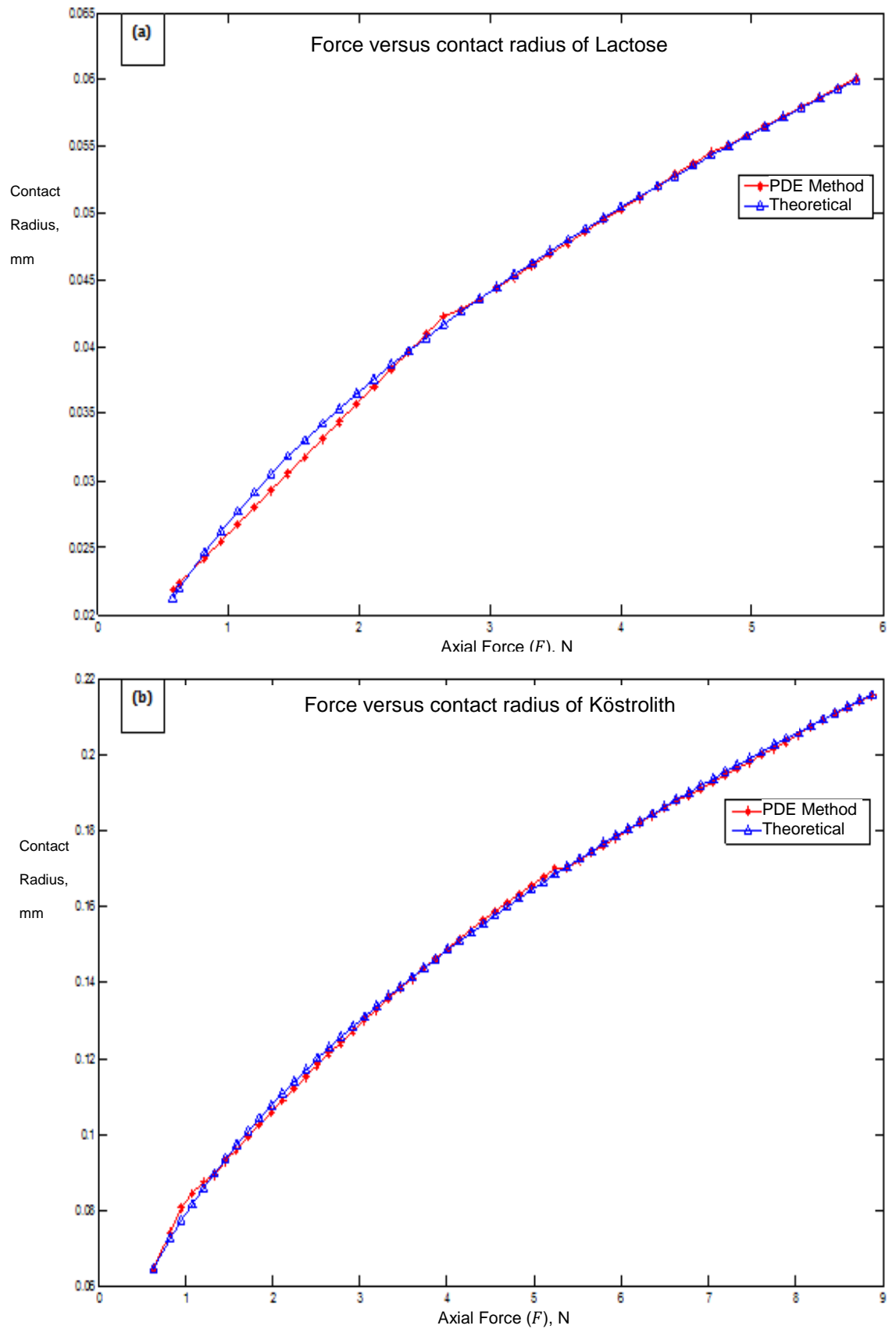


Figure 5.9: Comparison between the radius of contact area of the theoretical and PDE-based spherical (a) Lactose and (b) Köstrolith.

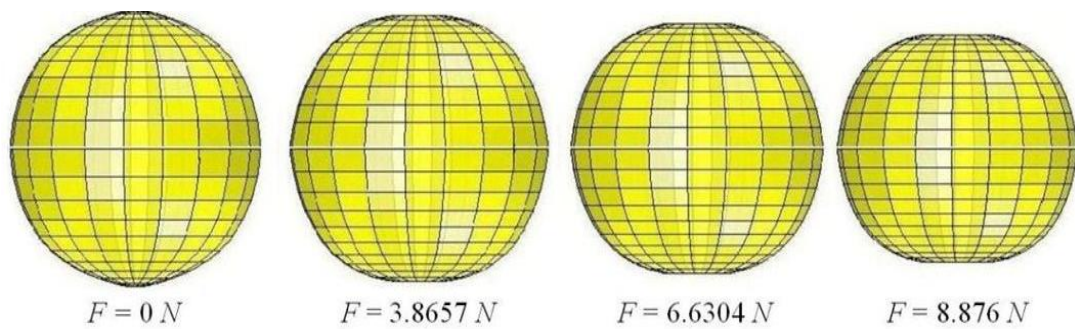


Figure 5.10: Solid PDE-based representation of compressed spherical tablets at different force values.

Figure 5.11 shows the theoretical and simulated displacements of a spherical tablet made of Köstrolith, subject to the axial force. The force-displacement data for this tablet have been plotted as Heckel graphs. The graph shows that the yield pressure of compressed Köstrolith is  $93.2314\text{ N/mm}^2$ . It is observed that the curve generated by the PDE method fits the theoretical one remarkably well. It shows that the simulation can be used as a tool to predict the compressibility of a spherical shaped pharmaceutical tablet. However, the Heckel graph for the Lactose cannot be plotted since there is no information regarding the mass of that material.

It is clear that the results for the compressed PDE-based representation of a spherical tablet are in close agreement with the elastic-plastic deformation model proposed in the literature. From all the results, it seems that the solution

associated with the particular PDE representing the shape of the tablet under axial compression can be related to the existing contact law model and defined key parameters of the overall shape to the PDE coefficients. Another interesting observation from the results is that the height and contact radius of the deformed PDE-based representation of a spherical tablet can be generated by a small set of parameters. However, this simulation can be applied only to the case involving the axial compression of an object generated from circular-shaped boundary curves.

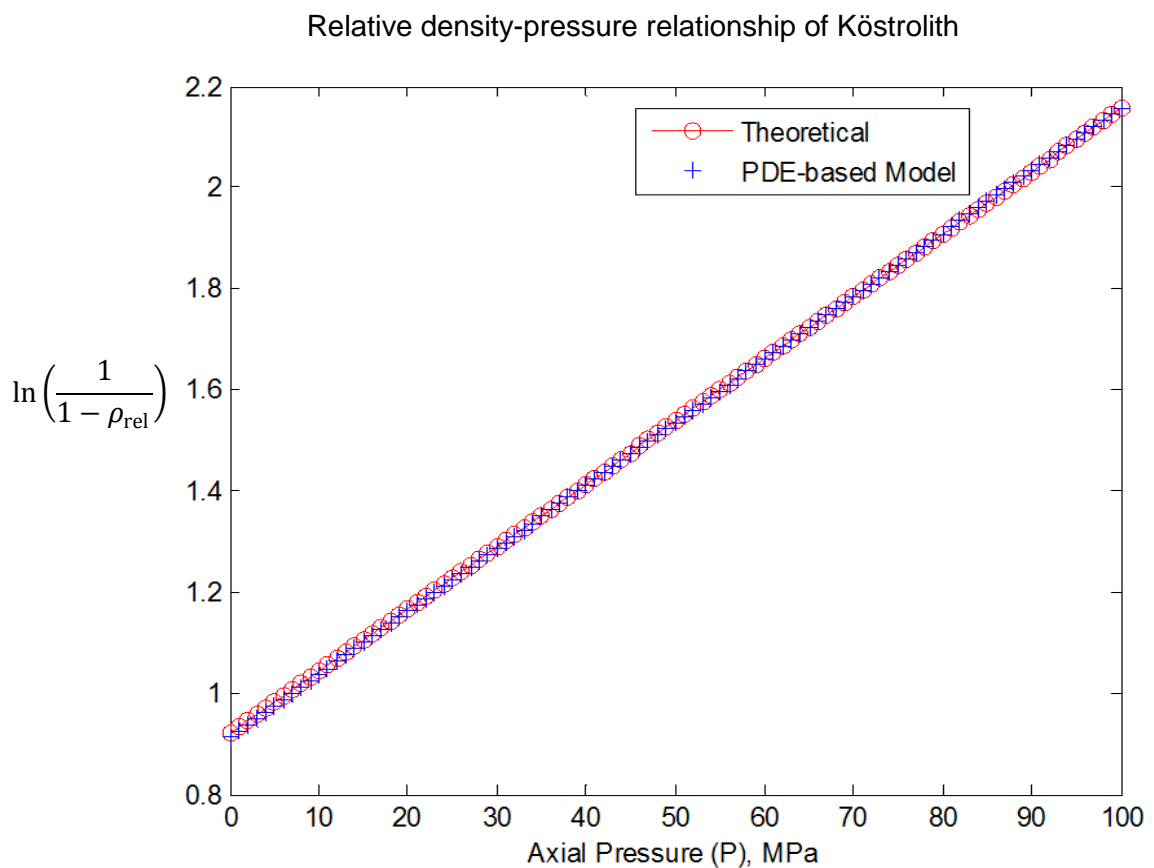


Figure 5.11: Heckel plot of theoretical and PDE-based model for the compressed spherical tablet.

## 5.4 Summary

In this chapter, the solution of the axisymmetric boundary value problem for a finite cylinder subject to a uniform axial load has been utilised in order to model the displacement components of a compressed PDE-based representation of a round tablet. The Heckel plot obtained from the developed model shows that the model is capable of predicting the compressibility of pharmaceutical materials since it fits the experimental data accurately. Furthermore, various case studies presented in this chapter show that the solution to a particular elliptic PDE can be exploited as a tool for representing the deformation and contact law for elastic-plastic spherical tablets. This is due to the fact that the spine and radius of the PDE-based object are determined analytically. The results obtained from the PDE-based simulation are compared with the theoretical ones. It is found that the analytic solution of the elliptic PDE can be utilised to represent the physical changes of the deformed object.

## **Chapter 6**

### **Automatic Design Optimisation**

#### **6.1 Introduction**

This chapter describes the methodology for automatic design optimisation of solid pharmaceutical dosage forms involving flat-faced round and spherical tablets, and a spherical capsule. Solid tablets of a cylindrical and spherical shape have been created in Chapter 4, using the PDE method. The shape of a spherical capsule presented in Section 6.2.2 is also modelled using the same method. The optimisation of both dosage forms is performed by combining the PDE method and a standard method for numerical optimisation. The objective is to obtain an optimal shape for the tablets and also to predict the optimal thickness of a spherical capsule shell.

## 6.2 Optimal Design of Pharmaceutical Tablets for Strength

This section shows how automatic design optimisation of solid pharmaceutical tablets and capsules can be carried out using the parametric model discussed in Chapter 3. The work in this chapter focuses on the design of tablets possessing the maximum tensile strength subject to required volume. This is because all produced solid dosage forms need to have at least minimum mechanical strength to uphold any potential load such as film coating, packaging and handling before use.

Normally, the shape of the initial object is designed closer to the optimal shape due to the designer's experience (Eisinger and Ruprecht 2002). This can save time because the designer does not have to consider alternative designs which would clearly not hold the required functionality. Hence, tablets in cylindrical and spherical shapes are created as the initial geometry shape of tablets as shown in Figures 4.6(a) and 4.6(b). The shape of a spherical capsule shell with its preliminary thickness and size will be discussed later in this chapter. It is assumed that both dosage forms are finite, homogeneous and isotropic.

The design optimisation of these dosage forms is performed by solving a constrained optimisation problem, formulated on the basis of the objective function, together with the boundary conditions (positional and interior curves) as-

sociated with the geometry of the dosage form and the required constraints. As mentioned in Chapter 3, there is a wide variety of methods for numerical optimisation, such as Interior-point and Active Set methods (Hei et al. 2008). The selection of a particular method is problem specific and needs more consideration in terms of cost and time taken to assess the value of the objective function (Ugail 2003). The best method is the one that can minimise the number of design variables and thus requires only a small number of function evaluations (Ugail and Wilson 2003).

It has been reported in Leyffer (2005) that the Interior-point method has better speed in solving the problem than the Active Set method. However, the Active Set method is more robust and suitable for warm starts (Leyffer 2005). The term warm start refers to a strategy used to solve an integer optimisation problem by giving an advanced starting point and reducing the number of iterations needed to find the optimal solution (John and Yıldırım 2008). Therefore, the Active Set method is capable of solving constrained nonlinear optimisation problems in a shorter time compared with other methods.

In the Active Set method, the optimisation problem is split into two groups: an active set and an inactive set, where the active set refers to a subset of the constraints that are locally active (Eitrich and Lang 2006). Mathematically, the equality constraints are always included in the active set while the inequality con-

straints need to be identified as active or inactive (Bergounioux and Kunisch 2002). The inactive constraints are essentially ignored. The optimisation process begins with the active set until a point that minimises the objective function is found. If all constraints and optimal conditions are satisfied, then the optimal solution is obtained.

The optimisation in this thesis is carried out using the Active Set method. The MATLAB Optimisation Toolbox has been used to run the constrained nonlinear minimisation problem, while a subroutine to produce the solution of the elliptic PDE has been developed in C<sup>++</sup>. Moreover, the same subroutine used for mesh generation as mentioned in Chapter 4 has been used. It has been written in an m-file in order to display the resulting shapes after the optimisation process has finished. Given that both programs are needed simultaneously, a MATLAB Executable (MEX) file is built to provide an interface between MATLAB R2008a and Visual Studio 2008. This file is dynamically loaded when the m-file is compiled and allows the referred C<sup>++</sup> file to be called from within MATLAB as though it were a built-in function.

Figure 6.1 outlines the optimisation process in searches for optimal shapes of pharmaceutical tablets. As it can be seen from the flow diagram, the process starts with an initial design, which is set as input data. These data are used to

evaluate constraint's functions and then calculate a value for the objective function. These values are passed through an optimisation engine in order to generate a new design. This process is continued until the optimum result is found.

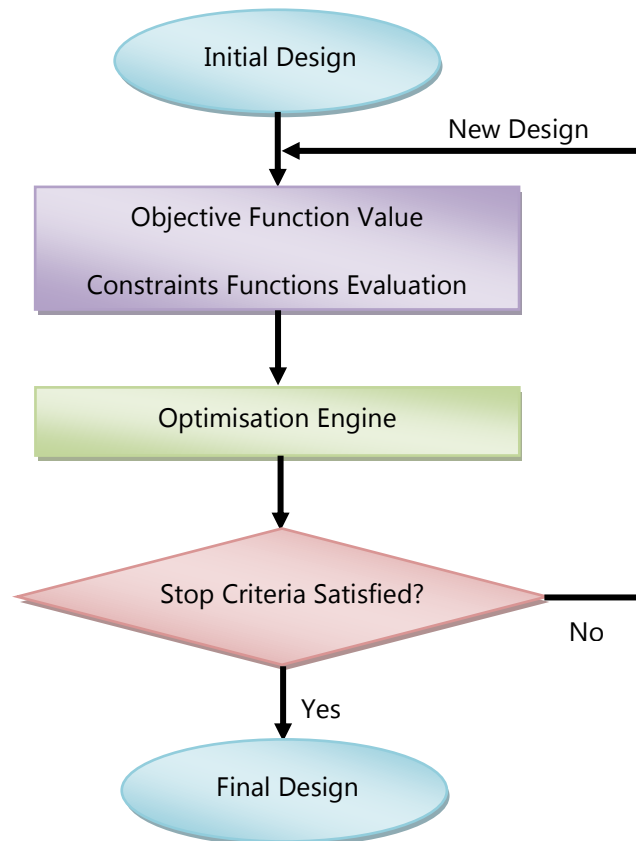


Figure 6.1: Optimisation flow diagram.

### 6.2.1 The Flat-faced Round Tablet

The automatic optimisation of the flat-faced round tablet shown in Figure 4.6(a) is discussed. The material properties and the initial dimension of this tablet can be found in Chapter 5, Section 5.2.1. Assuming that the tablet is located at the

bottom of a bottle filled with tablets, such a tablet experiences a stress. This is due to the weight of the rest of the tablets in the bottle and hence, this tablet becomes either slightly deformed or damaged. Therefore, the required strength of the tablet needs to be measured by calculating the maximum tensile strength within the tablet. This is done by means of axisymmetric boundary value analysis, whereby the force is applied on the top plane of the tablet, as caused by the weight of the other tablets in the bottle. It is also assumed that the bottom plane of the tablet is fixed at  $z = 0$ .

As mentioned above, the objective of the optimisation is to determine the maximum tensile strength of a round tablet, subject to a given volume. Therefore, it is important to analyse the calculation of the maximum tensile strength that occurs in the solution for every design, as required in the optimisation process. In this case, Equation (2.5) is employed to measure the strength of the round tablet occurring in the whole structure. In order to express Equation (2.5) in terms of pressure, the yield force,  $F_y$ , is replaced by the yield pressure,  $P_y$ , which can be obtained from the Heckel model. This model has been explained in Section 2.2.1, and its equation can be seen in Equation (2.1). Therefore, the axial tensile strength is transformed into

$$\sigma_T^a = \frac{P}{\ln\left(\frac{\pi t c^2 \rho_{\text{true}}}{\pi t c^2 \rho_{\text{true}} - m}\right) - A}, \quad (6.1)$$

where  $t$ ,  $c$  and  $m$  represent the thickness, radius and mass of the tablet respectively,  $A$  is a Heckel parameter and  $\rho_{\text{true}}$  denotes the true density. The thickness of the tablet is measured by considering the axial displacement,  $\omega_z$ , of the tablet once the load is applied to its top plane. The axial displacement of the compressed flat-faced round tablet is measured using the model proposed in Chapter 5 (Equation (5.18)).

In order to perform the automatic optimisation on the PDE-based representation of a round tablet, Equation (6.1) needs to be represented by analytic expressions relating the coefficients associated with the solution of the fourth-order elliptic PDE. Therefore, the objective function is then re-written as

$$\sigma_1^a = \frac{P}{\ln\left(\frac{\pi(h_0 + \omega_z)(A_{1x}^2 + A_{1y}^2)\rho_{\text{true}}}{\pi(h_0 + \omega_z)(A_{1x}^2 + A_{1y}^2)\rho_{\text{true}} - m}\right) - A}, \quad (6.2)$$

where  $h_0$  is the initial height of the tablet. The value of the constant  $A$  is chosen between 0.8402 and 0.8738 (obtained from the results in Section 5.2.2) and the tablet is loaded by applying a pressure,  $P$ , at the top plan of the tablet within the range from 20 to 60 N/mm<sup>2</sup>.

The design space is further restricted by choosing a constraint to represent the volume of the tablet. In this case, the volume is fixed to 235 mm<sup>3</sup>, which can be calculated using the expression given by

$$\frac{1}{3} \sum_{i=1}^M (\mathbf{x}_i \cdot \mathbf{n}_i) \mathcal{A}_i = 235, \quad (6.3)$$

where  $\mathbf{n}_i$  and  $\mathcal{A}_i$  are the unit normal vector and area of the  $i^{\text{th}}$  defining surface respectively. It is worth mentioning that Equation (6.3) represents a means for the numerical computation of the volume enclosed within a closed surface. The value of  $M$  depends on the number of rectangular faces that are representing the outer surface of the tablet in question since the PDE-based representation of a tablet is generated from a cuboid mesh. The unit normal vector for a point on the surface is defined by the ratio of the cross product of  $\mathbf{x}_u$  and  $\mathbf{x}_v$  to the magnitude of the cross product, as below

$$\mathbf{n} = \frac{\mathbf{x}_u \times \mathbf{x}_v}{|\mathbf{x}_u \times \mathbf{x}_v|}, \quad (6.4)$$

where  $\mathbf{x}_u$  and  $\mathbf{x}_v$  are given in Equations (4.10) and (4.11) respectively. Note that only the faces comprising the outer surface are used in Equation (6.3).

This work considers only the boundary conditions of the tablet's body (Patch 2) when performing the design optimisation, since it is assumed that the tablet is axially compressed by other flat surfaces. Therefore, only the body of the tablet is deformed. Emphasis is made on the fact that only the translation in the  $z$  direction and dilations in the  $xy$  plane of these boundary curves within the de-

defined limits, are considered. With the above formulation, the radius and height of each curve are set as

$$4.5 \leq r|_{P_{21}, d_{21}, d_{22}, P_{22}} \leq 5.15, \quad [\text{mm}] \quad (6.5)$$

$$0 = z_{P_{21}} \leq z_{d_{21}} \leq z_{d_{22}} \leq z_{P_{22}} \leq 3.5, \quad [\text{mm}] \quad (6.6)$$

respectively. These allow the design parameters to be varied within the specific ranges in order to obtain a favourable range of shapes, together with the required volume of the tablet.

The Active Set method finds the design with the lowest possible value of the chosen merit function from the design space. The optimisation took 27 minutes on a MATLAB R2008a with a 2.20 GHz Intel Core 2 Duo T7500 processor, to obtain the maximum strength after four iterations, starting from a randomly chosen solution point. Two optimal shapes: perfect round and curved-edge round tablets are found with maximum tensile strength, as shown in Figures 6.2(a) and 6.2(b) respectively. The values of the design curves obtained for both optimal designs are given in Table 6.1. Note that the optimal design in Figure 6.2(a) shows a shape similar to the original one, with a relative reduction in height of 50%.

Table 6.1: Values used for the design parameters associated with the round tablet.

Boundary curve	Optimal (Straight round tablet)		Optimal (Curved-edge round tablet)	
	Height (mm)	Radius (mm)	Height (mm)	Radius (mm)
$P_{21}$	0.0	5.0	0.0	4.83
$d_{21}$	0.3	5.0	0.9	5.15
$d_{22}$	0.34	5.0	2.0	5.15
$P_{22}$	2.99	5.0	2.93	4.83
Tensile strength, $\sigma_T^a$	103.095 N/mm <sup>2</sup>		103.333 N/mm <sup>2</sup>	

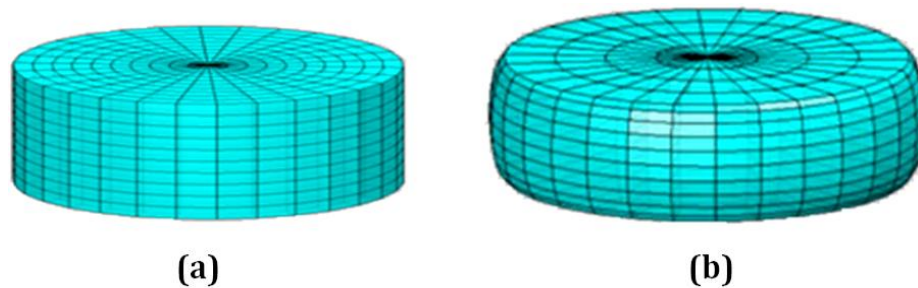


Figure 6.2: Optimal shapes for tablets with maximum tensile strength: (a) straight and (b) curved-edge round tablets.

### 6.2.2 The Spherical Tablet

In this section, the optimal design of a spherical tablet is obtained in a similar fashion to the one used for the flat-faced round tablet. This particular shape of tablet is created by means of two individual surface patches. It is important to

note that the number of design parameters in this shape is almost doubled when compared with the preceding example. This is due to the fact that two patches are now required. The aim of this example is the same as the previous one, which is to predict the optimal shape of a tablet with maximum tensile strength. Again, the translation in the  $z$  direction and dilations in the  $xy$  plane of all boundary curves are considered.

In contrast to the round tablet, it is assumed that this tablet is diametrically compressed by two point loads. Hence, the spherical tablet composed of Köstrolith experiences a stress on its upper and lower hemispheres. The micro-yield strength,  $s_y$ , Young modulus and Poisson's ratio of Köstrolith can be found in Table 5.2. In this example, Equation (2.10) is used in the optimisation routine as the objective function, which can be written in terms of PDE coefficients as

$$\sigma_T^s = \frac{2E^2 F_{ep} (1 - 2\gamma)}{\pi^3 (A_{1x}^2 + A_{1y}^2) (s_y (1 - \gamma^2))^2}. \quad (6.7)$$

In this case, the constraints are written as

$$7.7 \leq \frac{\pi s_y \omega_z r_{p21}}{2} \left( 1 - \frac{1}{3} \sqrt{\frac{r_{p21}}{\omega_z} \left( \frac{s_y \pi (1 - \gamma^2)}{2E} \right)^2} \right) \leq 9.9, \quad [\text{N}] \quad (6.8)$$

$$0.7 \leq r_{p21} \leq 0.8, \quad [\text{mm}] \quad (6.9)$$

$$r_{p22} \leq r_{d22} \leq r_{d21} \leq r_{p21}, \quad [\text{mm}] \quad (6.10)$$

$$r_{P_{22}} = \frac{\pi S_y r_{P_{21}} (1 - \nu^2)}{2E}, \quad [\text{mm}] \quad (6.11)$$

$$\frac{1}{3} \sum_{i=1}^M (X_i \cdot n_i) \mathcal{A}_i = 1.44. \quad [\text{mm}^3] \quad (6.12)$$

Equation (6.8) represents the axial force constraint, while Equation (6.9) shows the range of the radius of the tablet. The boundary curve  $P_{21}$  is chosen as the great circle, which divides the sphere into two congruent hemispheres. Therefore, only the boundary curves which correspond to the upper hemisphere are considered (as can be seen in Equation (6.10)) because it is assumed that the case discussed here has loading symmetry. These curves can be reflected as the conditions of the lower hemisphere, such as

$$P_{22} = P_{11}, \quad d_{22} = d_{11}, \quad d_{21} = d_{12}. \quad (6.13)$$

The radius of  $P_{22}$  is used to represent the radius of the contact area. This constraint is shown in Equation (6.11). The volume constraint in Equation (6.12) is similar to the previous one but this time the volume is fixed to  $1.44 \text{ mm}^3$ .

With the above formulation, the automatic optimisation was performed and the shape possessing the required characteristics was found after five iterations. For this particular case, the optimisation took 43 minutes to obtain a satisfactory optimal design, as shown in Figure 6.3(a). The final size and axial position of each curve obtained for the optimal design can be seen in Table 6.2. The result-

ing optimal shape has a relative vertical reduction and horizontal enlargement in size of 7.31% and 0.67% respectively. The maximum tensile strength for the tablet in spheroidal shape with radius 0.7047 mm was found to be equal to 77.1736 N/mm<sup>2</sup>.

In order to vary the geometry of the tablet with the same properties, the optimisation routine has been performed once again by changing the axial force and the radius constraints. In this example, the force is set between 8.5 N to 10.5 N, and the radius of  $P_{21}$  is varied from 0.75 to 0.85 mm. The other constraints remain the same as in Equations (6.10) – (6.12). A spheroidal tablet is obtained after the optimisation routine has been performed for 39 minutes.

The result suggests that a spheroidal tablet with radius 0.7561 mm and height 1.2669 mm, as presented in Figure 6.3(b), has a tensile strength equal to 69.1043 N/mm<sup>2</sup>. Note that the tensile strength of the tablet shown in Figure 6.3(b) is slightly lower than the one in Figure 6.3(a). This is because the decrease in the value of tensile strength is related to the increase in the tablet's size (Fu et al. 2004).

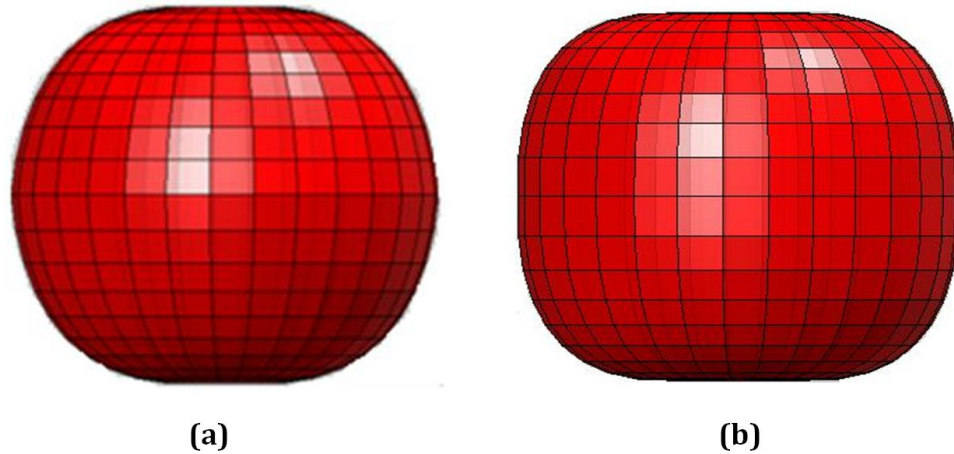


Figure 6.3: Spheroidal tablets with maximum tensile strength. (a) Resulting configuration with a tensile strength equal to  $77.1736 \text{ N/mm}^2$ . The tensile strength of a spheroidal tablet in (b) is  $69.1043 \text{ N/mm}^2$ .

Table 6.2: Values for the design parameters associated with the spherical tablet used in the optimisation.

Boundary curve	Optimal tablet in Figure 6.3(a)		Optimal tablet in Figure 6.3(b)	
	Height (mm)	Radius (mm)	Height (mm)	Radius (mm)
$P_{11}$	0.0512	0.0883	0.0666	0.0948
$d_{11}$	0.1381	0.4251	0.1501	0.5625
$d_{12}$	0.3756	0.6255	0.3501	0.6975
$P_{21}$	0.7000	0.7047	0.7000	0.7561
$d_{21}$	1.0245	0.6255	1.0499	0.6975
$d_{22}$	1.2620	0.4251	1.2500	0.5625
$P_{22}$	1.3489	0.0883	1.3335	0.0948

### 6.2.3 The Spherical Capsule

The aim of this section is to identify the optimal thickness of a soft capsule shell whilst possessing a predefined level of strength. Softgel capsules are another popular oral dosage form for medicine, which are used to mask the unpleasant taste and odour of substances. Most of them consist of a gelatine-based shell, which can encapsulate oil or liquid fill. In capsule production, all manufacturers aim to produce quality gelatine shells with the defined thickness and mechanical strength as well as the ability to survive all the manipulations of the encapsulation machine (Reich 2004).

In order to optimise the thickness of the shell, the parametric design of a solid capsule shell in spherical shape is discussed first. The procedure is similar to that for the spherical tablet. However, for the capsule, two spheres with different radii are needed. The first sphere with radius,  $r = a$ , represents the outer surface, while the other one with radius,  $r = b$  (where  $a > b$ ) creates the inner surface. Figure 6.4(a) illustrates the upper hemisphere of these spheres. In order to create a solid shell, both parametric surfaces are connected by the parameter  $w$  as given by

$$\mathbf{S}(\chi(u, v), w) = \chi(u, v)_{r=b} + w[\chi(u, v)_{r=a} - \chi(u, v)_{r=b}]. \quad (6.14)$$

The solid PDE-based representation of a spherical soft capsule shell generated by 800 cuboids is shown in Figure 6.4(b).

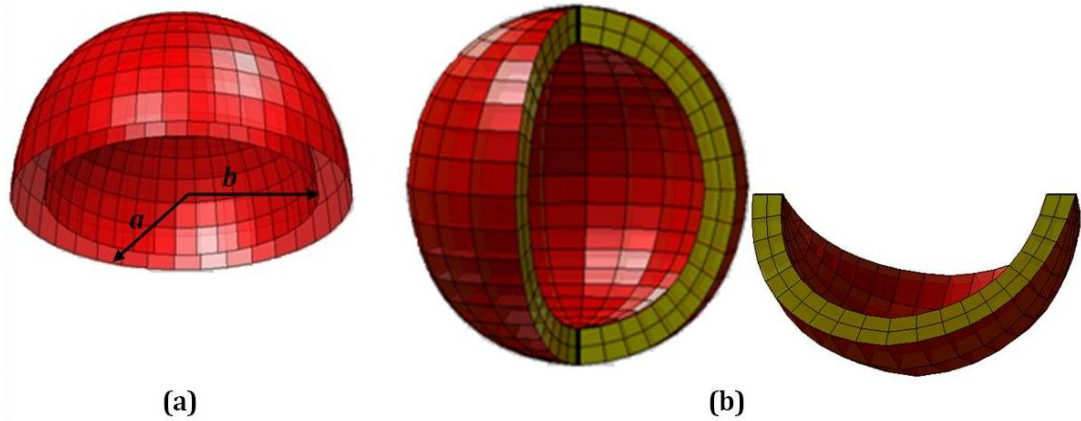


Figure 6.4: (a) Surface shape of upper hemisphere of the shell. (b) Solid PDE-based representation of a spherical soft shell.

To verify the quality, consistency and resilience of softgel capsules, the breaking force test needs to be conducted. As reported by Pharmatron (2010), the test is the same as that applied to tablets in which the capsule is compressed by two platens with a certain amount of force until it bursts. Therefore, either Equation (2.4) or Equation (2.5) can be used to measure the tensile strength of a soft-shelled capsule. In this thesis, Equation (2.4) is chosen as the objective function of the optimisation instead of Equation (2.5) because no information is available regarding the yield force of a spherical gelatine capsule.

During the compression test, an external pressure,  $P_{\text{ext}}$ , is applied to the outer surface of the spherical soft-shelled capsule. This capsule is also subject to an internal pressure,  $P_{\text{int}}$ , at its inner surface. It is assumed that the capsule shell is

thin and linearly elastic. The pressure at the outer surface of the capsule is exerted by the platens, whereas the internal pressure corresponds to the liquid pressure. As it is important to keep the tensile strength of this dosage form to the maximum, the thickness and size of the soft capsule need to be determined properly. The thickness of the capsule shell is measured by considering the radial displacement of the pressurised sphere.

This study employs the displacement model found in the work conducted by González Castro and Fitt (2002). The Biharmonic Love's stress function in spherical coordinates, which is given by

$$X(r, \theta) = \sum_{n=0}^{\infty} (A_n r^{-n-1} + B_n r^{-n+1} + C_n r^n + D_n r^{n+2}) P_n \cos \theta, \quad (6.15)$$

where  $A_n, B_n, C_n$  and  $D_n$  are arbitrary constants while  $P_n \cos \theta$  represents the  $n^{\text{th}}$  degree Legendre polynomial. Equation (6.15) has been used by the authors to find the expression for the radial displacement. The stress and displacement components in terms of  $X(r, \theta)$  are given by

$$\sigma_r = \left[ (2 - \gamma) \cos \theta \frac{\partial}{\partial r} - \frac{\gamma \sin \theta}{r} \frac{\partial}{\partial \theta} \right] \nabla^2 X - \frac{\partial^2}{\partial r^2} \left( \cos \theta \frac{\partial}{\partial r} - \frac{\sin \theta}{r} \frac{\partial}{\partial \theta} \right) X, \quad (6.16)$$

$$\begin{aligned} \tau_{r\theta} = & \left[ -\sin \theta (1 - \gamma) \left( \frac{\partial}{\partial r} - \frac{\cot \theta}{r} \frac{\partial}{\partial \theta} \right) \right] \nabla^2 X \\ & + \sin \theta \left[ \frac{\partial}{\partial r} \left( \frac{-1}{r \sin \theta} \frac{\partial}{\partial \theta} \right) \left( \cos \theta \frac{\partial}{\partial r} - \frac{\sin \theta}{r} \frac{\partial}{\partial \theta} \right) \right] X, \end{aligned} \quad (6.17)$$

$$\mu_r = -\frac{2(1+\gamma)}{3E} \cos \theta \nabla^2 X - \frac{1+\gamma}{E} \frac{\partial}{\partial r} \left( \cos \theta \frac{\partial}{\partial r} - \frac{\sin \theta}{r} \frac{\partial}{\partial \theta} \right) X, \quad (6.18)$$

where

$$\nabla^2 X = \frac{\partial^2 X}{\partial r^2} + \frac{2}{r} \frac{\partial X}{\partial r} + \frac{1}{r^2 \sin \theta} \frac{\partial}{\partial \theta} \left( \sin \theta \frac{\partial X}{\partial \theta} \right). \quad (6.19)$$

By substituting Equation (6.15) into Equation (6.18), the displacement model is written as (González Castro 2004)

$$\begin{aligned} \mu_r = & -\frac{2(1+\gamma)}{3E} [(1-2\gamma)B_1 r^{-2} + (10\gamma-5)D_1 r] - \frac{2(1+\gamma)}{5E} [(8-12\gamma)B_2 r^{-3} \\ & + 5C_2 + (28\gamma-7)D_2 r^2] \cos \theta - \frac{(1+\gamma)}{E} \sum_{n=2}^{\infty} \frac{P_n \cos \theta}{(2n+3)(2n-1)} \\ & \left\{ [n(n+1)(2n+3)(2n-1)] A_{n-1} r^{-n-2} \right. \\ & + [n(2n+3)(3-2n)(4\gamma-n-3)] B_{n-1} r^{-n} \\ & + 2(5n^2-1-8n^2\gamma+2\gamma-2n-8n^3\gamma+6n^3+2n\gamma) B_{n+1} r^{-n-2} \\ & + [n(n+1)(2n+3)(2n-1)] C_{n+1} r^{n-1} \\ & + [4(3n\gamma-5\gamma+n^3+2.5-n^4+4n^3\gamma+12n^2\gamma)-11n-21n^2] D_{n+1} r^{n+1} \\ & \left. + [2n(2n+3)(2\gamma(2n+1)-(3n+2))] D_{n-1} r^{n-1} \right\}. \quad (6.20) \end{aligned}$$

The constants  $A_n, B_n, C_n$  and  $D_n$  in Equation (6.20) can be found by applying the boundary conditions for the compression problem as follows

$$\sigma_r|_{r=a} = -P_{\text{ext}}, \quad \text{for } \frac{\pi}{2} - \psi \leq \theta \leq \frac{\pi}{2} + \psi \quad (6.21a)$$

$$\sigma_r|_{r=b} = -P_{\text{int}}, \quad (6.21b)$$

$$\tau_{r\theta}|_{r=a,b} = 0, \quad (6.21c)$$

where  $\psi$  represents the angle that describes the region of contact between the capsule and the platens. Note that the condition in Equation (6.21a) depends on  $\theta$  because it is assumed that the pressure from the platens acted over the region  $\frac{\pi}{2} - \psi \leq \theta \leq \frac{\pi}{2} + \psi$ , as can be seen in Figure 6.5. After substituting Equations (6.15) – (6.17) into Equations (6.21a) – (6.21c), the constants in Equation (6.20) are obtained. The long expressions of these constants are shown in **Appendix C**.

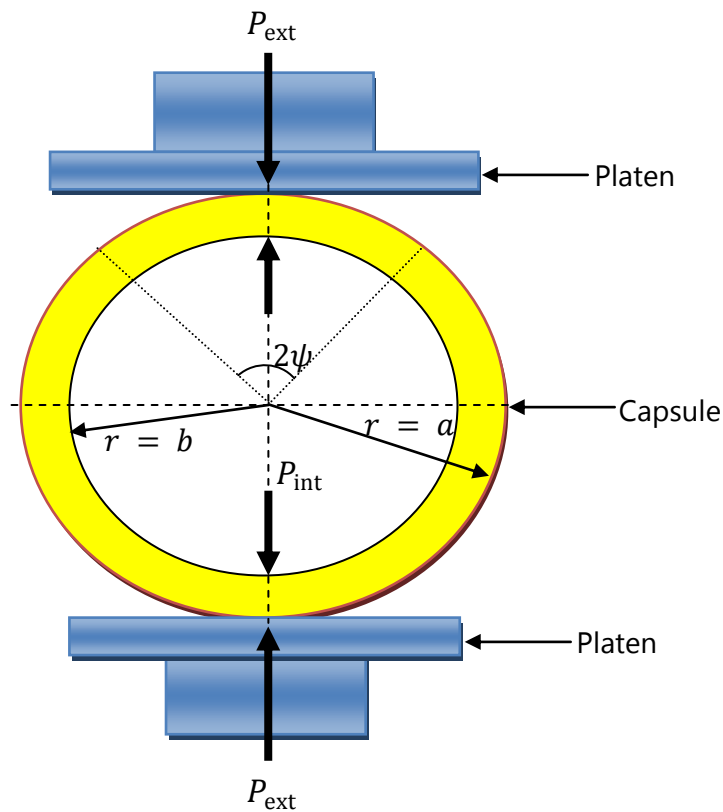


Figure 6.5: Mathematical representation of the compression test for a spherical gel capsule.

Similar to the case of a spherical tablet, the work in this section considers only the upper part of the capsule, due to the geometry and loading symmetries. A pressure ranging from 31.36 to 36.56 N/mm<sup>2</sup> is applied to the outer surface of the capsule throughout the compression test (Pharmatron 2010), while the pressure on its inner surface is assumed to be 7.33 N/mm<sup>2</sup>. As far as the material properties are concerned, the Young's modulus and Poisson's ratio of the gelatine are 0.11 N/mm<sup>2</sup> and 0.4 respectively (Markidou et al. 2005). For this particular example, the volume of the spherical capsule is fixed to 65.45 mm<sup>3</sup> while the fill volume is equal to 34 mm<sup>3</sup>. These volumes are calculated using the same expression as the previous cases.

With the above information and by expressing the objective function in terms of pressure and boundary curves, the complete optimisation problem is then written in the form as below

$$\text{Max } \sigma_T^d = \frac{P_{\text{ext}} r_{d22}^2 |_{r=a}}{r_{P21} |_{r=a} (r_{P21} |_{r=a} - r_{P21} |_{r=b})}, \quad (6.22)$$

subject to

$$\frac{1}{3} \sum_{i=1}^M (\mathbf{x}_{i(r=a)} \cdot \mathbf{n}_i) \mathcal{A}_i = 65.45, \quad [\text{mm}^3] \quad (6.23a)$$

$$\frac{1}{3} \sum_{i=1}^M (\mathbf{X}_{i(r=b)} \cdot \mathbf{n}_i) \mathcal{A}_i = 34, \quad [\text{mm}^3] \quad (6.23b)$$

$$2.5 \leq r_{p_{21}} \Big|_{r=a} + \mu_r \leq 2.8, \quad [\text{mm}] \quad (6.23c)$$

$$2.0 \leq r_{p_{21}} \Big|_{r=b} + \mu_r \leq 2.3, \quad [\text{mm}] \quad (6.23d)$$

$$1.25 \leq r_{d_{22}} \Big|_{r=a} + \mu_r \leq 1.35, \quad [\text{mm}] \quad (6.23e)$$

$$31.36 \leq P_{\text{ext}} \leq 36.56, \quad [\text{N/mm}^2] \quad (6.23f)$$

where  $r_{d_{22}} \Big|_{r=a}$  represents the radius of the contact area, while  $r_{p_{21}} \Big|_{r=a} = a$  and  $r_{p_{21}} \Big|_{r=b} = b$ . The automatic optimisation was performed in 51 minutes after the initial feasible point is specified as 31.4 N/mm<sup>2</sup>, 1.28 mm, 2.7 mm and 2.1 mm for  $P_{\text{ext}}$ ,  $r_{d_{22}} \Big|_{r=a}$ ,  $r_{p_{21}} \Big|_{r=a}$  and  $r_{p_{21}} \Big|_{r=b}$  respectively. The optimal thickness of a capsule shell with maximum tensile strength is obtained after 9 iterations. As can be seen in Figure 6.6, it is evident that the thickness of the gelatine shell decreases gradually as the tensile strength increases. In other words, a capsule with thin shell has a high tensile strength. The result for the case discussed in this section shows that a spherical softgel capsule with diameter 5 mm and thickness 0.4252 mm has a maximum strength of 53.66 N/mm<sup>2</sup>.

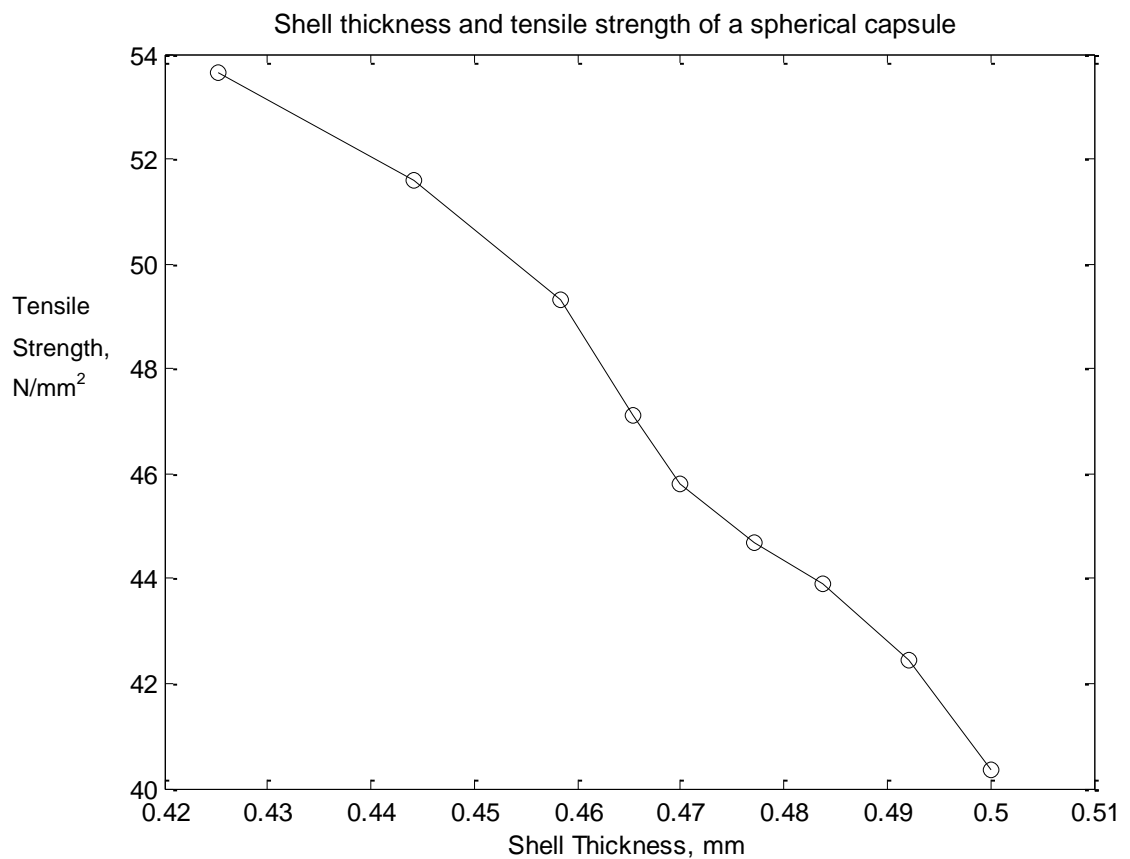


Figure 6.6: Relationship between the thickness of a capsule shell and the tensile strength in each iteration during the optimisation process.

### 6.3 Summary

A methodology for the automatic design optimisation for pharmaceutical tablet shapes has been described in this chapter. A flat-faced round and a spherical shaped tablet, together with a spherical capsule, have been used as the initial shape in the optimisation problem. The boundary curves which define the initial shape have been used as the starting point for the numerical optimisation using

the Active Set method. The problem has been solved according to the corresponding objective function, together with the boundary conditions associated with the geometry of the tablet and the required constraints. Based on the obtained results, it can be seen that the PDE method can be used to address optimisation problems in tablet production. Several shapes of tablet with maximum strength and specific volume have been found using this approach.

## **Chapter 7**

### **Conclusions**

This chapter consists of a summary of the work and conclusions about the achievements that have been made. This chapter also provides suggestions for possible improvements and directions for future work that could be undertaken to further develop this line of research.

#### **7.1 Summary**

There are many parametric surface generation techniques available nowadays, such as the Bézier, Basis spline (B-spline) and Non-uniform rational B-splines (NURBS). There is also a technique based on the use of Partial Differential Equations (PDEs), known as the PDE method. Of these methods, the PDE method is the most convincing method for representing any object shape since it can gen-

erate surfaces of complex geometries from a small number of parameters. The shape of the surfaces generated by this method is based on a boundary representation and can easily be modified since it is characterised by data distributed along the boundaries. Thus, this work employs the PDE method for designing a parametric representation of tablets in various shapes and sizes.

In tablet production, volume and surface area play an important role in determining the mechanical strength of the pharmaceutical tablet. Therefore, this work measured the volume and surface area of the generated PDE-based tablets by using formulae related to parametric surfaces. The values of these parameters have been obtained numerically using MATLAB.

The analytic solution of the elliptic PDE has been extended to a higher dimension in order to generate a solid representation of objects in general and tablets in particular. This is due to fact that the formulation of Bloor-Wilson PDE method generates only the surface of any given object, in this case, the tablet's surface. The generated solid tablet can be trimmed by changing the region defined by independent variables. Additionally, the shape and size of these tablets have been modified by taking advantage of the characteristics of the extended PDE method.

In Chapter 5, the displacement component of a compressed PDE-based representation of a flat-faced round tablet has been measured by using one of the solutions of the Love's stress function. The result is plotted in a Heckel diagram and compared with the experimental data. It is found that the theoretical Heckel's parameter is similar to the experimental one. However, the model seems to underestimate the initial volume of the particle bed. This may be attributed to the lack of detailed information on powder behaviour at low pressure. In the case of a spherical tablet, the deformation model of a granule, as found in the literature, has been used to measure the displacement of a compressed tablet in that particular shape; hence the physics is related to the parametric shape of the tablet in question under specific circumstances. Again, the result obtained from the simulation of a compressed parametric spherical tablet is analysed using the Heckel model and has been compared with the theoretical one.

A methodology for automatic design optimisation for pharmaceutical tablet shapes is also described in this work. The objective is to obtain an optimal shape and size for a particular tablet and also to predict the optimal thickness of a spherical capsule's shell, with maximum tensile strength. Given that the PDE method has proven useful in addressing optimisation problems in biological and industrial applications, the design optimisation of pharmaceutical tablets is

also carried out with the use of a similar approach. The problem has been solved according to the objective function, which is to maximise the tensile strength, together with the boundary conditions associated with the geometry of the tablet and the required constraints.

## **7.2 Contributions**

This section discusses the contributions in detail and how the aims and objectives are fulfilled.

### **I. Pioneer Work Utilising the PDE Method in the Pharmaceutical Industry.**

The PDE method has been applied in many areas as a technique in CAGD. However, this method has never been introduced into the pharmaceutical industry. Thus, this work is the first attempt to utilise the PDE method as a technique to generate the geometry of pharmaceutical tablets. Several shapes of tablets such as flat-faced round, convex round, oval, spherical and oblong tablets have been generated using this method. Furthermore, computer based simulation algorithm based on a surface representation model has been proposed in this thesis in order to simulate the powder compaction process, which is the most important stage in the tablet production.

## **II. Solid PDE-based Representation of an Object.**

Most objects in the physical world are best described by their volume. Even though the shape of such objects can be modelled by a surface representation, in many applications such as simulations of automotive productions or surgical operations, the information associated with the entire volume of such an object is more relevant than information about its surface. Therefore, solid modelling has become an important aspect in geometric modelling.

Solid modelling has been performed by modifying the formulation of a geometric surface. In this thesis, a new parameter,  $w$ , in domain  $0 \leq w \leq 1$  has been introduced into the solution to a particular elliptic PDE. This parameter generates interior points of the PDE-based object from the spine towards its surface. In order to visualise the generated solid PDE-based representation of a tablet, a subroutine has been written in a MATLAB file. In the mesh generation process, all generated points are used as vertices of rectangular faces to create a uniform cuboid meshes, thereby forming the shape of the tablet.

## **III. Mathematical Expressions for a Tablet's Height and Radius.**

Simple expressions representing the height and the radius of a PDE-based representation of a tablet have been achieved by exploiting the formulation of the extended PDE method. These expressions are suitable for a tablet

which is formed by a set of circular-shaped boundary curves, with the symmetry axis coinciding with the z-axis. In this thesis, these expressions have been used to modify the initial shape of pharmaceutical tablets in order to achieve the required designs. Furthermore, they are used in the simulation as a tool for representing the deformation of elastic-plastic spherical tablets. This is due to the fact that the spine and radius of the PDE-based object are determined analytically.

#### **IV. Axial Displacement Model.**

This thesis has proposed a pressure-displacement model to study the compressibility of pharmaceutical powders in a cylindrical die. The model has been developed by utilising the solution of the axisymmetric boundary value problem for a finite cylinder subject to a uniform axial load. The developed model has been applied to the PDE-based representation of a cylindrical tablet and the simulation result, which is presented in the Heckel graph, has been compared with the experimental results. It is found that the theoretical Heckel's parameter is quite similar to the experimental ones. However, the output of this model is sensitive to the change of the elastic properties, such as the Young's modulus and the Poisson's ratio.

## V. Simulation Algorithm for Tablet Compaction.

PDE-based simulations of compressed flat-faced round and spherical tablets have been carried out in Chapter 5. Different deformation models have been used in the simulation process to measure the displacement of a compressed PDE-based representation of flat-faced round and spherical tablets and hence relating the physics to the parametric shape of the tablet in question under some specific circumstances. The results obtained from the PDE-based simulation show that the analytic solution of the elliptic PDE can be utilised to represent the physical changes of the deformed object.

## VI. Simulation Results

The Heckel plot of each simulation result shows a good agreement with the experimental and theoretical ones. The graphs show that the yield pressure of  $\alpha$ -lactose monohydrate is within the range between  $93.5 \text{ N/mm}^2$  to  $102.04 \text{ N/mm}^2$  while Köstrolith presents a yield pressure equal to  $93.2314 \text{ N/mm}^2$ . These findings could be explored and offer a good point of reference for future work in pharmaceutical research. Given that the study of powder compaction has become popular, the results shown in this thesis can be used as a benchmark by other researchers in the future for modelling powder compaction.

## **VII. Shape Optimisation of PDE-based Representation of Tablets.**

This work has demonstrated the potential of the PDE method for improving old methodologies for designing pharmaceutical tablets. Optimal designs of tablets with particular volume and maximum strength have been obtained using an automatic design optimisation, which is performed by combining the PDE method with a standard method for numerical optimisation. The formulation of the optimisation problem discussed in this thesis involves as few design parameters as possible. Additionally, the concise parameterisation characteristics of the PDE method can be used to carry out automatic design optimisation in a practical setting, where the time taken for tablet testing can be significantly reduced and the future development of pharmaceutical technologies encouraged.

### **7.3 Research Limitations**

The results and contributions presented in this thesis show that the research has some limitations, which are highlighted as follows:

- I. It is worth noting that the example of the tablet used throughout this thesis may give the reader the impression that the shape of the tablet is somehow restricted to round shapes, formed by circular-shaped boundary curves in particular. This is not the case, since different tablet shapes can easily be

formed using the PDE method by changing the shape of the boundary curves. However, the study of mechanical behaviour of other tablet shapes has not been carried out in this thesis.

- II. It is highlighted that the developed axial displacement model, which has been shown in Chapter 5, can be applied only to the Single Ended Compression (SEC) process of powder in a cylindrical die. Moreover, the validity of this model is verified only at low pressure, where it indicates the deformation of the powder. Furthermore, from the simulation results obtained, this model seems to underestimate the initial volume of the particle bed. Therefore, more experimental results are needed to verify the validity of this model.
- III. In this thesis, the deformation of a compressed spherical tablet is measured using a model developed for a spherical granule found in Antonyuk et al. (2010). This is mainly due to the fact that the author assumes that both tablets and granules in that particular shape have similar mechanical behaviours.
- IV. There is a lack of data and information related to the properties of softgel capsules, such as the size, shell thickness and mechanical strength. This is because the study of soft gelatine capsules is still new in the pharmaceutical industry. Therefore, the optimisation of the spherical softgel capsule dis-

cussed in Section 6.2.3 has been carried out by assuming the initial thickness of the shell and its liquid pressure.

## 7.4 Future Work

For future work, broader plans have been made concerning the scope of this research, which currently focuses on the compactness of flat-faced cylindrical and spherical tablets. The limitations previously discussed may be improved in the future with regard to continuation of this research domain.

- I. The axial displacement model developed in Chapter 5 is valid only for the specific compaction process, which in this case is SEC and the powder is compressed using flat-faced punches. The work in this thesis can be improved by considering not only the SEC process but also the Double Ended Compression (DEC) process. In addition, other shapes of tablets, such as a convex round and oval tablets produced through the compaction process (SEC or DEC) using punches with curved surfaces, need to be considered. Therefore, a more general model for characterising the stress distribution can be developed. This can be achieved with the same approach as that used in Section 5.2, using a different set of boundary conditions.
- II. As mentioned in the previous section, the validity of the developed axial displacement model is verified on only one set of experimental data, which

considers  $\alpha$ -lactose monohydrate. In the future, simulation of powder compression using this model can be carried out to investigate whether the model is compatible with experimental data of other pharmaceutical powders, such as Microcrystalline Cellulose (MCC) and Hydroxypropylmethyl Cellulose (HPMC).

- III. The design optimisation focused on one loading direction exclusively, where an axial load was applied to the tablets in a direction parallel to the  $z$ -axis. In the future, the optimisation with different loading conditions, such as diametrical or triaxial compression can be performed to obtain various shapes of tablet with maximum strength.
- IV. It is interesting to consider whether parameterisation and manipulation of the geometry of PDE-based representation of tablets, as well as tablet compression, can be simulated interactively. This would involve the development of an interactive platform, whereby the physical and mechanical properties of tablets could potentially be assessed under specific and controlled conditions. This platform may potentially be used by pharmaceutical scientists with little programming knowledge and therefore may help reducing costs and time of experimental processes.

## Bibliography

- Adolfsson, Å. S., Gustafsson, C. & Nyström, C. (1999) Use of tablet tensile strength adjusted for surface area and mean interparticulate distance to evaluate dominating bonding mechanisms. *Drug Development and Industrial Pharmacy*, 25(6), pp. 753-764.
- Antonyuk, S., Heinrich, S., Tomas, J., Deen, N. G., Van Buijtenen, M. S. & Kuipers, J. A. M. (2010) Energy absorption during compression and impact of dryelastic-plastic spherical granules. *Granular Matter*, 12(1), pp. 15-47.
- Antonyuk, S., Tomas, J., Heinrich, S. & Mörl, L. (2005) Breakage behaviour of spherical granulates by compression. *Chemical Engineering Science*, 60(14), pp. 4031-4044.
- Athanasopoulos, M., Ugail, H. & González Castro, G. (2010) On the development of an interactive talking head system. *Proceedings of the 2010 International Conference on Cyberworlds*. Singapore, 20th-22nd October 2010, Washington: IEEE Computer Society, pp. 414-420.
- Bacher, C., Olsen, P. M., Bertelsen, P., Kristensen, J. & Sonnergaard, J. M. (2007) Improving the compaction properties of roller compacted calcium carbonate. *International Journal of Pharmaceutics*, 342(1-2), pp. 115-123.
- Baxter Brown, J. M. (1973) *Introductory solid mechanics*, London: John Wiley & Sons.
- Belic, A., Skrjanc, I., Bozic, D. Z., Karba, R. & Vrecer, F. (2009) Minimisation of the capping tendency by tableting process optimisation with the application of artificial neural networks and fuzzy models. *European Journal of Pharmaceutics and Biopharmaceutics*, 73(1), pp. 172-178.

- Benkhaldoun, F. & Seaid, M. (2008) New finite-volume relaxation methods for the third-order differential equations. *Communications in Computational Physics*, 4(4), pp. 820-837.
- Bergounioux, M. & Kunisch, K. (2002) Primal-dual strategy for state-constrained optimal control problems. *Computational Optimization and Applications*, 22(2), pp. 193-224.
- Bilalis, N. (2000) *Computer aided design-CAD*. [online]. Technical University of Crete. Available from: [http://www.adi.pt/docs/innoregio\\_cad-en.pdf](http://www.adi.pt/docs/innoregio_cad-en.pdf) [Accessed: 14th June 2012].
- Birkbeck, N., Levesque, J. & Amaral, J. N. (2007) A dimension abstraction approach to vectorization in MATLAB. *Proceedings of the International Symposium on Code Generation and Optimization*. San Jose, California, 11-14th March 2007, Washington: IEEE Computer Society, pp. 115-130.
- Bloor, M. I. G. & Wilson, M. J. (1989) Generating blend surfaces using partial differential equations. *Computer-Aided Design*, 21(3), pp. 165-171.
- Byrd, R. H. & Waltz, R. A. (2009) An active-set algorithm for nonlinear programming using parametric linear programming. *Optimization Methods and Software*, 26(1), pp. 47-66.
- Chtourou, H. D., Guillot, M. & Gakwaya, A. (2002) Modeling of the metal powder compaction process using the cap model. Part I. Experimental material characterization and validation. *International Journal of Solids and Structures*, 39(4), pp. 1059-1075.
- Chuang, S. H. & Pan, C. C. (1998) Rough cut tool path planning for B-spline surfaces using convex hull boxes. *The International Journal of Advanced Manufacturing Technology*, 14(2), pp. 85-92.
- Coons, S. A. (1963) An outline of the requirements for a computer-aided design system. *Spring Joint Computer Conference Proceedings*. Detroit, Michigan, 21st-23rd May 1963, New York: ACM, pp. 299-304.
- Coube, O., Cocks, A. C. F. & Wu, C. Y. (2005) Experimental and numerical study of die filling, powder transfer and die compaction. *Powder Metallurgy*, 48(1), pp. 68-76.
- Cox Gad, S. (2008) *Pharmaceutical manufacturing handbook: Production and processes*. New Jersey: John Wiley & Sons, Inc.
- Cunningham, J., Sinka, I. & Zavaliangos, A. (2004) Analysis of tablet compaction. I. Characterization of mechanical behavior of powder and powder/tooling friction. *Journal of Pharmaceutical Sciences*, 93(8), pp. 2022-2039.

- Dey, N. S., Majumdar, S. & Rao, M. E. B. (2008) Multiparticulate drug delivery systems for controlled release. *Tropical Journal of Pharmaceutical Research*, 7(3), pp. 1067-1075.
- Dimas, E. & Briassoulis, D. (1999) 3D geometric modelling based on NURBS: a review. *Advances in Engineering Software*, 30(9-11), pp. 741-751.
- Ding, H. -J., Lee, X. -Y. & Chen, W.-Q. (2005) Analytic solutions for a uniformly loaded circular plate with clamped edges. *Journal of Zhejiang University - Science A*, 6(10), pp. 1163-1168.
- Du, H. & Qin, H. (2005) Dynamic PDE-based surface design using geometric and physical constraints. *Graphical Models*, 67(1), pp. 43-71.
- Eichie, F. E. & Kudehinbu, A. O. (2009) Effect of particle size of granules on some mechanical properties of paracetamol tablets. *African Journal of Biotechnology*, 8(21), pp. 5913-5916.
- Eiliazadeh, B., Briscoe, B. J., Sheng, Y. & Pitt, K. (2003) Investigating density distributions for tablets of different geometry during the compaction of pharmaceuticals. *Particulate Science and Technology: An International Journal*, 21(4), pp. 303-316.
- Eiliazadeh, B., Pitt, K. & Briscoe, B. J. (2004) Effects of punch geometry on powder movement during pharmaceutical tableting processes. *International Journal of Solids and Structures*, 41(21), pp. 5967-5977.
- Eisinger, R. & Ruprecht, A. (2002) Automatic shape optimization of hydro turbine components based on CFD, *TASK Quarterly*, 6(1), pp. 101-111.
- Eitrich, T. & Lang, B. (2006) Efficient optimization of support vector machine learning parameters for unbalanced datasets. *Journal of Computational and Applied Mathematics*, 196(2), pp. 425-436.
- Elkhider, N., Chan, K. L. A. & Kazarian, S. G. (2007) Effect of moisture and pressure on tablet compaction studied with FTIR spectroscopic imaging. *Journal of Pharmaceutical Sciences*, 96(2), pp. 351-360.
- Enciu, P., Gerbaud, L. & Wurtz, F. (2010) Automatic differentiation applied for optimization of dynamical systems. *IEEE Transactions on Magnetics*, 46(8), pp. 2943-2946.
- Engel, G., Garikipati, K., Hughes, T. J. R., Larson, M. G., Mazzei, L. & Taylor, R. L. (2002) Continuous/discontinuous finite element approximations of fourth-order elliptic problems in structural and continuum mechanics with applications to thin beams

- and plates, and strain gradient elasticity. *Computer Methods in Applied Mechanics and Engineering*, 191(34), pp. 3669-3750.
- Farin, G. (2002) A history of curves and surfaces in CAGD. In: Farin, G., Hoschek, J. & Kim, M. -S., eds. *Handbook of Computer Aided Geometric Design*. Amsterdam: Elsevier, pp. 1-21.
- Frenning, G. (2008) An efficient finite/discrete element procedure for simulating compression of 3D particle assemblies. *Computer Methods in Applied Mechanics and Engineering*, 197(49-50), pp. 4266-4272.
- Frenning, G. (2010) Compression mechanics of granule beds: A combined finite/discrete element study. *Chemical Engineering Science*, 65(8), pp. 2464-2471.
- Fu, X., Dutt, M., Bentham, A. C., Hancock, B. C., Cameron, R. E. & Elliott, J. A. (2006) Investigation of particle packing in model pharmaceutical powders using X-ray microtomography and discrete element method. *Powder Technology*, 167(3), pp. 134-140.
- Fu, Y., Jeong, S. H. & Park, K. (2005) Fast-melting tablets based on highly plastic granules. *Journal of Controlled Release*, 109(1-3), pp. 203-210.
- Fu, Y., Yang, S., Jeong, S. H., Kimura, S. & Park, K. (2004) Orally fast disintegrating tablets: developments, technologies, taste-masking and clinical studies. *Critical Reviews in Therapeutic Drug Carrier Systems*, 21(6), pp. 433-76.
- Gabaude, C. M. D., Guillot, M., Gautier, J. C., Saudemon, P. & Chulia, D. (1999) Effects of true density, compacted mass, compression speed, and punch deformation on the mean yield pressure. *Journal of Pharmaceutical Sciences*, 88(7), pp. 725-730.
- González Castro, G. & Fitt, A. D. (2002) A mathematical model for tonometry. In: Buikis, A., Ciegis, R. & Fitt, A. D., eds. *Progress in Industrial Mathematics at ECMI 2002. 12th conference of the European Consortium for Mathematics in Industry*. Berlin Heidelberg, Germany: Springer-Verlag, pp. 285-290.
- González Castro, G. (2004) *The mathematical modelling of human eyes*. PhD thesis, University of Southampton.
- González Castro, G., Athanasopoulos, M., Ugail, H., Willis, P., & Sheng, Y. (2010). Cyclic animation using Partial Differential Equations. *The Visual Computer*, 26(5), pp. 325-338.
- González Castro, G., Ugail, H., Willis, P. & Palmer, I. (2008) A survey of Partial Differential Equations in geometric design. *The Visual Computer*, 24(3), pp. 213-225.

- Grinchenko, V. T. (2003) The Biharmonic problem and progress in the development of analytical methods for the solution of boundary-value problems. *Journal of Engineering Mathematics*, 46(3), pp. 281-297.
- Han, L. H., Elliott, J. A., Bentham, A. C., Mills, A., Amidon, G. E. & Hancock, B. C. (2008) A modified Drucker-Prager Cap model for die compaction simulation of pharmaceutical powders. *International Journal of Solids and Structures*, 45(10), pp. 3088-3106.
- Hancock, B. C., Colvin, J. T., Mullarney, M. P. & Zinchuk, A. V. (2003) The relative densities of pharmaceutical powders, blends, dry granulations, and immediate-release tablets. *Pharmaceutical Technology*, 27(1), pp. 64-80.
- Harris, L. V. A. & Meyers, F. (2007) Engineering design graphics: Into the 21st century. *Engineering Design Graphics Journal*, 71(3), pp. 9-23.
- Hassanpour, A. & Ghadiri, M. (2004) Distinct element analysis and experimental evaluation of the Heckel analysis of bulk powder compression. *Powder Technology*, 141(3), pp. 251-261.
- Heckel, R. W. (1961) Density-pressure relationship in powder compaction. *Transaction of the Metallurgical Society of AIME*, 221(1), pp. 671-675.
- Hei, L., Nocedal, J. & Waltz, R. A. (2008) A numerical study of Active-set and Interior-point methods for bound constrained optimization. In: Bock, H. G., Kostina, E., Phu, H. X. & Rannacher, R. eds. *Modeling, Simulation and Optimization of Complex Processes*. Berlin Heidelberg: Springer, pp. 273-292.
- Herbold, E. B., Nesterenko, V. F., Benson, D. J., Cai, J., Vecchio, K. S., Jiang, F., Addiss, J. W., Walley, S. M. & Proud, W. G. (2008) Particle size effect on strength, failure, and shock behavior in pol-tetrafluoro-ethylene-Al-W granular composite materials. *Journal of Applied Physics*, 104(10), pp. 1-11.
- Ilić, I., Kása, P., Dreu, R., Pintye-Hódi, K. & Srčić, S. (2009) The compressibility and compactibility of different types of lactose. *Drug Development and Industrial Pharmacy*, 35(10), pp. 1271-1280.
- Iveson, S. M. & Page, N. W. (2005) Dynamic strength of liquid-bound granular materials: The effect of particle size and shape. *Powder Technology*, 152(1-3), pp. 79-89.
- John, E. & Yıldırım, E. (2008) Implementation of warm-start strategies in interior-point methods for linear programming in fixed dimension. *Computational Optimization and Applications*, 41(2), pp. 151-183.

- Kabir, M., Lovell, M. & Higgs, C. (2008) Utilizing the explicit finite element method for studying granular flows. *Tribology Letters*, 29(2), pp. 85-94.
- Kasik, D. J., Buxton, W. & Ferguson, D. R. (2005) Ten CAD challenges. *IEEE Computer Graphics and Applications*, 25(2), pp. 81-92.
- Krull, F. N. (1994) The origin of computer graphics within general motors. *IEEE Annals of the History of Computing*, 16(3), pp. 40-56.
- Lavoué, G. (2008) Basic background in 3D object processing. In: Dugelay, J. -L., Baskurt, A. & Daoudi, M., eds. *3D Object Processing: Compression, Indexing and Watermarking*. Chichester, UK: John Wiley & Sons, Ltd, pp. 5-43.
- Leyffer, S. (2005) The return of the active set method. *Oberwolfach Reports*, 2(1), pp. 107-109.
- Li, F., Pan, J. & Sinka, C. (2009) Contact laws between solid particles. *Journal of the Mechanics and Physics of Solids*, 57(8), pp. 1194-1208.
- Liang, S. & Jeffrey, D. J. (2009) An efficient analytical approach for solving fourth order boundary value problems. *Computer Physics Communications*, 180(11), pp. 2034-2040.
- Liang, Y., Wang, H. & Ren, X. (2008) Analytical solution for spatially axisymmetric problem of thick-walled cylinder subjected to different linearly varying pressures along the axis and uniform pressures at two ends. *Science in China Series G: Physics Mechanics and Astronomy*, 51(1), pp. 98-104.
- Loop, C. (1994) Smooth spline surfaces over irregular meshes. *The 21st annual conference on Computer graphics and interactive techniques – SIGGRAPH'94, Conference Proceedings*. Orlando, 24-29th July 2004, New York: ACM, pp. 303-310.
- Love, A. E. H. (1892) *A treatise of the mathematical theory of elasticity*. Cambridge: Cambridge University Press.
- Markidou, A., Shih, W. Y. & Shih, W. -H. (2005) Soft-materials elastic and shear moduli measurement using piezoelectric cantilevers. *Review of Scientific Instruments*, 76(6), pp. 064302(1-7).
- Monterde, J. & Ugail, H. (2006) A general 4th-order PDE method to generate Bézier surfaces from the boundary. *Computer Aided Geometric Design*, 23(2), pp. 208-225.
- Nokhodchi, A. (2005) An overview of the effect of moisture on compaction and compression. *Pharmaceutical Technology*, 29(1), pp. 46-66.

- Owolabi, B. I. O., Afolabi, T. A. & Adebowale, K. O. (2010) Effect of heat moisture treatment on the functional and tableting properties of corn starch. *African Journal of Pharmacy and Pharmacology*, 4(7), pp. 498-510.
- Panien, M., Schreurs, G. & Pfiffner, A. (2006) Mechanical behaviour of granular materials used in analogue modelling: insights from grain characterisation, ring-shear tests and analogue experiments. *Journal of Structural Geology*, 28(9), pp. 1710-1724.
- Patra, S. (2010) *Design and modelling of axial micro gas turbine*. BTech thesis, National Institute of Technology Rourkela, India.
- Peiró, J., Formaggia, L., Gazzola, M., Radaelli, A. & Rigamonti, V. (2007) Shape reconstruction from medical images and quality mesh generation via implicit surfaces. *International Journal for Numerical Methods in Fluids*, 53(8), pp. 1339-1360.
- Perkins, M., Ebbens, S. J., Hayes, S., Roberts, C. J., Madden, C. E., Luk, S. Y. & Patel, N. (2007) Elastic modulus measurements from individual lactose particles using atomic force microscopy. *International Journal of Pharmaceutics*, 332(1-2), pp. 168-175.
- Pharmatron, S. (2010) *Breaking-force tests for empty and filled hard capsules and soft-gels*. [online]. Available from: <http://www.pharmatron.ch/newsroom/publications/breaking-force-tests-for-empty-and-filled-hard-capsules-and-softgels/> [Accessed 09th March 2012].
- Pitt, K. G. & Heasley, M. G. (2011) *Determination of the tensile strength of elongated tablets*. Powder Technology. [online]. Available from: <http://www.sciencedirect.com/science/article/pii/S0032591011007467#FCANote> [Accessed 04th April 2012].
- Pitt, K. G., Stanley, P. & Newton, J. M. (1988) Tensile fracture of doubly convex cylindrical discs under diametral loading. *Journal of Material Science*, 23(8), pp. 2723-2728.
- Pungotra, H., Knopf, G. K. & Canas, R. (2008) Efficient algorithm to detect collision between deformable B-spline surfaces for virtual sculpting. *Computer-Aided Design*, 40(10-11), pp. 1055-1066.
- Reich, G. (2004) Formulation and physical properties of soft capsules. In: Podczek, F. & Jones, B. E., eds. *Pharmaceutical Capsules*, London: Pharmaceutical Press, pp. 201-212.
- Reynolds, T. D., Mitchell, S. A. & Balwinski, K. M. (2002) Investigation of the effect of tablet surface area/volume on drug release from Hydroxypropylmethylcellulose controlled-release matrix tablets. *Drug Development and Industrial Pharmacy*, 28(4), pp. 457-466.

- Sánchez, H., Moreno, A., Oyarzun, D. & García-Alonso, A. (2004) Evaluation of NURBS surfaces: An overview based on runtime efficiency. *WSCG SHORT Communication Papers Proceedings*. Czech Republic, 2nd-6th February 2004, Plzen: UNION Agency-Science Press, pp. 235-242.
- Santos, H. M. M. & Sousa, J. J. M. (2008) Tablet compression. In: Gad S. C., ed. *Pharmaceutical Manufacturing Handbook: Production and Process*. New York: John Wiley & Sons, pp. 1133-1163.
- Sburlati, R. (2009) Three-dimensional analytical solution for an axisymmetric Biharmonic problem. *Journal of Elasticity*, 95(1), pp. 79-97.
- Schulz, B. M. & Schulz, M. (2006) The dynamics of wet granular matter. *Journal of Non-Crystalline Solids*, 352(42-49), pp. 4877-4879.
- Sekula, E. (2010) The structure of turbulent jets: Application of experimental and environmental methods. PhD thesis, Universitat Politècnica De Catalunya, Spain.
- Shahat, A., Keyhani, A. & Marwali, M. (2011) Sizing high speed micro generators for smart grid systems. In: Keyhani, A. & Marwali, M., eds. *Smart Power Grids*. Berlin Heidelberg: Springer, pp. 177-234.
- Shang, L., Jiachuan, S., Li, H. & Fan, C. (2008) Simulation of 3D garment based on six pieces of Bezier curved surfaces. *International Conference on Computer Science and Software Engineering, Conference Proceedings*. Wuhan Hubei, 12-14<sup>th</sup> Dec. 2008, Washington: IEEE Transactions on Visualization and Computer Graphics, pp. 1082-1085.
- Sheng, Y., Sourin, A., González Castro, G. & Ugail, H. (2010) A PDE method for patchwise approximation of large polygon meshes. *The Visual Computer*, 26(6-8), pp. 975-984.
- Sheng, Y., Willis, P., González Castro, G. & Ugail, H. (2008) PDE-based facial animation: Making the complex simple. In: Bebis, G., Boyle, R., Parvin, B., Koracin, D., Remagnino, P., Porikli, F., Peters, J., Klosowski, J., Arns, L., Chun, Y. K., Rhyne, T. M. & Monroe, L., eds. *Advances in Visual Computing: 4th International Symposium*. Berlin: Springer, pp. 723-732.
- Siepmann, J., Kranz, H., Peppas N. A. & Bodmeier, R. (2000) Calculation of the required size and shape of Hydroxypropyl Methylcellulose matrices to achieve desired drug release profiles. *International Journal of Pharmaceutics*, 201(2), pp. 151-164.
- Siiriä, S. & Yliruusi, J. (2007) Particle packing simulations based on Newtonian mechanics. *Powder Technology*, 174(3), pp. 82-92.

- Sinha, T., Curtis, J. S., Hancock, B. C. & Wassgren, C. (2010) A study on the sensitivity of Drucker-Prager Cap model parameters during the decompression phase of powder compaction simulations. *Powder Technology*, 198(3), pp. 315-324.
- Song, C. M., Lim, S. J. & Tong, J. C. (2009) Recent advances in computer-aided drug design. *Briefings in Bioinformatics*, 10(5), pp. 579-591.
- Sonnergaard, J. M. (1999) A critical evaluation of the Heckel equation. *International Journal of Pharmaceutics*, 193(1), pp. 63-71.
- Sonnergaard, J. M. (2006) Quantification of the compactibility of pharmaceutical powders. *European Journal of Pharmaceutics and Biopharmaceutics*, 63(3), pp. 270-277.
- Sovány, T., Kása Jr, P. & Pintye-Hódi, K. (2009) Comparison of the halving of tablets prepared with eccentric and rotary tablet presses. *American Association of Pharmaceutical Scientists PharmSciTech*, 10(2), pp. 430-436.
- Spaniol, B., Bica, V. C., Ruppenthal, L. R., Volpato, M. R. & Petrovick, P. R. (2009) Compressional behavior of a mixture of granules containing high load of *Phyllanthus niruri* spraydried extract and granules of adjuvants: Comparison between eccentric and rotary tablet machines. *American Association of Pharmaceutical Scientists PharmSciTech*, 10(3), pp. 1013-1023.
- Swaminathan, V. & Kilsig, D. O. (2000) The effect of particle morphology on the physical stability of pharmaceutical powder mixtures: The effect of surface roughness of the carrier on the stability of ordered mixtures. *Drug Development and Industrial Pharmacy*, 26(4), pp. 365-373.
- Timoshenko, S. P. & Goodier, J. N. (1970) *Theory of elasticity*. 3rd edn., New York: McGraw Hill.
- Tomas, J. R. (2001) Assessment of mechanical properties of cohesive particulate solids. Part 1: Particle contact constitutive model. *Particulate Science and Technology: An International Journal*, 19(2), pp. 95-110.
- Tornincasa, S. & Monaco, F. D. (2010) The future and the evolution of CAD. In: Ekinović, S., Uctug, Y. & Calvet, J. V., eds. *14th International Research/Expert Conference "Trends in the Development of Machinery and Associated Technology"*. Mediterranean Cruise, 11-18th September 2010, Conference Proceedings. [online]. <http://www.tmt.unze.ba/proceedings2010.php>, pp. II(1-18).
- Tousey, M. D. (2002) Optimal tablet press operation: Machine versus granulation. *Pharmaceutical Technology*, 26(1), pp. 52-60.

- Ugail, H. & Sourin, A. (2008) Partial differential equations for function based geometry modelling within visual Cyberworlds. *Proceedings of the 2008 International Conference on Cyberworlds*. Hangzhou, China, 22nd-24th September 2008, Los Alamitos: IEEE Computer Society, pp. 224-231.
- Ugail, H. & Wilson, M. J. (2003) Efficient shape parametrisation for automatic design optimisation using a partial differential equation formulation. *Computers & Structures*, 81(28-29), pp. 2601-2609.
- Ugail, H. & Wilson, M. J. (2005) Modelling of oedemous limbs and venous ulcers using partial differential equations. *Theoretical Biology and Medical Modelling*, 2(28), pp. 1-9.
- Ugail, H. (2003) Parametric design and optimisation of thin-walled structures for food packaging. *Optimization and Engineering*, 4(4), pp. 291-307.
- Ugail, H. (2004) Spine based shape parameterisation for PDE surfaces. *Journal Computing*, 72(1), pp. 195-206.
- Ugail, H. (2006) Method of trimming PDE surfaces. *Computers & Graphics*, 30(2), pp. 225-232.
- Van der Velden, A. & Koch, P. (2010) Isight design optimization methodologies. *ASM Handbook - Application of Metal Processing Simulations*, 22B(1), pp. 1-24.
- Waimer, F., Krumme, M., Danz, P., Tenter, U. & Schmidt, P. C. (1999) The influence of engravings on the sticking of tablets. Investigations with an instrumented upper punch. *Pharmaceutical Development and Technology*, 4(3), pp. 369-375.
- Wellmann, C., Lillie, C. & Wriggers, P. (2008) Comparison of the macroscopic behavior of granular materials modeled by different constitutive equations on the microscale. *Finite Element in Analysis and Design*, 44(5), pp. 259-271.
- Wu, C. Y. & Seville, J. P. K. (2009) A comparative study of compaction properties of binary and bilayer tablets. *Powder Technology*, 189(2), pp. 285-294.
- Wu, C. Y., Best, S. M., Bentham, A. C., Hancock, B. C. & Bonfield, W. (2005) A simple predictive model for the tensile strength of binary tablets. *European Journal of Pharmaceutical Sciences*, 25(2-3), pp. 331-336.
- Wu, C. Y., Hancock, B. C., Mills, A., Bentham, A. C., Best, S. M. & Elliott, J. A. (2008) Numerical and experimental investigation of capping mechanisms during pharmaceutical tablet compaction. *Powder Technology*, 181(2), pp. 121-129.

- Wu, C. Y., Thornton, C. & Li, L. Y. (2003) Coefficients of restitution for elastoplastic oblique impacts. *Advanced Powder Technology*, 14(4), pp. 435-448.
- Xie, Z. & Farin, G. E. (2004) Image registration using hierarchical B-splines. *IEEE Transactions on Visualization and Computer Graphics*, 10(1), pp. 85-94.
- Yap, S. F., Adams, M. J., Seville, J. P. K. & Zhang, Z. (2008) Single and bulk compression of pharmaceutical excipients: Evaluation of mechanical properties. *Powder Technology*, 185(1), pp. 1-10.
- You, L., Comninou, P. & Zhang, J. J. (2008) Solid modelling with fourth order partial differential equation. *International Journal of Computers*, 4(2), pp. 452-461.
- Yu, D. -G., Branford-White, C., Yang, Y. -C., Zhu, L. -M., Welbeck, E. W. & Yang, X. -L. (2009) A novel fast disintegrating tablet fabricated by three-dimensional printing. *Drug Development and Industrial Pharmacy*, 35(12), pp. 1530-1536.
- Zhang, J. J. & You, L. (2002) PDE based surface representation - vase design. *Computers & Graphics*, 26(1), pp. 89-98.
- Zhang, J. J. & You, L. (2004) Fast surface modelling using a 6th order PDE. *Computer Graphics Forum*, 23(3), pp. 311-320.
- Zhang, Y., Law, Y. & Chakrabarti, S. (2003) Physical properties and compact analysis of commonly used direct compression binders. *American Association of Pharmaceutical Scientists PharmSciTech*, 4(4), pp. 489-499.

## Appendix A

### Pseudocode for Cuboid Mesh Generation

The pseudocode below shows how to generate a cuboid mesh for a PDE-based representation of an object. The process has been explained in detail on page (70 - 72).

#### **GenerateCuboidMesh(F)**

##### **Input:**

Height ( $h$ ) and Radius ( $r$ ) of Boundary Curves

Domain  $du, dw, dv$

**Output:** Cuboid Meshes

1. Initialise  $h$  and  $r$   
Call **PDEMethod** ( $h, r$ ) to calculate PDE coefficients  
Return (**PDECoefficients**)

2. Set Domain  $du = dw = [0, 1]$  and  $dv = [0, 2\pi]$   
Call **MeshGrid** ( $du, dv, dw$ ) to generate vector  $\mathbf{u}, \mathbf{v}$  and  $\mathbf{w}$   
Return  $(\mathbf{u}, \mathbf{v}, \mathbf{w}, sx, sy, sz)$  where  $sx, sy$  and  $sz$  are the number of points on  $x$ -,  $y$ - and  $z$ -axis respectively.
  
3. Calculate **ExtendedPDE** ( $\mathbf{u}, \mathbf{v}, \mathbf{w}, \mathbf{PDECoefficient}$ ) to generate nodes  
Return **(Nodes)**
  
4. Generate **Face1(Nodes)** patch parallel to  $yz$ -plane until  $sx$ -layer  
Generate **Face2(Nodes)** patch parallel to  $xy$ -plane until  $sz$ -layer  
Generate **Face3(Nodes)** patch parallel to  $zx$ -plane until  $sy$ -layer

## Appendix B

### Experimental Data of Compressed Powder

Tables below show a set of force-displacement data of compressed  $\alpha$ -lactose monohydrate together with its properties, which were prepared at the Institute of Pharmaceutical Innovation (IPI), University of Bradford. The last two columns of the second table give the value of pressure and relative density. These values are used to plot the Heckel graph, as shown in Figure 5.3.

<b>Weight (g)</b>	0.3
<b>True Density</b>	1.3
<b>Compensation Test Equation:</b> $y = 0.00002x - 0.0267$	

Force (N)	Displacement (x)	Thickness (mm)	Relative Density (D)	Pressure (MPa)	Ln(1/1-D)
3.891	-6.032	6.0588	0.484956734	0.049541751	0.663504
3.891	-5.992	6.0188	0.488179692	0.049541751	0.669782
3.891	-5.951	5.9778	0.491527988	0.049541751	0.676345
7.782	-5.91	5.9369	0.494916043	0.099083501	0.683031
7.782	-5.869	5.8959	0.498357708	0.099083501	0.689868
11.672	-5.829	5.8559	0.501755208	0.14861252	0.696664
15.563	-5.788	5.8150	0.505286228	0.19815427	0.703776
19.454	-5.747	5.7741	0.508867297	0.247696021	0.711041
23.345	-5.707	5.7342	0.512410112	0.297237772	0.718281
31.126	-5.666	5.6933	0.516086186	0.396308541	0.725848
35.017	-5.628	5.6554	0.519546792	0.445850291	0.733025
42.799	-5.587	5.6146	0.523326353	0.544933793	0.740923
50.581	-5.547	5.5747	0.527066744	0.644017294	0.748801

58.362	-5.506	5.5339	0.53095692	0.743088063	0.757061
70.035	-5.465	5.4931	0.534897367	0.891713315	0.765497
81.707	-5.425	5.4533	0.538797922	1.040325835	0.773919
93.379	-5.384	5.4126	0.542856059	1.188938354	0.782757
108.943	-5.346	5.3749	0.546662572	1.387105357	0.791119
124.506	-5.305	5.3342	0.550832467	1.585259628	0.800359
143.96	-5.265	5.2946	0.554953471	1.832955649	0.809576
163.414	-5.224	5.2540	0.559243023	2.08065167	0.819262
186.759	-5.183	5.2134	0.563590992	2.377889441	0.829175
213.995	-5.146	5.1770	0.567559689	2.724668964	0.838311
245.121	-5.105	5.1366	0.572021127	3.120977504	0.848681
276.248	-5.064	5.0962	0.576553258	3.517298778	0.859328
315.156	-5.027	5.0600	0.580680492	4.01269082	0.869122
354.064	-4.986	5.0198	0.585333292	4.508082862	0.88028
396.863	-4.945	4.9796	0.590052036	5.053016654	0.891725
447.443	-4.904	4.9396	0.594828739	5.697021216	0.903445
498.024	-4.864	4.9007	0.599561042	6.34103851	0.915194
556.386	-4.823	4.8608	0.604474232	7.084126573	0.927539
618.639	-4.785	4.8241	0.609079763	7.876756387	0.939252
688.674	-4.744	4.7845	0.614120888	8.768469702	0.952231
762.599	-4.704	4.7460	0.619105527	9.709712036	0.965233
840.415	-4.663	4.7065	0.624294045	10.70049612	0.978948
926.013	-4.622	4.6672	0.629549269	11.79036371	0.993035
1019.392	-4.585	4.6321	0.634324133	12.97930206	1.006008
1120.554	-4.544	4.5931	0.639706955	14.26733665	1.020838
1233.387	-4.506	4.5574	0.644724163	15.70397102	1.034861
1322.876	-4.475	4.5282	0.648883147	16.84338036	1.046636
1416.255	-4.447	4.5020	0.652649649	18.03231871	1.057421
1513.526	-4.419	4.4760	0.656448717	19.27081155	1.068419
1618.577	-4.387	4.4461	0.660863209	20.60836243	1.081352
1731.411	-4.359	4.4203	0.664711975	22.04500953	1.092765
1848.135	-4.331	4.3947	0.668593998	23.53118566	1.104411
1968.75	-4.299	4.3651	0.673125915	25.06690354	1.11818
2093.256	-4.271	4.3396	0.677082846	26.65216316	1.130359
2217.762	-4.243	4.3141	0.681086574	28.23742279	1.142836
2338.377	-4.212	4.2855	0.685629999	29.77314067	1.157185
2458.992	-4.184	4.2599	0.689748353	31.30885855	1.170372
2575.717	-4.155	4.2332	0.694093156	32.7950474	1.184475
2692.441	-4.127	4.2075	0.698327038	34.28122353	1.198412
2813.056	-4.099	4.1820	0.702599814	35.81694141	1.212677
2929.781	-4.071	4.1563	0.706938431	37.30313027	1.227373
3046.505	-4.043	4.1306	0.711330967	38.78930639	1.242474
3163.229	-4.014	4.1040	0.715952842	40.27548252	1.258615
3276.063	-3.986	4.0782	0.720472215	41.71212963	1.274654
3385.006	-3.961	4.0554	0.724526561	43.09923498	1.289264
3493.948	-3.936	4.0326	0.7286268	44.48632761	1.30426
3599	-3.908	4.0067	0.733336604	45.82389122	1.321768
3700.161	-3.883	3.9837	0.737566265	47.11191307	1.337757
3793.541	-3.858	3.9606	0.741874148	48.30086416	1.354308
3886.92	-3.833	3.9374	0.746232653	49.48980251	1.371337
3972.518	-3.807	3.9132	0.75086435	50.5796701	1.389758
4058.116	-3.782	3.8899	0.755359666	51.66953768	1.407966
4139.823	-3.76	3.8695	0.759335261	52.70986352	1.42435
4217.639	-3.739	3.8501	0.763170084	53.7006476	1.440413

4295.456	-3.713	3.8256	0.768046345	54.69144442	1.461218
4369.381	-3.692	3.8061	0.77198567	55.63268675	1.478347
4439.416	-3.673	3.7885	0.775571905	56.52440007	1.4942
4505.559	-3.651	3.7678	0.779828118	57.3665589	1.513347
4563.921	-3.629	3.7470	0.784163871	58.10964696	1.533236
4622.283	-3.61	3.7291	0.78791374	58.85273503	1.550762
4672.864	-3.591	3.7112	0.791732843	59.49675232	1.568934
4719.554	-3.572	3.6931	0.795605914	60.09122786	1.587705
4758.462	-3.554	3.6759	0.799333412	60.58661991	1.606111
4789.588	-3.535	3.6575	0.803349753	60.98292845	1.626329
4812.933	-3.516	3.6390	0.807441188	61.28016622	1.647354
4828.497	-3.5	3.6233	0.8109374	61.47833322	1.665677
4836.278	-3.482	3.6054	0.814950983	61.57740399	1.687135
4836.278	-3.466	3.5894	0.818583658	61.57740399	1.706961
4832.387	-3.45	3.5733	0.82226677	61.52786224	1.727472
4820.715	-3.435	3.5581	0.82578716	61.37924972	1.747478
4805.151	-3.419	3.5418	0.829590208	61.18108272	1.769549
4781.807	-3.406	3.5283	0.83275657	60.88385768	1.788305
4754.571	-3.391	3.5128	0.836441665	60.53707815	1.810586
4719.554	-3.378	3.4991	0.839716668	60.09122786	1.830812
4680.646	-3.363	3.4833	0.843520284	59.59583582	1.854829
4633.956	-3.35	3.4694	0.846908049	59.00136028	1.876717
4587.266	-3.337	3.4554	0.850323137	58.40688473	1.899277
4532.795	-3.325	3.4424	0.853556456	57.71333842	1.921115
4474.433	-3.312	3.4282	0.857083841	56.97025036	1.945497
4412.18	-3.303	3.4179	0.859652893	56.17762054	1.963637
4349.927	-3.29	3.4037	0.863250687	55.38499073	1.989606
4279.892	-3.281	3.3933	0.865896612	54.49327742	2.009144
4209.857	-3.272	3.3829	0.868558807	53.6015641	2.029196
4139.823	-3.262	3.3715	0.871495829	52.70986352	2.051794
4065.897	-3.253	3.3610	0.874212859	51.76860845	2.073164
3991.972	-3.243	3.3495	0.87720869	50.82736612	2.097269
3921.938	-3.234	3.3391	0.879941001	49.93566554	2.119772
3848.012	-3.225	3.3287	0.882711028	48.99441047	2.143115
3774.087	-3.218	3.3202	0.884965141	48.05316814	2.16252
3704.052	-3.209	3.3098	0.887746068	47.16145482	2.186992
3630.127	-3.203	3.3023	0.889756486	46.22021249	2.205064
3563.983	-3.196	3.2940	0.892004629	45.37804092	2.225667
3497.839	-3.19	3.2867	0.893992072	44.53586936	2.244241
3435.586	-3.184	3.2794	0.895967129	43.74323955	2.263048
3373.333	-3.178	3.2722	0.897950932	42.95060973	2.282302
3318.862	-3.171	3.2641	0.90017634	42.25706342	2.30435
3264.39	-3.165	3.2570	0.902135741	41.56350437	2.324174
3217.701	-3.159	3.2501	0.90406039	40.96904156	2.344036
3171.011	-3.153	3.2431	0.905993273	40.37456602	2.364389
3132.103	-3.149	3.2383	0.907330062	39.87917398	2.378711
3093.195	-3.143	3.2316	0.909233174	39.38378194	2.399461
3062.068	-3.137	3.2249	0.911100319	38.98746066	2.420247
3030.942	-3.134	3.2213	0.912124893	38.59115212	2.431839
3007.597	-3.127	3.2139	0.914244078	38.29391435	2.45625
2984.252	-3.124	3.2104	0.915231372	37.99667658	2.46783
2968.689	-3.118	3.2041	0.917034159	37.79852231	2.489326
2953.125	-3.115	3.2008	0.917982857	37.60035531	2.500827
2941.453	-3.109	3.1945	0.919774104	37.45174279	2.522909

2933.671	-3.106	3.1914	0.920683579	37.35265928	2.53431
2929.781	-3.099	3.1843	0.922730002	37.30313027	2.56045
2929.781	-3.093	3.1783	0.924471935	37.30313027	2.583251
2933.671	-3.09	3.1754	0.925322699	37.35265928	2.594579
2941.453	-3.084	3.1695	0.927028921	37.45174279	2.617692
2953.125	-3.08	3.1658	0.928131881	37.60035531	2.632923
2968.689	-3.074	3.1601	0.929802691	37.79852231	2.656445
2988.143	-3.071	3.1575	0.930571549	38.04621833	2.667459
3011.488	-3.065	3.1519	0.932205134	38.3434561	2.691269
3034.833	-3.062	3.1494	0.932954918	38.64069387	2.70239
3065.959	-3.055	3.1430	0.934847971	39.03700241	2.731032
3100.976	-3.052	3.1407	0.935532474	39.4828527	2.741594
3135.994	-3.046	3.1354	0.937113757	39.92871573	2.766428
3178.792	-3.043	3.1333	0.937755006	40.47363679	2.776677
3221.592	-3.037	3.1281	0.93929708	41.01858331	2.801763
3268.281	-3.033	3.1251	0.94021869	41.61304613	2.817062
3318.862	-3.027	3.1201	0.941721912	42.25706342	2.842529
3369.442	-3.024	3.1181	0.942322446	42.90106798	2.852887
3427.804	-3.018	3.1133	0.943785229	43.64415604	2.878576
3486.167	-3.015	3.1114	0.944341153	44.38725684	2.888514
3548.42	-3.012	3.1097	0.944874091	45.17988665	2.898135
3610.673	-3.005	3.1039	0.946625974	45.97251647	2.930431
3676.816	-3.002	3.1022	0.947137742	46.8146753	2.940066
3746.851	-2.996	3.0976	0.94854403	47.70638861	2.967029
3816.885	-2.993	3.0960	0.94903402	48.5980892	2.976597
3886.92	-2.986	3.0904	0.950753493	49.48980251	3.010917
3960.845	-2.983	3.0889	0.951221803	50.43104485	3.020472
4034.771	-2.977	3.0844	0.952616219	51.37229991	3.049475
4108.696	-2.974	3.0829	0.953086367	52.31354224	3.059447
4182.622	-2.968	3.0784	0.954486259	53.25479731	3.089741
4256.547	-2.965	3.0768	0.954958254	54.19603964	3.100166
4326.582	-2.961	3.0742	0.955765683	55.08775296	3.118254
4396.616	-2.955	3.0696	0.957197735	55.97945354	3.151164
4466.651	-2.952	3.0680	0.957696701	56.87116686	3.16289
4532.795	-2.949	3.0664	0.958220506	57.71333842	3.17535
4598.938	-2.943	3.0617	0.959684321	58.55549725	3.211015
4661.191	-2.939	3.0589	0.960548636	59.34812707	3.232687
4719.554	-2.936	3.0571	0.961124489	60.09122786	3.247391
4777.916	-2.93	3.0523	0.962646275	60.83431593	3.287323
4828.497	-2.927	3.0503	0.963273796	61.47833322	3.304265
4875.186	-2.924	3.0482	0.963926749	62.07279603	3.322204
4917.985	-2.921	3.0461	0.964605225	62.61772982	3.341191
4956.893	-2.918	3.0438	0.965309336	63.11312187	3.361285
4988.02	-2.911	3.0375	0.967336102	63.50944314	3.421485
5019.146	-2.908	3.0351	0.968093848	63.90575168	3.444956
5046.382	-2.905	3.0326	0.968877637	64.2525312	3.469829
5069.727	-2.902	3.0301	0.9696876	64.54976897	3.496198
5085.29	-2.899	3.0274	0.970548812	64.74792324	3.525021
5100.853	-2.896	3.0247	0.971411555	64.94607751	3.554753
5112.525	-2.892	3.0210	0.972622724	65.09469003	3.598042
5120.307	-2.889	3.0181	0.973539354	65.19377354	3.632097
5128.089	-2.886	3.0153	0.974457715	65.29285704	3.66742
5128.089	-2.886	3.0153	0.974457715	65.29285704	3.66742
5128.089	-2.883	3.0123	0.975428206	65.29285704	3.706156

5124.198	-2.88	3.0092	0.976425882	65.24331529	3.747606
5120.307	-2.877	3.0061	0.977425602	65.19377354	3.790939
5112.525	-2.877	3.0060	0.97747621	65.09469003	3.793183
5100.853	-2.874	3.0027	0.978528794	64.94607751	3.841042
5089.181	-2.871	2.9995	0.979583647	64.797465	3.891419
5073.618	-2.871	2.9992	0.97968531	64.59931072	3.896411
5058.054	-2.867	2.9949	0.981095625	64.40114372	3.968362
5042.491	-2.864	2.9915	0.982181571	64.20298945	4.027522
5023.037	-2.864	2.9912	0.98230933	63.95529343	4.034718
4999.692	-2.861	2.9877	0.983449195	63.65805566	4.101321
4976.347	-2.861	2.9872	0.983602907	63.36081789	4.110651
4953.002	-2.858	2.9838	0.984745778	63.06358012	4.182899
4925.767	-2.858	2.9832	0.984925581	62.71681333	4.194756
4898.531	-2.855	2.9797	0.986097283	62.3700338	4.275671
4867.404	-2.855	2.9790	0.986303351	61.97371253	4.290604
4836.278	-2.852	2.9754	0.987504155	61.57740399	4.382359
4805.151	-2.852	2.9748	0.987710811	61.18108272	4.399035
4770.134	-2.849	2.9711	0.988940949	60.73523242	4.504506
4735.117	-2.849	2.9704	0.989174114	60.28938213	4.525815
4696.209	-2.849	2.9696	0.989433317	59.79399009	4.550049
4657.301	-2.845	2.9648	0.991027893	59.29859805	4.713635
4618.393	-2.845	2.9641	0.991288068	58.80320601	4.743062
4579.484	-2.845	2.9633	0.991548387	58.30780123	4.773398
4540.577	-2.845	2.9625	0.99180883	57.81242192	4.804698
4497.777	-2.845	2.9617	0.99209549	57.2674754	4.840322
4458.87	-2.845	2.9609	0.99235622	56.77209609	4.873863
4419.961	-2.842	2.9571	0.993624118	56.27669131	5.055233
4381.053	-2.842	2.9563	0.993885658	55.78129927	5.097118
4346.036	-2.842	2.9556	0.994121162	55.33544898	5.136396
4311.019	-2.842	2.9549	0.994356776	54.88959869	5.1773
4276.001	-2.842	2.9542	0.994592509	54.44373567	5.21997
4244.875	-2.842	2.9536	0.994802136	54.04742712	5.259508
4217.639	-2.842	2.9531	0.994985638	53.7006476	5.295449
4190.403	-2.842	2.9525	0.995169206	53.35386808	5.332745
4167.059	-2.842	2.9520	0.995326597	53.05664304	5.365868
4151.495	-2.842	2.9517	0.995431561	52.85847604	5.388584
4135.932	-2.842	2.9514	0.995536541	52.66032177	5.411831
4124.26	-2.842	2.9512	0.995615288	52.51170925	5.429631
4116.478	-2.842	2.9510	0.995667798	52.41262575	5.441679
4108.696	-2.842	2.9509	0.995720313	52.31354224	5.453875
4108.696	-2.839	2.9479	0.99673364	52.31354224	5.724079
4108.696	-2.839	2.9479	0.99673364	52.31354224	5.724079
4108.696	-2.839	2.9479	0.99673364	52.31354224	5.724079
4116.478	-2.839	2.9480	0.996681018	52.41262575	5.708097
4124.26	-2.839	2.9482	0.996628402	52.51170925	5.692368
4135.932	-2.839	2.9484	0.996549494	52.66032177	5.669234
4147.604	-2.839	2.9487	0.996470599	52.80893429	5.646627
4163.168	-2.839	2.9490	0.996365415	53.00710129	5.61726
4178.731	-2.839	2.9493	0.996260261	53.20525556	5.58874
4198.185	-2.836	2.9467	0.997143007	53.45295158	5.857986
4213.749	-2.836	2.9470	0.997037682	53.65111858	5.821783
4237.093	-2.836	2.9474	0.99687975	53.94834362	5.769842
4256.547	-2.836	2.9478	0.996748173	54.19603964	5.728538
4279.892	-2.836	2.9483	0.996590325	54.49327742	5.681138

4307.128	-2.836	2.9488	0.996406232	54.84005694	5.628554
4330.473	-2.833	2.9463	0.997262896	55.13729471	5.900855
4357.708	-2.833	2.9469	0.99707856	55.4840615	5.835679
4384.944	-2.833	2.9474	0.996894286	55.83084102	5.774512
4416.07	-2.83	2.9450	0.997699067	56.22714956	6.074441
4447.197	-2.83	2.9456	0.997488211	56.62347084	5.98676
4478.323	-2.83	2.9463	0.99727745	57.01977938	5.906186
4509.45	-2.83	2.9469	0.997066772	57.41610065	5.831652
4540.577	-2.827	2.9445	0.997871825	57.81242192	6.15249
4575.594	-2.827	2.9452	0.997634541	58.25827221	6.046783
4614.502	-2.827	2.9460	0.997371024	58.75366426	5.941161
4649.519	-2.827	2.9467	0.997133979	59.19951455	5.854831
4688.427	-2.823	2.9435	0.998225414	59.69490659	6.334188
4731.226	-2.823	2.9443	0.997935208	60.23984038	6.182726

## Appendix C

### Coefficients of the Love's Stress Function in Spherical Coordinates

For the case of a compressed spherical softgel capsule, a Biharmonic Love's stress function in spherical coordinates,  $X(r, \theta)$ , is used to find the expression for the radial displacement,  $\mu_r$ . The boundary conditions in Equations (6.21a)-(6.21c) have been solved using MAPLE to find the coefficients in Equation (6.20). These are

$$B_1 = -\frac{3(-f_0 + P_{\text{int}} - P_{\text{ext}})(ab)^3}{4(b^3 - a^3)(2\gamma - 1)}, \quad (\text{C.1})$$

$$B_2 = \frac{5}{24} \frac{f_1 a^4 b^5}{(b^5 - a^5)(3\gamma - 2)}, \quad (\text{C.2})$$

$$D_1 = -\frac{3(P_{\text{int}} - P_{\text{ext}})b^3 - f_0 a^3}{10(b^3 - a^3)(\gamma + 1)}, \quad (\text{C.3})$$

$$D_2 = \frac{5}{28} \frac{f_1 a^4}{(b^5 - a^5)(\gamma + 1)}, \quad (\text{C.4})$$

$$\begin{aligned}
A_{n-1} = & \left\{ f_n(2n+3)[a^{n+4}b^5(2n+1)(n^4+2n^3-n^2-2n+4-4\gamma^2) \right. \\
& + a^{n+6}b^3n(n+2)(2n-1)(-n^2-2n-2\gamma+1) + a^{5-n}b^{2n+4}[2(n^2+n+1) \\
& (n^2-2) + 2n(n+2)(2n-1)\gamma + 4(2n+1)\gamma^2] + B_{n+1}(n+2)[(ab^5+ba^5) \\
& (2n+1)^2(6n+2-4\gamma(2n+1))(n^4+2n^3-n^2-2n+4-4\gamma^2) + na^3b^3 \\
& (n^2-1)(n+2)(2n-1)(2n+3)(8\gamma(2n+1)-12n-4) + (a^{2-2n}b^{2n+4} \\
& + a^{2n+4}b^{2-2n})(24n+8-16\gamma(2n+1))(\gamma^2(2n+1)^2-n^4-2n^3-3n^2-2n \\
& -1)] \left. \right\} \div \left\{ (2n^3+7n^2+6n)[(2n+1)^2(4\gamma^2-n^4-2n^3+n^2+2n-4)(ab^5 \right. \\
& + ba^5) + 2n(2n-1)(2n+3)(n-1)(n+1)(n+2)a^3b^3 + 4(a^{2-n}b^{2n+4} \\
& \left. + a^{2n+4}b^{2-n})(n^4+2n^3+3n^2+2n+1-\gamma^2(2n+1)^2) \right\}, \tag{C.5}
\end{aligned}$$

$$\begin{aligned}
B_{n-1} = & \left\{ f_n(2n-1)[a^{n+4}b^3(2n+3)(n+1)(n-1) + a^{n+6}b(2n+1)(-n^2-2n \right. \\
& -2\gamma+1) + 2a^{3-n}b^{2n+4}(n^2+n+2n\gamma+1+\gamma)] \left. \right\} \div \left\{ (2n-3)[(2n+1)^2 \right. \\
& (n^4+2n^3-n^2-2n+4-4\gamma^2)(ab^5+ba^5) - 2n(2n-1)(2n+3)(n-1) \\
& (n+1)(n+2)a^3b^3 + 4(\gamma^2(2n+1)^2-n^4-2n^3-3n^2-2n-1) \\
& \left. (a^{2-2n}b^{2n+4} + a^{2n+4}b^{2-2n}) \right\}, \tag{C.6}
\end{aligned}$$

$$\begin{aligned}
D_{n+1} = & \left\{ f_n(2n+3)[a^{n-5}b(2n+1)(-n^2+2-2\gamma) + 2a^{n+4}b^{2-2n}(-n^2-n+2n\gamma \right. \\
& -1+\gamma) + a^{3-n}b^3n(2n-1)(n+2)] \left. \right\} \div \left\{ (2n+5)[(2n+1)^2(n^4+2n^3-n^2 \right. \\
& -2n+4-4\gamma^2)(ab^5+ba^5) + 2na^3b^3(4n^5+12n^4+n^3-18n^2-5n+6) \\
& \left. + 4(a^{2-2n}b^{2n+4} + a^{2n+4}b^{2-2n})(n^4+2n^3+3n^2+2n+1-\gamma^2(2n+1)^2) \right\}, \tag{C.7}
\end{aligned}$$

$$\begin{aligned}
C_{n+1} = & \left\{ -f_n [a^{n+6} b^{2-2n} [4(2n+1)(2n-1)\gamma^2 + 2(n+1)(n-1)(2n-1)(2n+3)\gamma \right. \\
& + 2(2n-1)(-n^4 + 3n^3 - 2n^2 - n + 1)] + a^{5-n} b^3 (n+1)(n-1)(2n-1) \\
& (2n+3)(-n^2 + 2 - 2\gamma) + a^{3-n} b^5 (2n-1)(2n+1)(n^4 + 2n^3 - n^2 - 2n \\
& + 4 - 4\gamma^2)] + D_{n-1} (n-1) [(ab^5 + ba^5)(2n+1)^2 (-6n - 4 + 4\gamma(2n+1))(n^4 \\
& + 2n^3 - n^2 - 2n + 4 - 4\gamma^2) + 8(a^{2-2n} b^{2n+4} + a^{2n+4} b^{2-2n})(3n+2 - \gamma(4n \\
& + 2))(n^4 + 2n^3 + 3n^2 + 2n + 1 - \gamma^2(2n+1)^2) + 4a^3 b^3 n(n+1)(n+2)(2n-1) \\
& \left. (2n+3)(n-1)(3n+2 - 2\gamma(2n+1))] \right\} \div \left\{ (2n^3 - n^2 - 2n + 1) [(2n+1)^2 (-n^4 \right. \\
& - 2n^3 + n^2 + 2n - 4 + 4\gamma^2)(ab^5 + ba^5) + 2n(2n-1)(2n+3)(n^2 - 1)(n+2)a^3 b^3 \\
& \left. + (a^{2-2n} b^{2n+4} + a^{2n+4} b^{2-2n})(4n^4 + 8n^3 + 12n^2 + 8n + 4 - \gamma^2(2n+1)^2)] \right\}, \quad (C.8)
\end{aligned}$$

where  $f_0, f_1, \dots, f_n$  are coefficients of the expansion of an infinite series of Legendre polynomials. The expression for the radial displacement, shown in Equation (6.20), together with coefficients in Equations (C.1) – (C.8) is used in an optimisation process, which is discussed in Section 6.2.3, in order to find the optimal thickness of a spherical capsule.